Master Thesis, Department of Geosciences

Granite weathering, saprolitization and the formation of secondary clay particles, SW Bornholm

Nikolas Oberhardt

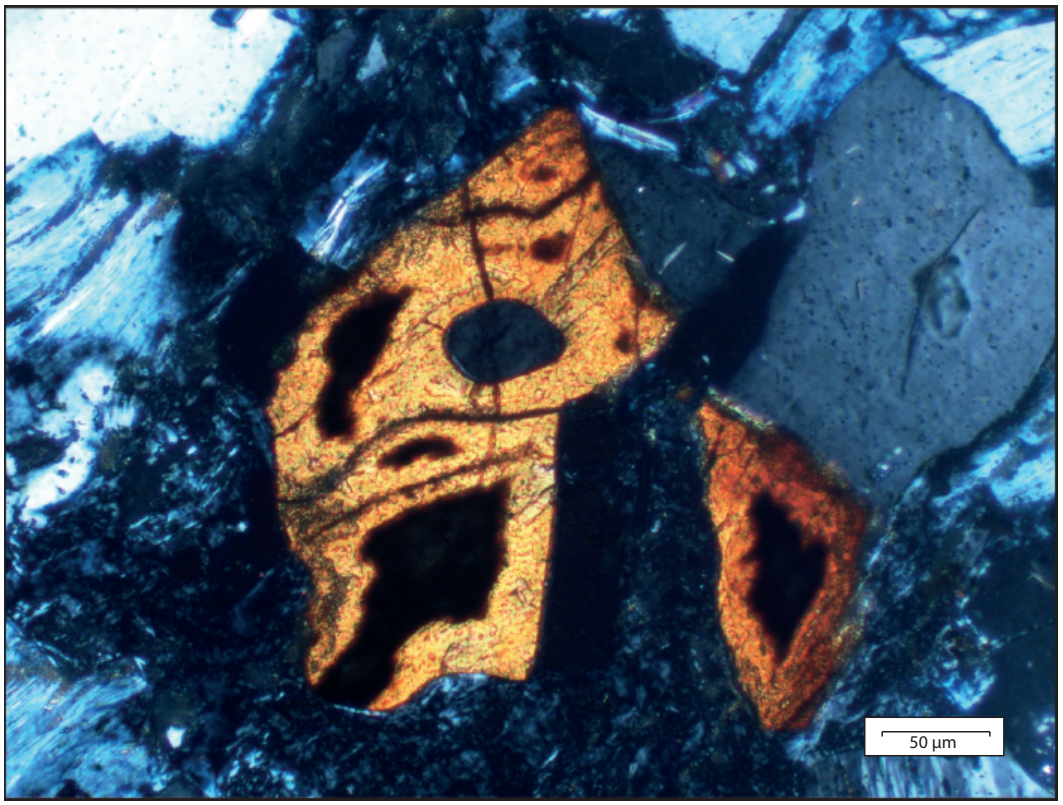

UNIVERSITY OF OSLO

FACULTY OF MATHEMATICS AND NATURAL SCIENCES

Granite weathering, saprolitization and the formation of secondary clay particles, SW Bornholm

Nikolas Oberhardt

Master Thesis in Geosciences

Discipline: Geology

Department of Geosciences

Faculty of Mathematics and Natural Sciences

University of Oslo

June 28th, 2013

Tutor(s): Prof. Henning Dypvik and Lars Riber, UIO

This work is published digitally through DUO – Digitale Utgivelser ved UiO

http://www.duo.uio.no

It is also catalogued in BIBSYS (http://www.bibsys.no/english)

To Konrad

Abstract

In situ weathering of the Mesoproterozoic, hornblende- and biotite-rich Rønne granite at Nygård kaolin pit provides a well preserved, Jurassic to Early Cretaceous saprolite section on Bornholm. Fresh Rønne granite could be sampled in the approximately 800 m distant granite quarry at Klippeløkken. This study comprises petrographical and mineralogical thin section-, XRD- and SEM- analysis to distinguish the mode of primary mineral dissolution and secondary clay mineral precipitation in the weathering profile. These analysis are based on sedimentary logging, regular interval sampling, gamma ray- and fracture/joint measurements in five weathering profiles at the inactive Nygård kaolin pit. The weathering classification of saprolitic lithology has been conducted according five facies, from fresh rock to highly weathered, friable soil. The weathering sequence has been interpreted based on the mineralogical and petrographical analysis. Specific clay mineral abundance of kaolinite>>>chlorite>>smectite>illite studied in the weathering profile have been used to interpret the depositional environment of the succession.

Three main generations of weathering could be determined accordingly, 1. subaerial weathering, where original plagioclase feldspar, hornblende and biotite was dissolved and illite, smectite, illite/smectite mixed-layers and kaolinite clay minerals were formed during Early- to Late Jurassic. 2. Mineral formations during burial of the profile, are associated with the precipitation of carbonate concretions, foremost siderite, and authigenic chlorite in ?Late Jurassic to Early Cretaceous. 3. Post-burial mineral reactions are mostly associated with oxidation conditions during seasonal changing groundwater percolation and the precipitation of hematite. Re-exposure and erosion of the overlying Rabekke Formation is suggested of Late Cretaceous to Early Cenozoic time. Transpressional tectonics have led to fault reactivation and obduction of the southeastern margin of Bornholm.

Corestone associations in the weathering section are well preserved and fracture/joint measurements revealed comparable strike directions with the adjacent granite quarry at Klippeløkken, suggesting only little to none tectonic impact between the two study localities. Tectonic stability, relatively low relief and prevailing humid and tropical climatic conditions can be addressed as driving parameters for the argillization of thick kaolinite deposits during the Mid Mesozoic on Bornholm.

The acquired results of this master thesis are used as comparison with other localities. An example of similar paleo-chemical weathering can be found at Ivö Klack (southern Sweden) also constituted by thick kaolinite deposits in the upper profile. In contrary, a recent weathering profile formed under more temperate arid conditions in NW Portugal displays arenization and kaolinite is replaced by gibbsite.

As part of the Utsira Project, a collaboration of the University of Oslo and Lundin Petroleum AS, it was the main focus of this study to provide lateral information of onshore weathering profiles, that may be used as comparison to marine weathering successions found in two drill cores from the Johan Svedrups field and the Edvard Grieg field in the North Sea.

Contents

1 Introduction

1.1 Background

The deep, in situ weathering profile at the Nygård kaolin pit, also referred to as Rabekke or Rabekkeværket clay pit (Gry, 1956, 1960; Gravesen et al., 1982), is located northwest of the town Rønne on Bornholm (Figure 1.1). Only a sparse saprolite section of 30 m length and 5m height remained accessible along the margin of the formerly kaolin pit, which currently is drowned by a lake of oozing groundwater (Figure 1.5). Active quarrying of the high-purity kaolinite was conducted by the Danish company *A/S Hasle Klinker- og Chamottestensfabrik* until the early 1990's. Ever since the quarry was left to the process of renaturation.

This research is part of the Utsira project "Petrography and porosity developments in reservoir formations on the Utsira High, importance of provenance, weathering vs. diagenesis" a cooperation between *Lundin Petroleum AS* and the *University of Oslo (UIO)*. Project chairman at the *University of Oslo* and supervisor for this thesis is Prof.Henning Dypvik. The "Utsira working group" further consists of Phd student Lars Riber (*UIO / Lundin AS*) who contributes as co-supervisor for three Master candidate members.

Observations of two drill cores from the Utsira High, in particular from the Edvard Grieg and Johan Svedrup field in the North Sea revealed the presence of thick in situ weathering crusts, which may have served as petroleum migration pathways and/or reservoir rocks. The Utsira High demarcates an intra-basinal, structural high forming the eastern flank of the Viking Graben (Laursen et al., 1995). The restrictive analytical ability to study highly 3-dimensional, heterogeneous weathering profiles only in vertical manner and by drill core correlation, was cause to quest for possible onshore analogues. Prospective localities to observe lateral trends and detailed mineralogical behavior within multiple, adjacent profiles in a coalescent weathering succession were found in Bornholm and southern Sweden [1]. This master thesis will elucidate the formation and weathering sequence of secondary clay minerals at the Nygård kaolin pit, derived from a granitoid parent rock.

[1] The onshore locality at Ivö Klack (southern Sweden), is used as comparison in the discussion chapter, further details are given in the master thesis of (Naqvi, 2013)

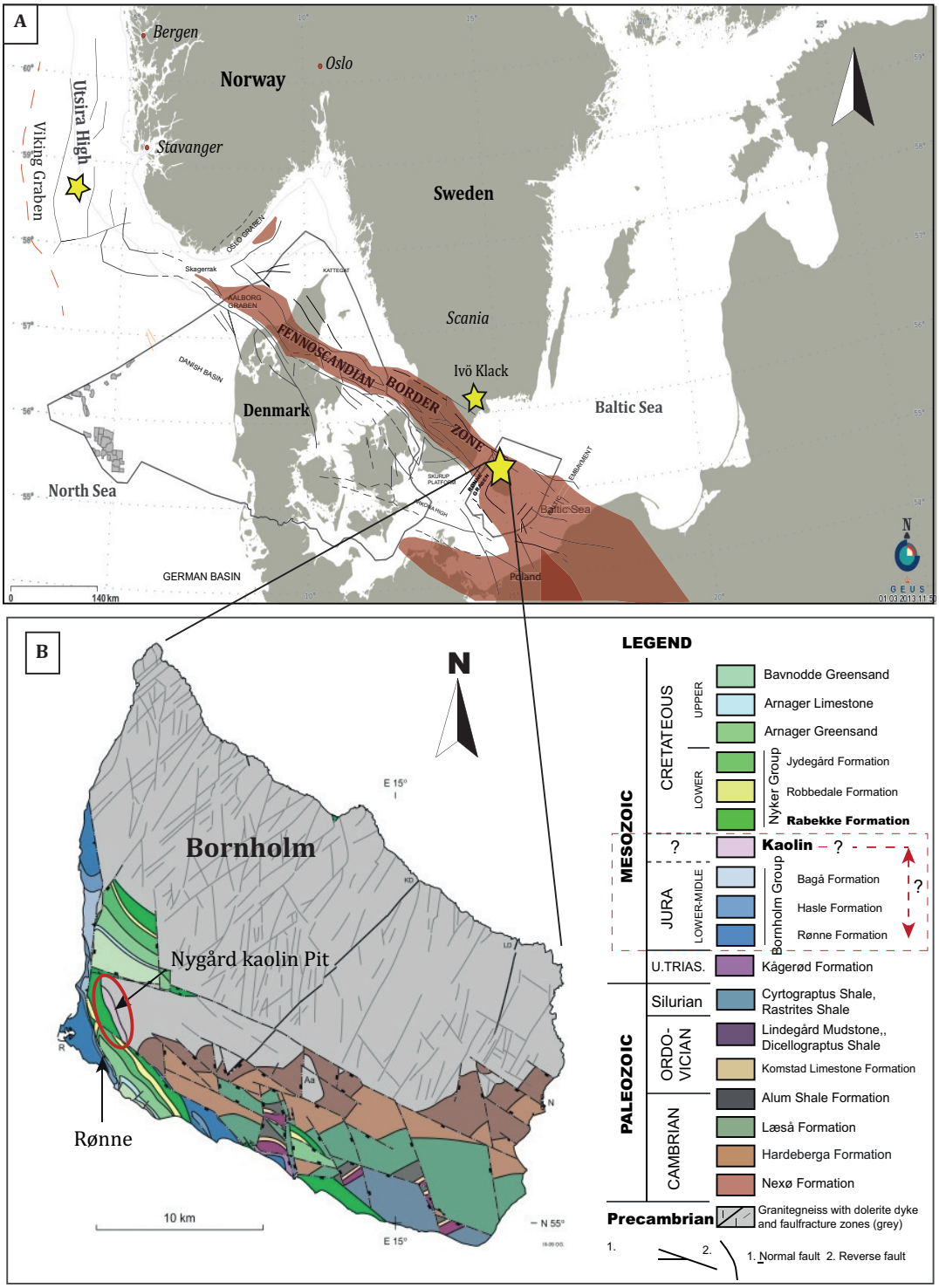

Figure 1.1: a) Map showing the study areas of the Utsira project group (UIO). Field localities are marked by stars. The principal structural units of the Fennoscandinavian Border Zone (Tornquist Zone) are displayed in transparent red color (modified after http://geuskort.geus.dk (2013) and Liboriussen et al. (1987)). b) Detailed map of Bornholm showing main geological units, the study area is marked by a red circle. The mosaic tectonic pattern and principal startigraphic column are illustrated, red dashed square marks the anticipated time range of weathering (modified from Graversen (2004))

This master thesis is based on sedimentological field mapping, sampling and the petrographical analysis of the saprolized, Paleozoic 'Rønne Granite' at the Bornholm onshore locality. The unweathered Rønne granite could be observed at two granite quarries in close vicinity of the weathering site. First, Bornholm's oldest granite quarry *Klippeløkken* located about 800 m north-east of the Nygård kaolin pit, where industrial quarrying of Rønne granite has been carried out since 1821 and second at the *Stubbegård* quarry approximately 1.5 km south-east of the study site (Figure 1.5).

1.1.1 Field locality Nygård kaolin pit

The observation site at the Nygård kaolin pit is situated at 55.10917°N latitude and 14.72798°E longitude, approximately 17 m above sea level. Bondam (1967) described that sole primary kaolin deposits spread about 3 km from Almegård north of the study site, to Kanegård in the south and show no more than 550 m lateral expansion (Figure 1.2). Strong thickness variations of the clay layer with a maximum value of about 30 m were also described by Bondam (1967). The saprolite kaolin deposit is seated directly upon dark, feldspar-rich granite, which constitutes the source rock for residual weathering. The weathering profile is partly covered by the Early Cretaceous sedimentary succession of the Rabekke formation (Gry, 1956, 1960).

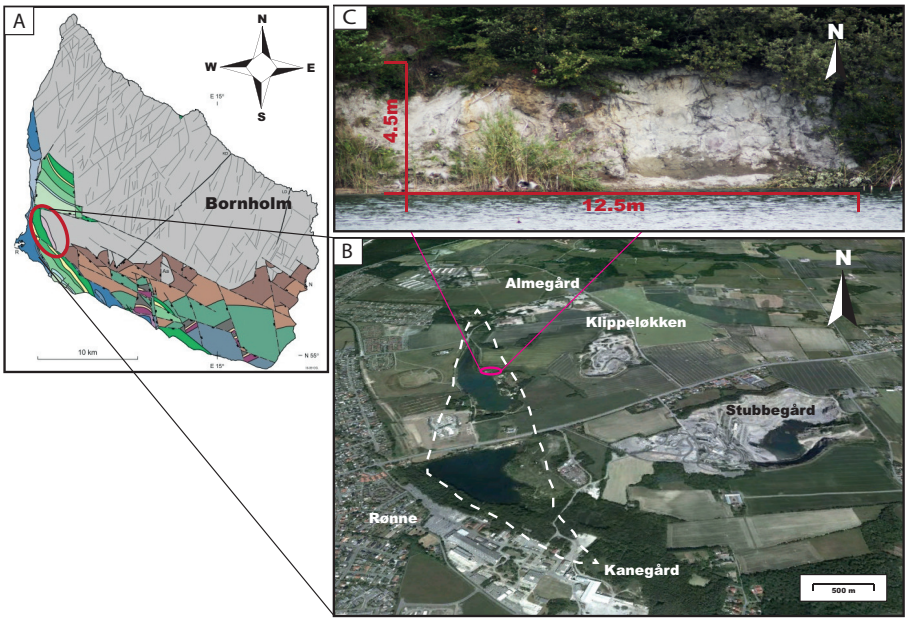

Figure 1.2: a) Outline of Bornholm and main geological units (for details see Figure 1.1), red circle marks the kaolin unit north-east of Rønne (modified from Graversen (2010)). b) Aerial photography of study localities and areal expansion of the kaolinite deposit outlined by white dashed line. The small red ellipsoid designates the outcrop of the weathering succession. Klippeløkken and Stubbegård granite quarries are displayed (modified from www.google.maps.com). c) represents the study site, at the northern hinge of the quarry pond (marked by the red ellipsoid) (Photo: Lars Riber (UIO))

The Rabekke Formation was first described and established by Gry (1956). Gravesen et al. (1982) denoted the formation as poorly sorted, fluviatile, medium to coarse grained, ferruginous sandstone, where kaolinitic, unconsolidated sand may interfere with mixed clay mineral associations. Gravesen et al. (1982) further stated that organic material is abundant and sideritic concretions could be observed frequently. Graff-Petersen and Bondam (1963) described the lower boundary of the Rabekke Formation observed at the Nygård kaolin pit as a "gradual contact" between the kaolinitic saprolite and the coastal-marine deposit. The Rabekke Formation as part of the Nyker Group could be distinguished over wide exposure, where the Nyker blocks are present (see Figure 1.3 and Figure 1.1) (Gravesen et al., 1982). Medium- to coarse-grained fluviatile sands of the lower Homanshald Member were observed in the Arnager-Sose block, resting uncomformably upon shoreline marine sandstones of the lower Jurassic Hasle Formation (Lindgren et al., 2008). Ostracods found in carbonaceous clays and silts of the upper Skyttegård Member indicate Lower-Upper? Berriasian age (Dörhöfer and Norris, 1977; Surlyk, 1980). The Paeleoecology of theropod dinosaur teeth discussed by Lindgren et al. (2008) suggest coastal plain, lagoonal, shallow marine to fresh water lacustrine environments during the Early Berriasian age for the studied fossil assemblage of the Skyttegård Member. The lower Homanshald Member was suggested to be of similar age, but a Tithonian origin can not be excluded, due to the low excess ability (Gravesen et al., 1982).

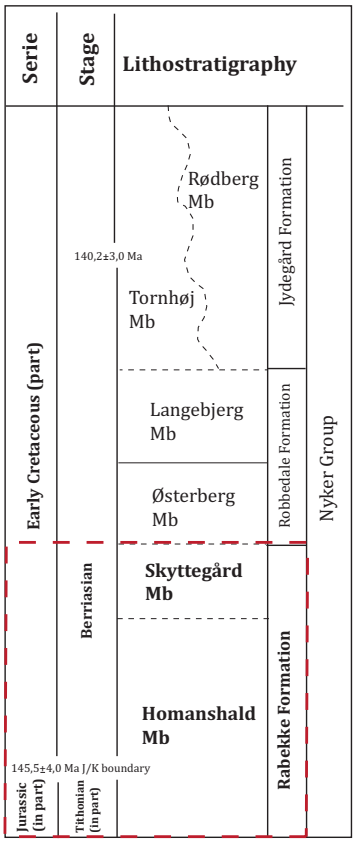

Figure 1.3: Lithostratigraphy of the Early Cretaceous, Bornholm. The red dashed square illustrates the discussed Rabekke Formation (modified after Gravesen et al. (1982); Petersen et al. (1996)).

1.1.2 Study objectives

The formation of clay sedimentary particles, with particular emphasis on the precipitation of kaolinite, at the Nygård kaolin pit is not clearly resolved in relation to the chronological classification of the weathering profile devlopement. Primarily exposure and weathering of crystalline bedrock at Nygård kaolin pit is suggested to be older than Late Jurassic- Early Cretaceous age. Due to the tropical and humid paleoclimatic conditions (Figure 1.8) prevailing during the most of the Mid-Mesozoic in southern Fennoscandia, it is suggested, that the

overlaying Rabekke Formation marks the upper age limit for the saprolite succession at the Nygård kaolin pit (Gravesen et al., 1996).

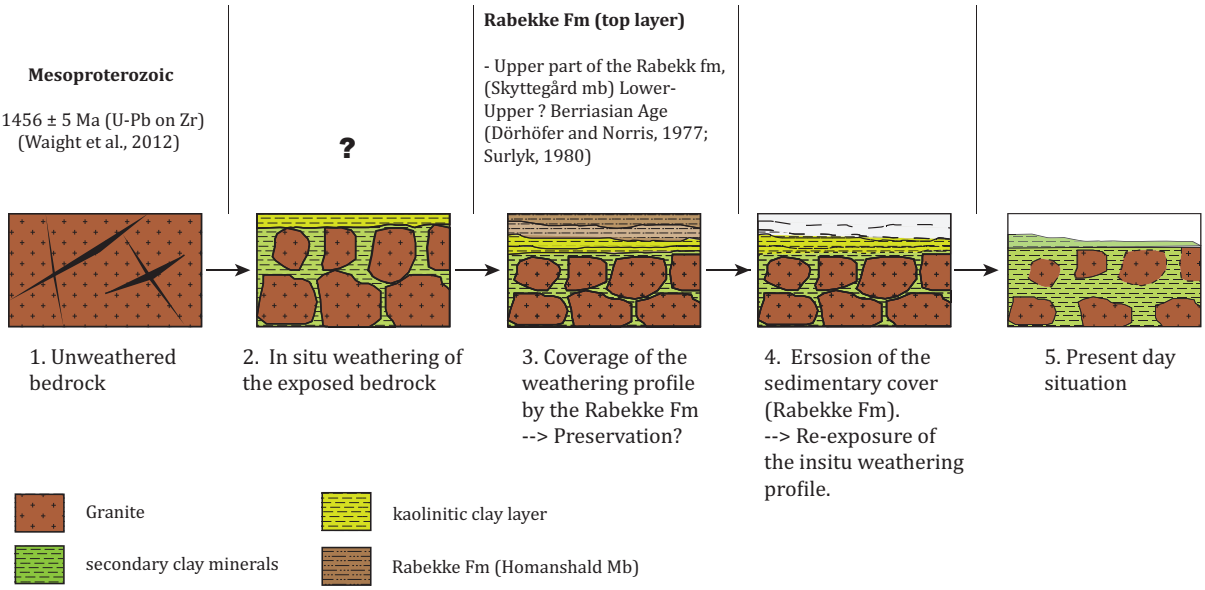

Figure 1.4: Simplified development of the weathering profile from unweathered Proterozoic bedrock to saprolite at the present display.

Burial and congruent coverage of the succession by podzolization processes and/or the near shore to lacustrine deposits of the Rabekke Formation (Graversen, 2004), may have led to the preservation of the weathering profile during Late Jurassic-Early Cretaceous. Recurrent obduction due to Late Cretaceous-Early Cenozoic fault reactivation tectonics along the western margin of the island led to partial erosion of Mesozoic sediments and may have induced the re-exposure of the weathering profile at Nygård (Gry, 1969; Gravesen et al., 1982; Liboriussen et al., 1987; Michelsen and Nielsen, 1991, 1993). Figure 1.4 attemps to display the general development in five steps. The regional tectonics, the paleoclimate, such as the measurable petrographical parameters resulting in the present succession, will be described and discussed comprehensively in this master thesis.

1.2 Previous work

First geological descriptions of primary kaolin deposits at Nygård were conducted by Graff-Petersen and Bondam (1963). Figure 1.5 illustrates the kaolin pit at Nygård during active quarrying and displays the areal exposure of the kaolin deposit. The areal exposure of the clay formation and a generalized profile section (Figure 1.6) through the Nygård clay pit could be established and the basic lithological characterization was conducted. Two principal clay horizons could be distinguished by the aid of XRD-bulk analysis: 1. the lower

Figure 1.5: Aerial photos of the study area, left picture taken in 1992 (Gravesen et al., 1996), right image show the present conditions of the drowned quarry pond (www.google.earth.com) (1). *1. Nygård Kaolin Pit, 2. Klippeløkken Granite Quarry and 3. Rønne Granitverket at Stubbegård*

"inhomogeneous" siliceous clays and 2. the upper multicolored clay layer with slightly higher mica content. The results of these observations indicated relatively short distance transportation and mineral reactions from siliceous corse grained sediments towards fine-grained micaceous sediments within cm range. Graff-Petersen and Bondam (1963) concluded, that " the final contribution of clay mineral to the sediment has been derived from weathered granites or granodiorites [...] with fairly high iron content".

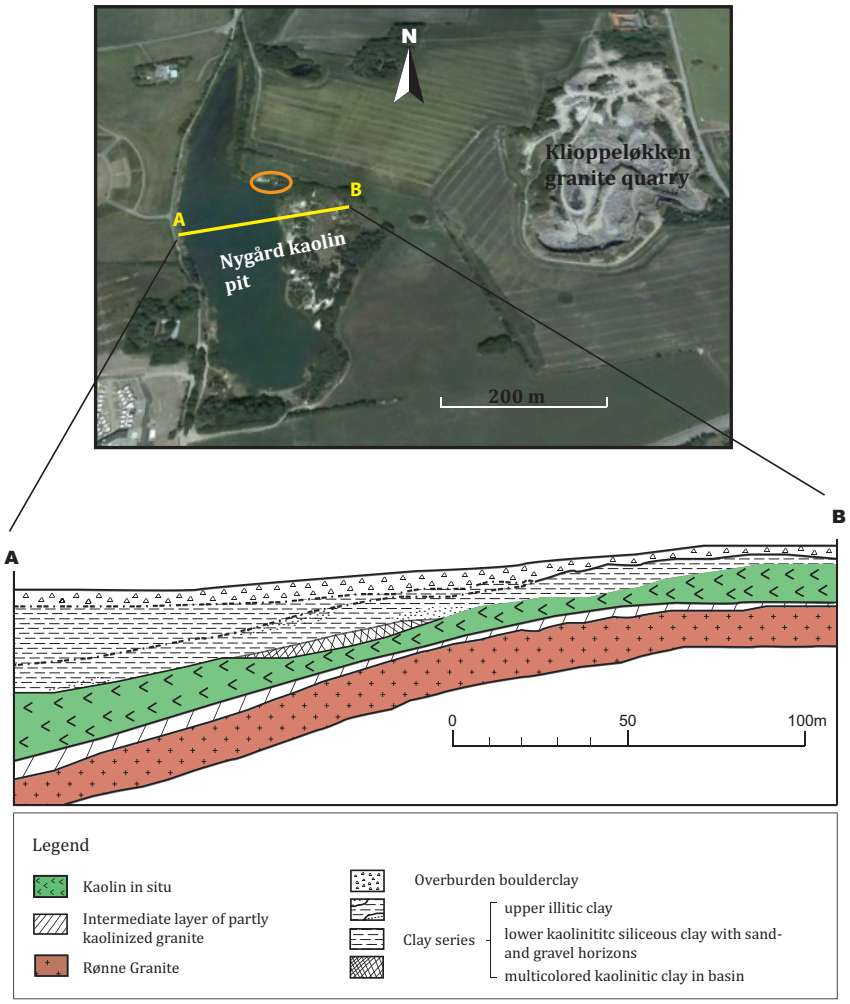

Figure 1.6: Aerial photo of the study location (modified after www.maps.google.com). Small orange circle marks the position of the observed weathering profile. Cross section A to B marks the approximate position of the profile established by Graff-Petersen and Bondam (1963). The section through the Nygård clay pit is illustrated below (modified from Graff-Petersen and Bondam (1963)).

Bondam (1967) returned to perform detailed geochemical analysis on the granitic source rock and on the "spectrum" of weathering residuals [2] at the Nygård clay pit. Chemical analysis was performed with emphasis on relative element distributions of oxides and the immobile

[2]Weathering residuals could be studied from the exposed underlaying bedrock to the overlying Rabekke Formation, which in the purpose of this thesis was not possible due to the oozed quarry pond.

aluminum phases. Different aspects of paragenesis or neo-genesis of secondary clay mineral phases, comprised the main focus of this work. Particular emphasis of this work was the evaluation and application of ion mobilization within the weathered section at Nygård.

Two main results could be studied by Bondam (1967) through geochemical analysis at Nygård: 1. a "paragenesis characterized by the occurrence of small amounts of calcite [...] resulting in the extension of the stability field of potash-feldspar in the residual rocks [...] which favors the formation of illites in these residuals" and 2. a "paragenesis is free of calcite [...] comprising kaolins which are practically devoid of illites." [3]. A rather general decription of the outcrop by Bondam (1984) was followed by a consolidation of the formerly established geochemical analysis in Bondam and Störr (1988). SEM and TEM observations were added and minor scale transformation reactions of the leaching conditions within the transitions zone from granite to residual weathering product were studied.

1.3 Geological setting

1.3.1 Bornholm and the structural geology of the Fennoscandian Border Zone

Bornholm is an island in the Baltic Sea, located within the Danish-Polish Furrow (Figure 1.7). The island represents the uplifted horst block of a complex intercontinental fault zone, the composited Tornquist zone, also referred to as the Fennoscandian Border Zone (Fig.1a) (Sorgenfrei and Buch, 1964; Baartman and Christensen, 1975; Liboriussen et al., 1987; Graversen, 2010). This zone defines the border between the stable Fennoscandian-Baltic Shield and the metastable Danish-Polish Trough (Liboriussen et al., 1987).

The Tornquist Zone is composited of two main segments (Figure 1.7), the Sorgenfrei-Tornquist Zone located to the north-west and the the Teisseyre-Tornquist zone to the south-east (EUGENO-S, 1988; Berthelsen, 1998).

Due to structural and tectonic differences it was suggested to subdivide the Sorgenfrei-Tornquist Zone into the Skagerak-Kattegat segment, which confines a stable, more elevated platform to the north-west and the Bornholm-Skåne segment, representing a rather compression dominated block faulted structure to the south-east (Sorgenfrei and Buch, 1964; EUGENO-S, 1988; Michelsen and Nielsen, 1991, 1993).

Along the western margin of the island Bornholm the Rønne Graben is situated, a smaller pull-apart basin located within the Bornholm fault complex. This right lateral, wrench faulted graben formed in Late Carboniferous- Early Permian time (Graversen, 2010). The graben structure cuts approximately perpendicular from NE-SW through the regional NW-SE trend of

[3]Bondam (1967) appears in Danish language, followed in Bondam (1968) by the English publication.

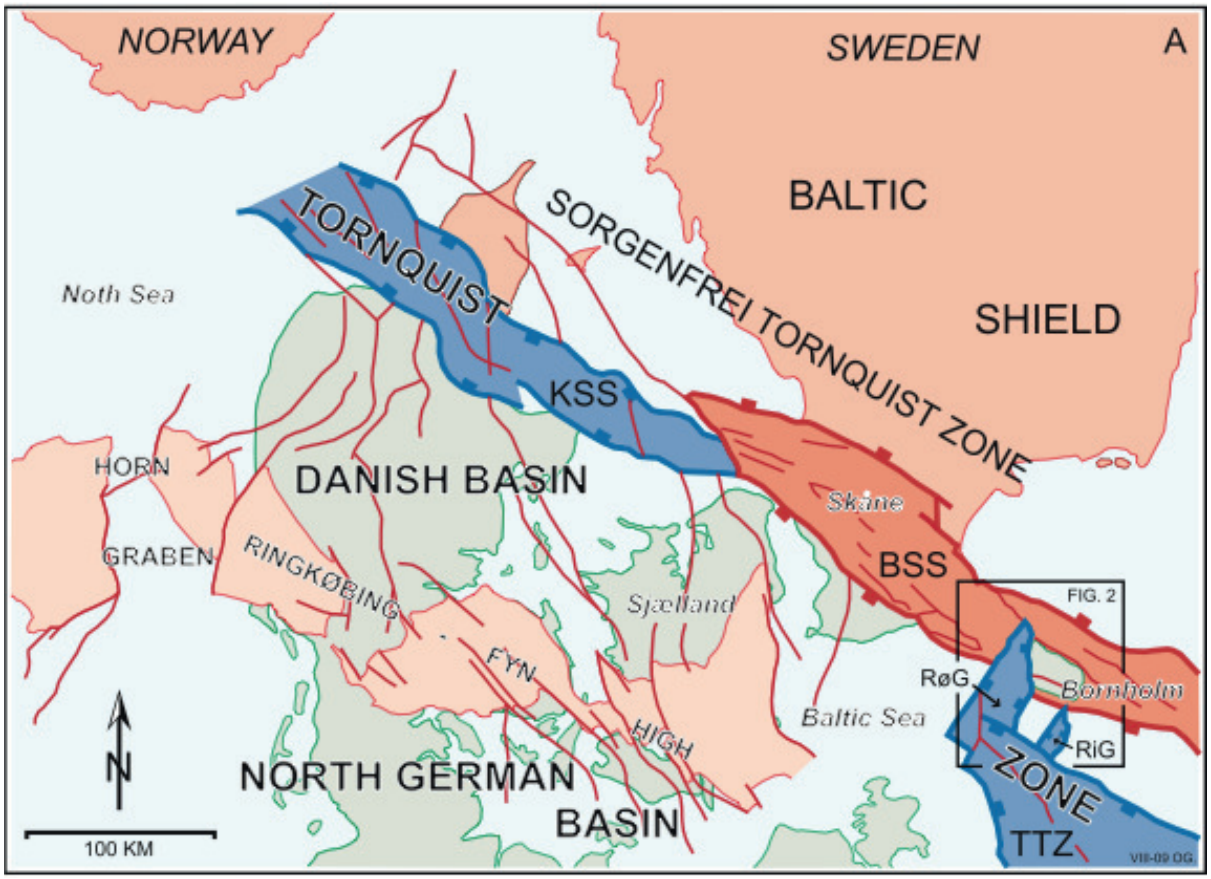

Figure 1.7: Structure map representing the main segments of the Sorgenfrei-Tornquist Zone. KSS: Kattegat-Skagerak segment; BSS: Bornholm-Skåne segment; TTZ: Teisseyre-Tornquist Zone (Graversen (2010))

the Sorgenfrei-Tornquist Zone and determines the converging zone of the Sorgenfrei-Tornquist segment (north-west) and the Teisseyre-Tornquist Zone (south-east) (Petersen et al., 2003; Vejbæk and Andersen, 2002; Liboriussen et al., 1987).

1.3.2 Paleotectonics and paleoclimate during the Mesozoic

To understand the mode and formation of deep chemical weathering crusts, it is necessary to elucidate the basic tectono-startigraphic setting and the paleoclimatic conditions in Fennoscandia during Pre-Tertiary.

Late Paleozoic-Mesozoic: Opening of the Danish-Polish Furrow, induced by early rifting movements along the Arctic-Atlantic Zone, resulted in strong transtensional stresses in the southern most Baltic Shield, triggering the formation of the Sorgenfrei-Tornquist Zone and the intracratonic Danish Basin (Pitman and Talwani, 1972).

This stage marks the early Pangean breakup, comprising the initial widening of the Baltic Shied and the early formation of fault block structures along with the formation of in- and extrusive volcanic rocks (Petersen et al., 2003).

Triassic: During the Early Mesozoic, northern Europe was still dominated by the continental regime of Pangea. In Late Triassic to Early Jurassic, the breaking up of Pangea was accompanied by progressing subsidence and widening of the North-European basins, opening pathways for a marine transgression (Early Liassic) from the Tethys sea located in southeast. Formerly arid, continental conditions changed gradually to more humid climate, when seaways opened their path into the Pangean interior (Ahlberg et al., 2003). During the Triassic, southern Sweden was situated at about 35° N and drifted approximately to 50° N during the Mesozoic (Lidmar-Bergström, 1983).

Jurassic: The transition from Triassic to the Jurassic was dominated by the Early Kimmerian tectonic phase (Norling and Bergström, 1987). Bölau (1973) suggested, that the progressive fragmentation of Northwest Europe, due to the development of the rift movement, originated in the Paleozoic Variscian-orogeny with its acme by the end of the Jurassic. During the Jurassic, the Central North Sea Graben, such as the Danish- Polish Furrow developed into the dominant fracture zones in the Alpine foreland (Lidmar-Bergström, 1983). In general, tectonic movements along the Fennoscandian border zone actively controlled deposition and erosion, leaving different patterns of continuous sedimentary successions and hiati in different tectonic blocks (Ahlberg et al., 2003). During the Early Jurassic, southern Sweden was still situated at 35 ° N slowly moving towards 40 ° N during Middle and Late Jurassic. Brinkmann and Sanders (1969); Störr and Bellmann (1975) suggest a climatic shift from humid to drier conditions during the Late Jurassic, due to the gradual break up of Pangea and northward rifting of Fennoscandia.

Cretaceous: The rifting of the Arctic- North Atlantic continued during Cretaceous times (Pitman and Talwani, 1972). The first inversion tectonics can be recognized in the Central European marginal troughs, resulting in significant erosion of the former depositional troughs (Ahlberg et al., 2003). In the Danish-Polish trough the compressional inversion tectonics died out in Scania. The Upper Cretaceous successions are dominated by a worldwide transgression, which led to a climate stabilization, caused by an increase in the ratio of oceanic to continental area (Hays and Pitman, 1973). Paleo sea-level observations of Kominz et al. (2008) suggest a maximum Campanian transgression of 75-100 m above recent sea-level.

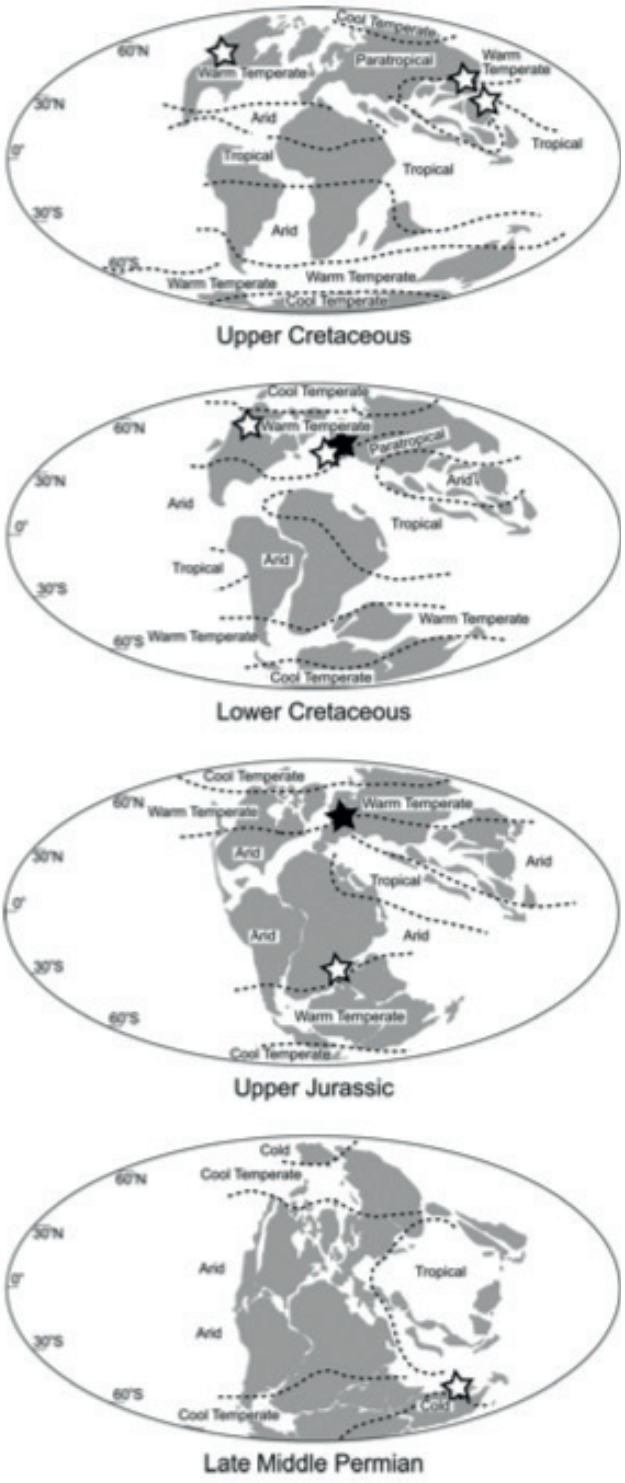

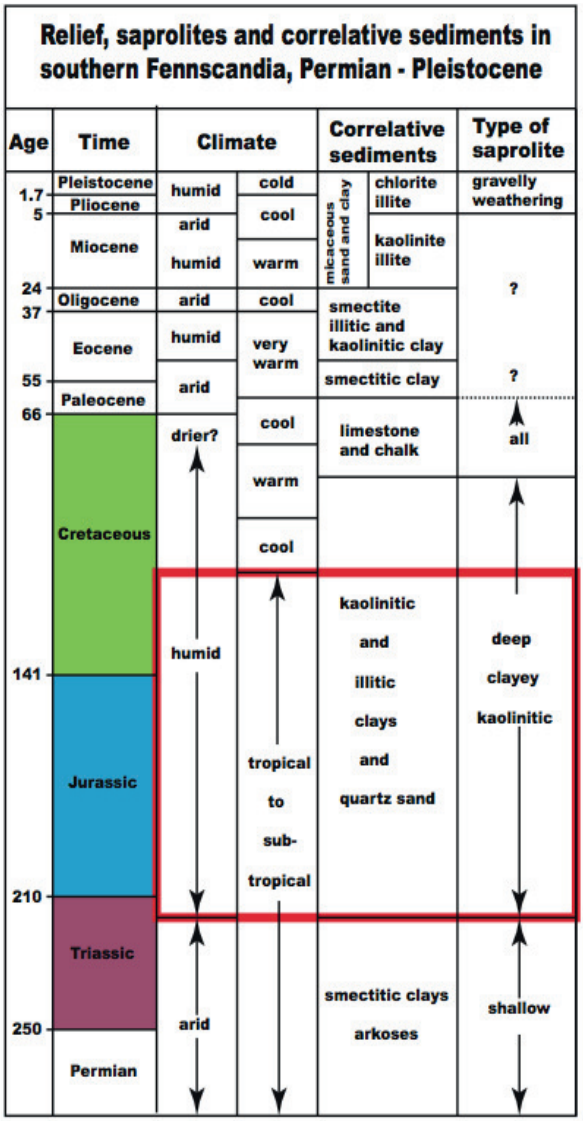

Figure 1.8: Summary figure for the paleotectonical and paleoclimatical development during the Mesozoic. The red marked area shows humid, tropical climatic conditions, during kaolinitization in Fennoscandinavia is thought to occur (modified after Scotese (2002) and Lidmar-Bergström (1983))

1.4 Weathering

Weathering can be defined as the change in degree of consolidation and composition of a rock mass by the action of atmospheric and hydrospheric agencies (Jackson and Sherman, 1953). Ollier et al. (1984) defined the process of weathering as the breakdown and alteration of materials at the Earth′s surface to products that are more in equilibrium with newly imposed physico- chemical conditions. Three major modes of weathering can be determined, 1. physical weathering, involving the unconsolidation of consolidated rock through mechanical decomposition by retaining their original mineralogy and 2. chemical weathering leading to a change in the chemical composition of the rock assemblage through mineral reactions. The 3. mode includes the disintegration of rocks by plant growth, animals and particular bacterias, which play an extremely important role in the processing of soils, gathered under the term of biotic weathering (Ollier et al., 1984). Changes in rock composition, caused by deuteric mineral reactions in igneous rocks directly after their crystallization and hydrothermal agencies are termed ”alteration” (Jackson and Sherman, 1953).

1.4.1 Weathering of granite

Granite is a granular, phaneritic, intrusive (plutonic) igneous rock, generally consisting of three main mineral compartments.

1. **Feldspar**, which can be subdivided into the solid solution series of plagioclase between calcium-end member anorthite ($CaAl_2Si_2O_8$) and the sodium-end member albite ($NaAlSi_3O_8$) and the alkali-feldspar solid solution series between $NaAlSi_3O_8$ (albite) with one of the temperature dependent varieties of potassium-rich feldspars of $KAlSi_3O_8$ sanidine, orthoclase and microcline. [4]

2. **Quartz**, (SiO_2) which under low (acidic) pH-conditions constitutes as weathering inert phase.

3. **Mica**, which mainly is comprised of biotite ($K(Mg,Fe)_3(AlSi_3)O_{10}(OH)_4$) and muscovite ($KAl_2(AlSi_3O_10)(OH)_2$).

Tectonically undisturbed intrusions of massive character, normally display no defined orientation pattern or internal structures (Ollier et al., 1984). Undisturbed bedrock formations with no tectonic history or dislocations due to cooling are very sparse to non-existing, therefore fractures and joints are most common within these rock types. Velde et al. (1991) and Turcotte

[4] Named in decreasing temperature depended order.

(1986) stated that the formation of fractures and joints in granitic rocks follow a ”fractal-manner” which could be observed on many different scales. The fracture pattern in crystalline rock, often reflect fracture angles of 60°and 120°(see Figure 1.9). This fracture pattern is the direct response to main forces and their stress directions acting on the bedrock. The joints and fractures control the rate and the depth of weathering, allowing meteoric fluids to access the bedrock and thereby increasing the rate of in situ chemical weathering and mineral reactions (Ollier et al., 1996). Ollier et al. (1996) further stated, that the presence of biotite is extremely important, because biotite appears to be a ′weak link′ in the weathering process and therefore a major parameter for the weathering intensity. Biotite-rich fractured granites and granodiorites tend to weather deeply, by deeper water circulation in joints and enhanced mineral reactions of the mica fraction (Ollier et al., 1996).

1.4.2 The formation of weathering crusts

The formation of thick weathering crusts, depends on the following essential parameters, according to Petrov (1967); Störr and Bellmann (1975):

- A period of tectonic stability that enables intensive, undisturbed chemical weathering.
- Tropical to moderate humid climate, that assure the presence of precipitating water for dissolved ion transport.
- Source rock mineralogy of solvent primary minerals, such as plagioclase, mica or hornblende as weathering unstable mineral phases must be present in combination with joint and fracture systems allowing fluid drainage through the profile.
- Drainage capacity and vertical conductivity controls the qualitative precipitation of secondary mineral phases.

1.4.2.1 Types of weathering crusts

The use and definition of weathering products from a crystalline parent rock, have led to some confusion, therefore it is necessary to emblaze the terms further used in this work.

- A saprolite is defined as a soft and typically clay-rich rock, which usually is thoroughly decomposed. Saprolites are chemical weathering products, formed in place of igneous, metamorphic or sedimentary protoliths. They can be characterized according to the degree of preservation of rock structures from the unweathered parent rock. The formation of saprolitic covers is commonly associated with humid, tropical to subtropical climates (Bates and Jackson, 1987).

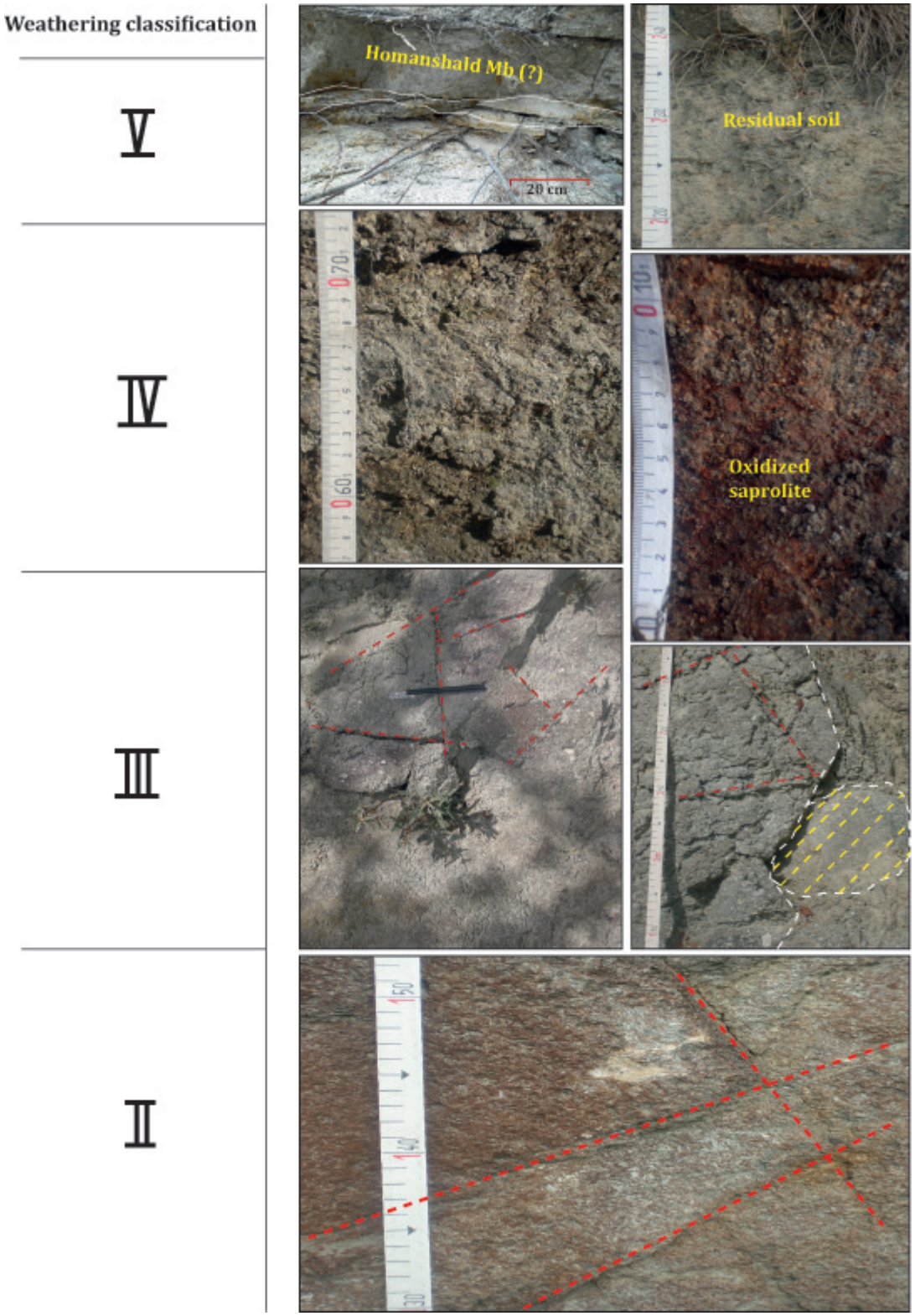

Figure 1.9: Saprolite formation, template displaying increasing degree of weathering from bottom to top, of random images from Nygård kaolin pit. Note that weathering facies I has been neglected in this image, photos of the fresh granite are included in the chapter results.

- In comparison to saprolites, regolith crusts do not preserve the internal structure of their weathering educt. It is used to describe the layer or mantel of fragmental and unconsolidated rock material, constituting the primer soil formation, which often was exposed to reworking processes. Regoliths can be formed in place or deposited after transport and might therefore include rock debris of fluvial, aeolian and biotic accumulations (Bates and Jackson, 1987)

- Laterites are among more controversive group of weathering products. Eggleton and Taylor (1998) postulated a more careful definition of the word laterite from ferricrete, which rather describes the transport bounded formation of ferrigeneous concrete, than the formation of hardened iron- or aluminum-rich weathering crusts. Laterites form under hot, tropical conditions and are characterized by their strong oxidation stain in color and confine in comparison to saprolithes more advanced denudation.

1.4.2.2 Spheroidal weathering, the formation of core-stones

The formation of spheroidal weathering in granite and other crystalline rocks is a highly discussed topic with many different suggested causes. Due to the chemical emphasis on mineral formation and the saprolitic nature of the weathered substrate in this thesis, focus will be put on the constant volume hypothesis for the formation of such structures. Granitic boulders can be observed to consist of completely rounded corestones, surrounded by thin concentric sheets or layers of rock (Ollier, 1971). These boulders, found in field, could easily be misjudged to be sedimentary derived, due to their spherical and rounded appearance. Corestones are formed in situ within tens to hundred of meters buried in the ground. It is commonly accepted, that the term of exfoliation is most suitable for the formation of sheet or layer-like weathering (Ollier, 1971).

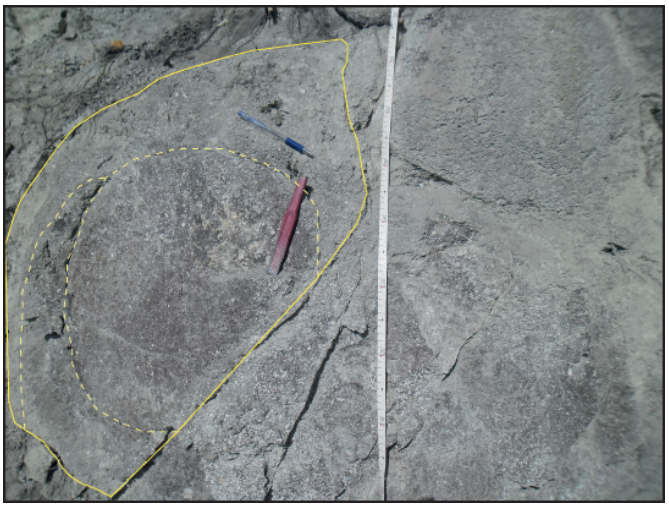

Figure 1.10: Rudimentary weathering rindlets (indicated by yellow lines) of the Rønne Granite at Klippeløkken granite quarry.

Ollier (1971) proposed that spheroidal weathering is caused by periodic chemical alteration under constant volume conditions. Inhomogeneity and fracturing of the bedrock, such as percolation pathways for weathering fluids may also be driving agents for the formation of corestones. The proposal of Ollier (1971) is especially considerable for saprolitic weathering of primary mineral phases, where the internal rock structure is often preserved. The preservation

of the original rock texture can be a sign for a nearly isovolumetric replacement by secondary minerals. Fritz and Ragland (1980) stated that the boundaries between concentric rindlet around the corestones are formed from coalescence of solution channels that tend to form parallel to the fresh rock contact. The solution channels are suggested to be formed by micro-cracks induced by residual stress released after erosion unloading (Ollier, 1971; Fritz and Ragland, 1980). Commonly accepted is the theory, that fracture sets in crystalline bedrock tend to form cubic- or block-like features of rock. Circulating fluids drain along the block surfaces and it seems likely, that the edges of these blocks are more affected by weathering than the block planes, which might contribute to the spherical formation of the corestones (Prasad and Sarracino, 1989).

1.4.3 Kaolinite weathering

Kaolinite weathering or kaolinitization of primary minerals of source rock confines the weathering under acidic to neutral pH-conditions. Predominantly alkali and alkaline earth‘s, such as Mg, Ca and K are dissolved and transported via pore fluids (see Figure 1.11). The dissolution of these elements lead to the relative accumulation of less mobile elements in the remaining mineral phases, such as Si, Fe, Al and Ti (Schmitz, 2008). Hereby secondary phases, like clay minerals (kaolinite), Fe- and Ti- oxides (i.e. hematite, rutile or ilmenite) and -hydroxides (i.e. goethite) are formed (compare Millot et al. (1970); Störr (1983); Meunier (2005)).

The kaolinitization model after Krumb (1998) displays the formation of thick kaolinitic layers with respect to the climatic conditions, vegetation, characteristics of the parent rock, processes of podsolisation, tectonic setting, such as the drainage capacity of the weathering rock and determines these factors as driving agents for specific chemical formation of kaolinite successions. According by the contact zone between fresh rock and weathered section, distinguished as saprock and saprolite in a intact weathering sequence, is dominated by three-layer silicates like smectite-, illite-rich clay minerals. This coincides with the observations made by Bondam (1967), who found increasing amounts of smectite with increasing depth at the Nygård locality. Above the greenish stained smectite- to illite-rich clay layers increasingly degraded kaolintic clay was found, displaying a shift in coloration with similar composition (Buchwald, 1971). With increasing height in the profile and prolonged weathering, three-layer silicates become increasingly unstable may degenerate into 1:1 kaolinite (Schmitz, 2008). Kaolinite foremost forms through recrystallization (neogenesis) as secondary mineral phase of dissolved original phases of plagioclase (anorthite ($CaAl_2Si_2O_8$) + albite ($NaAlSi_3O_8$)), potassic feldspar ($KAlSi_3O_8$) and biotite mica ($K(Mg,Fe)_3(AlSi_3)O_{10}(OH)_4$) (Nahon, 1991; Meunier, 2005). The formation of cation-rich clay minerals like smectite, vermiculite and mixed-layer minerals are associated with the initial stage of the kaolinitization, alongside the

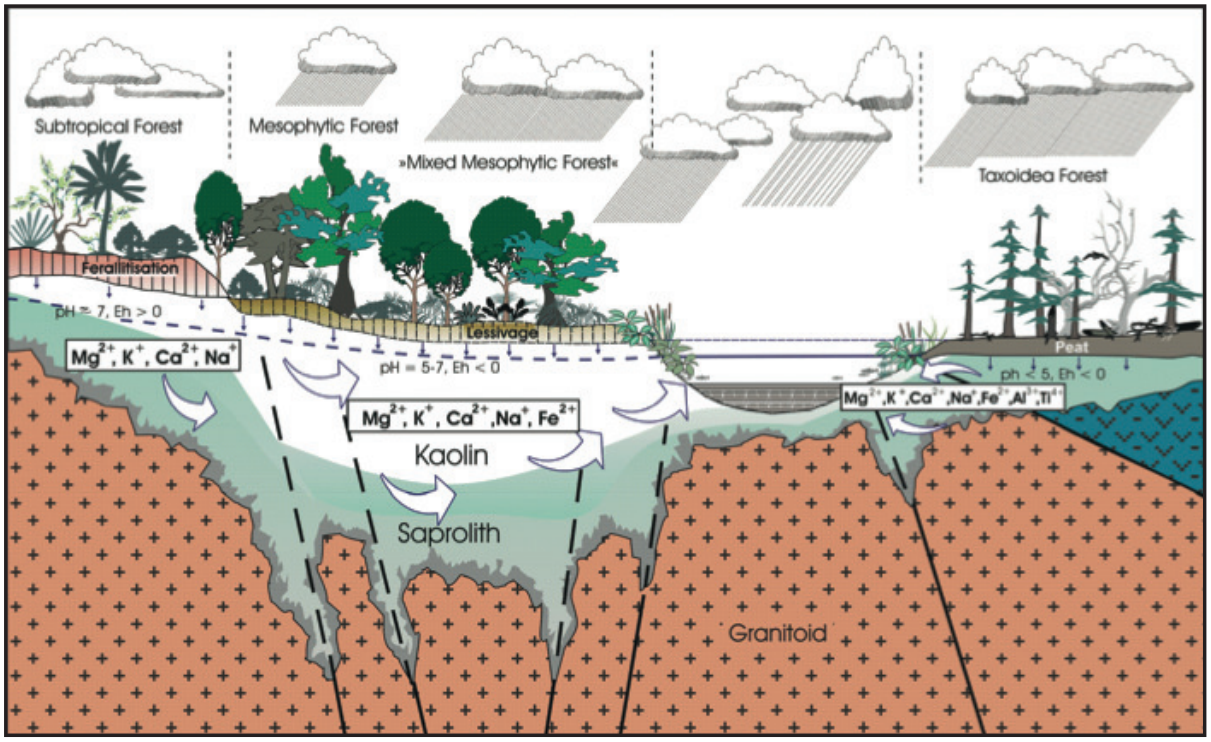

Figure 1.11: Simplified summary model of kaolinitization under subtropical to tropical, humid climatic conditions (after Krumb (1998))

layer silicate illite (Schmitz, 2008). With progressing weathering and increasing drainage conductivity, swelling clays like smectite become increasingly unstable, which leads to an enrichment of kaolinite and illite (Righi and Meunier, 1995). Kaolinite dominated clay mineral phases comprise, together with Ti- and Fe-oxides and hydroxides, residual quartz, accessory minerals like zircon and mineral relicts of the protolith the typical mineral associations of kaolinite zone (Heim, 1990). Very high drainage discharge of percolating fluids in tropical, humid conditions with extreme times of precipitation, may lead to the formation of thick latertic covers on top of the kaolinite zone, due to the enhanced solution of SiO_2 (Heim (1990) in Schmitz (2008)).

2 Methods

2.1 Fieldwork

Fieldwork at the Nyård Kaolin Pit (Figure 1.2a), was conducted from the 10 th to the 15 th of September 2012 [1]. Logging of the weathering profile, regular interval sampling and strike-slip measurements of preserved fracture sets, such as gamma-ray measurements have been performed in field.

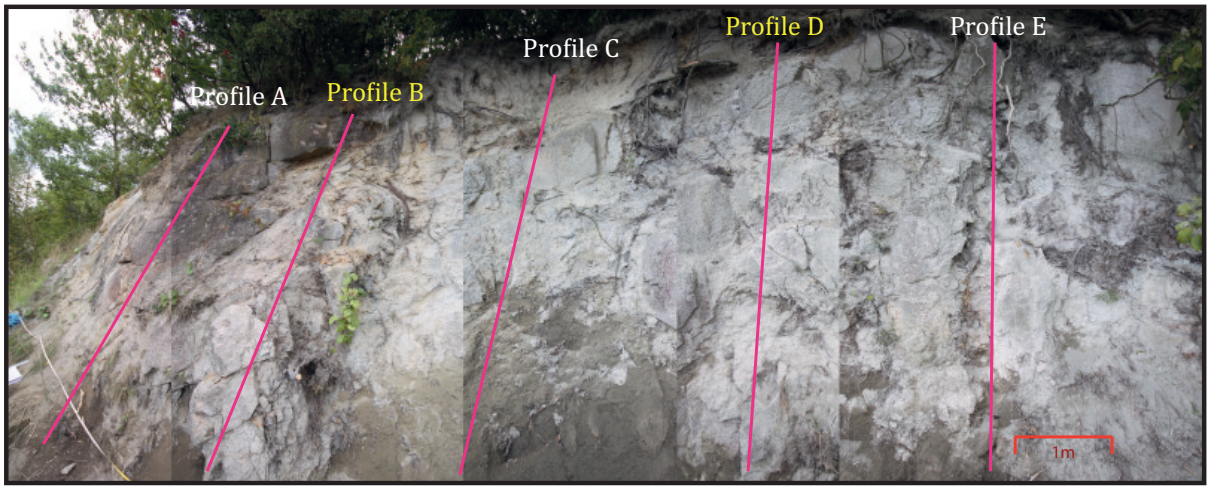

Figure 2.1: Close up mosaic image of the study section at the Nygård kaolin pit, illustrated with the five analysed profiles (for location in quarty compare with Figure 1.2 and Figure 1.6).

At the first approach, the study site was hard to access and plant overgrowth had to be removed carefully not to destroy the still preserved, but friable rock structure of the granitoid source rock in the saprolite around the corestones. Fine rootlets could be observed within the complete succession intruding in fractures and more soft parts of the profile.

The observed profiles were distinguished according the presence and frequent distribution of core-stones. Five sections were chosen and logged from bottom to top under sediment geological aspects, with respect to grain size, lithology, fracturing, color and friability of hand

[1] The author also attended the fieldwork at Ivö Klack from the 16 th to the 18 th of September 2012, the results of this locality are included into the discussion of this work and are presented in detail by (Naqvi, 2013).

specimen. These observations contributed to the macroscopical classification of weathering degree (given in roman numbers from I (fresh rock) to V (residual soil)) in field after Ollier et al. (1984) (see Figure 1.9).

Further, detailed sketches of each section, such as of the overall profile have been drawn in ratio 1:10 (1m=10 cm) (see Figure D.1 in the appendices). For the digitalization of the logs, it seemed most appropriate to combine the sedimentary logs and the section sketches, to provide the highest possible accuracy. In addition, detailed photographs of the study site have been included for the creation of the final logs, which are illustrated in the results chapter. The lower saprolite horizon is therefore displayed in sketch form, whereas the overlaying residual soil is displayed as sedimentary succession.

2.1.1 Sampling

155 samples out of 5 profiles (A-E) were collected from the weathered succession (Figure 2.1) and 2 samples (Q1-12 and Q2-12) of the fresh granite from the Klippeløkken quarry. The samples were extracted in regular intervals of 10 cm within each profile, to gain detailed information of small scale changes in lithology from less alternated corestones to friable saprolite and clay-rich residual material. The exact height of each section was determined by installing a fixed measuring band, which also provided a scale. In addition to the two unweathered samples from the granite quarry 31 samples (11 from profile B and D, such as 3 from profile A, C and E respectively) were chosen for detailed XRD, thin-section and SEM analysis. Sample Raf 3B-1985 was included, due to the lack of a sample of the almost pure kaolinite. The sample was collected in 1985 by Prof. Henning Dypvik (UIO). The samples were named e.g. AR1-12 to AR 28-12, where the prefix A marks the individual profile and the prefix R stands for the locality (Rabekke); the first number, e.g. 28 determines the sample number (the sample numbers up to 20 indicates the height from where the probe was taken in the specific profile, by multiplying the sample number times 10, e.g. no. 20 x 10 = 200 cm in the profile). The suffix -12 defines the year of sampling (2012), to assure that each sample provides distinct recognition.

2.1.2 Gamma Ray measurements

Gamma ray measurements were conducted by the aid of a hand-held scintillation detector (*Canberra SG-2P Radiagem 2000*). The device detects natural emitted gamma radiation from K, Th and U (according *Canberra Industies Inc.*, 2010).

The acquired measurements are given in counts per second (cps). γ-ray detection was performed at every height of each profile at the Nygård locality where samples have been extracted, hence in regular intervals of approximately 10 cm.

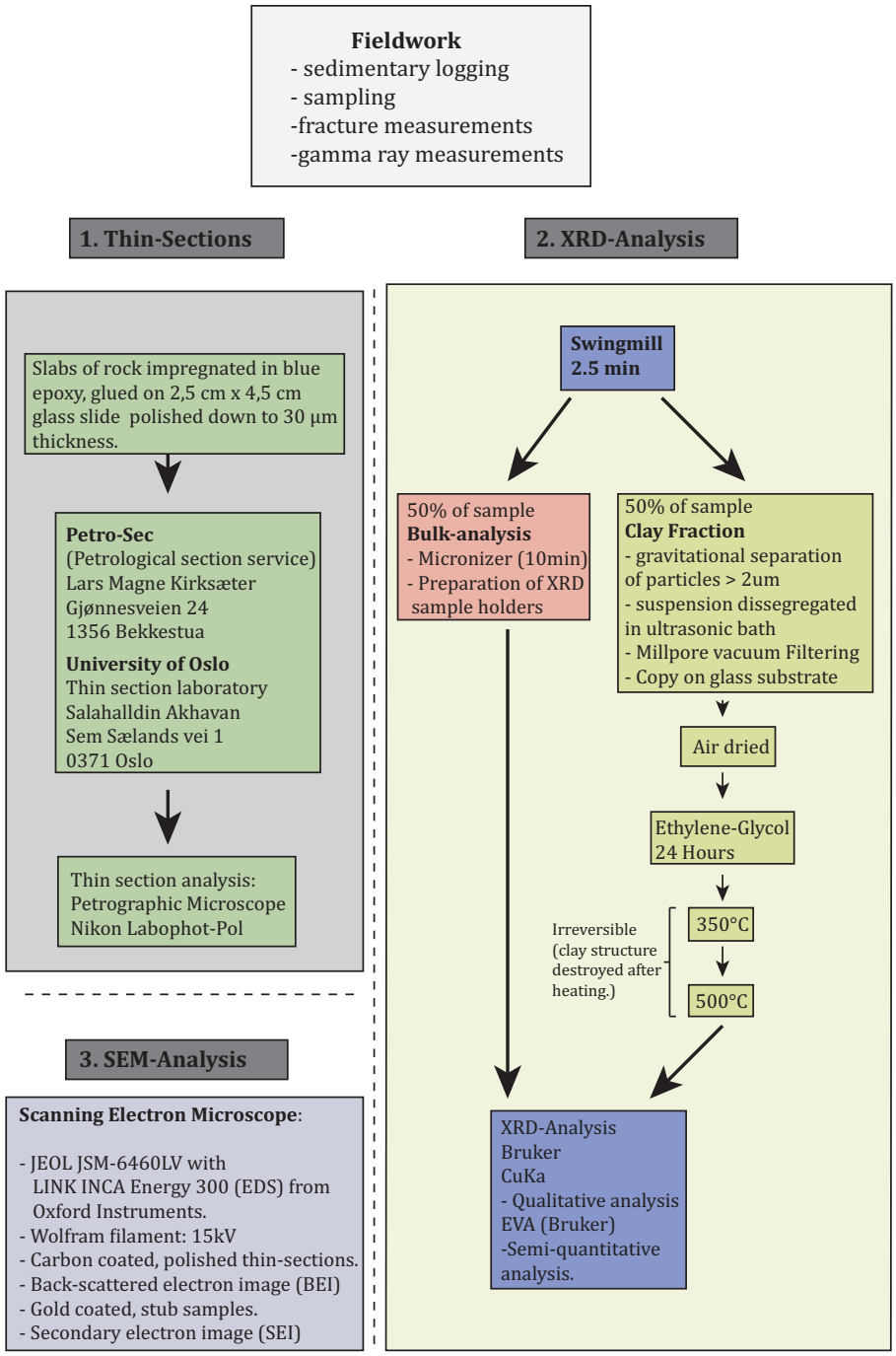

Figure 2.2: Methodology summary table.

2.2 Petrographical and mineralogical analysis

The petrological analysis of the weathered bedrock material at the Nygård kaolin pit, such as the fresh ”Rønne Granite” has been performed using microscopic thin-section observation, scanning electron microscopy (SEM) on selected samples of thin sections and stub samples

and X-ray diffractometry (XRD) of the bulk rock assemblage and the fraction $< 2\,\mu m$. The methodology of each analytical approach will be discussed in detail in this chapter. The used laboratory techniques and petrological analysis were conducted under the guidance and supervision of Prof. Henning Dypvik, Maarten Aerts (XRD, sediment laboratory), Berit Løken Berg (SEM, CL) and Lars Riber (UIO). A summary of all steps taken for the mineralogical and petrographical sample analysis is given at the end of the chapter (Figure 2.2).

2.2.1 Thin sections

Thin sections of selected samples (Table 2.1) were partly prepared by Lars Magne Kirksæter at the Petrological Section Service (Petro-Sec) and by Salahalldin Akhavan of the petro-technical department at the UIO. The rock samples were impregnated in blue epoxy, glued after drying onto 2.5 cm x 4.5 cm glass slides and then polished to a thickness of about $30\,\mu m$. The thin section analysis comprised detailed observation of 34 samples (according subsection samples). Results from this investigation are summarized in Figure B.1 to Figure B.3 in the appendices. For the analysis, a *Nikon Labophot-Pol* petrographic microscope has been used. The optical analysis has been conducted to elaborate particular mineral-mineral relations, qualitative determination of minerals, such as the quantitative distribution of original and secondary minerals in the samples in terms of finding an appropriate classification for the given weathering facies and to distinguish different crystal growth generations in the section. During the analytical work for this thesis, the petrographical microscope constituted a major role for the investigation of the samples. All thin sections have been studied under plain polarized light (ppl), to distinguish mineral characteristics, such as relief, isotropy and pleochroism. Cross polarized light (xpl) was used for the observation of zoning and twinning, the determination of birefringence color, such as the conoscopic image.

Little to no signs transportation was studied within the samples of the weathering profile (see chapter results fracture measurements) and the reworking of the weathering products appeared on minor scale according the optical analysis of thin sections. Therefore igneous characteristics were assumed for the microscopical observation of the slides and the analysis were carried out by means of their plutonic source rock.

2.2.1.1 Point counting of minerals

The mineral content was optically quantified in 20 representative samples (Table 2.1). 400 point counts have been conducted for each slide to estimate an allegoric average of the mineral content. The counting was conducted on a *Nikon Labophot-Pol* petrographic microscope, under plain polarized light (ppl) and cross polarized light (xpl), together with a *Swift Model F automatic point counter* with automatic top frame sample holder.

Table 2.1: Number of samples prepared for thin section analysis. Sections used for point counting are illustrated in bold font.

Thin section summary			
Thin section nr.	Sample	Thin section nr.	Sample
1)	AR 3-12	18)	**DR 3-12**
2)	AR 18-12	19)	**DR 7-12**
3)	AR 28-12	20)	**DR 9-12**
4)	**BR 1-12**	21)	**DR 10-12**
5)	**BR 2-12**	22)	**DR 13-12**
6)	**BR4-12**	23)	**DR 19-12**
7)	**BR 5-12**	24)	**DR 20-12**
8)	**BR 7-12**	25)	**DR 24-12**
9)	**BR 13-12**	26)	**DR 28-12**
10)	**BR 16-12**	27)	**DR 31-12**
11)	**BR 19-12**	28	**DR 37-12**
12)	**BR 21-12**	29)	ER 1-12
13)	**BR 23-12**	30)	ER 14-12
14)	**BR 28-12**	31)	ER 30-12
15)	CR 3-12	32)	**Q 1-12**
16)	CR 14-12	33)	**QR 2-12**
17)	CR 25-12	34)	**RaF 3B-1985**

2.2.2 Scanning Electron Microscopy (SEM)

The scanning electron microscope is used for surface morphological observation, such as the structural and chemical characterization of heterogeneous, organic and inorganic materials (Goldstein et al., 2003). Surface morphologies were studied of substrates glued on brass stubs, coated in gold, using secondary electron imaging (SEI), such as structural and chemical analysis of thin sections coated in carbon, using back scattered electron imaging (BSE) were observed in great detail, within nm to µm range. The analysis were conducted on a *JEOL JSM-6460LV*, with a *LINK INCA Energy 300 (EDS)* from the company *Oxford Instuments*.

The *JEOL JSM-6460 LV* is operating with an standard Wolfram filament (15 kV) and has detectors for secondary-electron images (SEI), backscattered electron image (BSE), cathodo-luminescence (CL), such as X-ray detectors for element determination and element mapping. For scanning electron microscopy a charged electron beam is induced by heating the wolfram filament ”shooting” the produced electrons on the analyzed specimen in a rectangular pattern. The electrically charged atom surfaces of the sample produces X-rays, back-scattering electron images (BSE) and secondary electron images (SEI) in interaction.

Back-scattering images (BSE) were used for thin section observations to analyze texture and composition of the compartments. Depending on density and electronic charge of the analyzed substrate backscattering images of heavy minerals, such as zircon or iron oxides in the samples revealed brighter images compared to other minerals, like quartz or feldspar, due to their higher reflectance capacity of electrons.

Secondary electron imaging (SEI) was used for three-dimensional, morphological analysis of mineral surfaces of stub samples coated in gold. Grain mount specimens glued on brass substrates reflect the incoming SE electron beam only from their outermost shell and thus have a comparably low energy, which in contrary to BEI creates higher resolution images that lets the user acquired well determined images of the surface topography of the observed specimen.This technique was foremost used to identify etch pitted surfaces of feldspar grains and to determine other weathering features to gain information about the dissolution and precipitation hierarchy.

Elemental analysis of minerals could be performed by the "Point & Count" method as an integrated X-ray detector feature of the *JEOL JSM-6460LV* to investigate the chemical constitution of the present mineral phases in the samples.

2.2.3 X-ray diffractometry (XRD)

X-ray diffractometry (XRD) was used to characterize the mineralogical composition and semi-quantitative distribution of characterized phases in 34 selected samples (Table 2.1 accordingly). The data was collected on a *Bruker D8 Advanced* (40kV and 40mA) diffractometer, with a *Lynxeye XE High-Resolution Energy-Dispersive 1D Detector*, using *CuK*α radiation and later analyzed by the aid of the analytical software program *Diffrac.EVA*.

Determination of the mineralogical composition by X-ray diffraction is possible, due to mineral specific atomic structure, displaying phase characteristic distances in the mineral lattice, referred to as d-spacing. The d-value, given in Ångström (1Å = 10^{-10}m), describes the distance between two crystallographic planes of which the incoming x-ray beam, with certain wavelength (λ), is diffracted in an angle (2θ) in which x-rays are scattered strongly at material specific manner (Figure 2.3) (Goldstein et al., 2003).

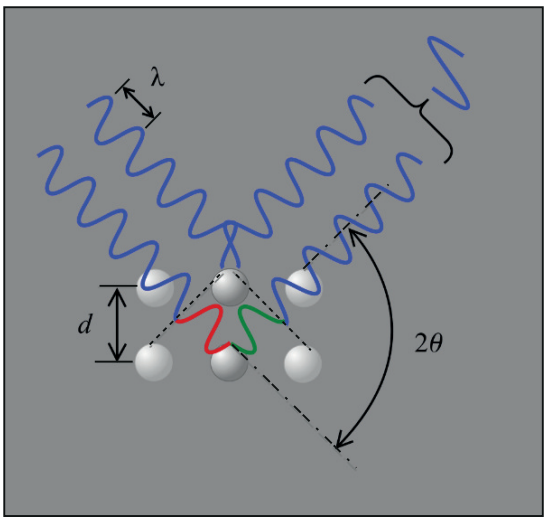

Figure 2.3: Diffraction according to Bragg's law. Strong scattering of the incoming (red) and the diffracted (green) beam, with the wavelength of $n\lambda$ occurs only at angle θ (http://commons.wikimedia.org).

Measured diffraction angles of the x-ray beam are recorded as peaks in a diffractogram, according their specific Ångström value. The qualitative peak analysis has been performed with the *Bruker* software Diffrac EVA. The semi-quantitative evaluation was achieved by distinguishing the count numbers of the mineral peak intensity of specific d-values (Table 2.2 for bulk sample analysis and Table 2.3 for clay fraction analysis) and calculating the percentage of the given mineral phases in each sample, based on the qualitative observations.

The semi-quantitative approach represents a non-absolute method, where the outcome might comprise imprecise results. Therefore, semi-quantitative values are referred to as "XRD-percentages".

All selected samples for XRD analysis were in the first step powderized with the aid of a "swing-mill". Solid samples, like those of the fresh granite and less weathered probes had to be crushed manually first, using mortar and pestle. A total amount of approximately 8-15 grams was used for powderization in the mill. For the purpose of standardization, the crushing was conducted at same moment of torsion (45Nm) and crushing time of 2.5 minutes. This was not applicable for samples of the fresh Rønne granite, which had to be crushed double time. Since most of the samples taken from the lower most 50 cm of the study section were still moist, due to capillary water from the adjacent quarry pond at the Nygård kaolin pit, they primarily underwent low temperature drying (55 °C) in the oven for about 12 hours, before crushing. To avoid cross-contamination all parts of the equipment involved were cleaned thoroughly after each sample preparation. The powderized fraction of the samples was then subdivided: 1. Approximately 5 g for bulk section analysis and 2. the rest for further preparation of clay fraction analysis.

2.2.3.1 Bulk-analysis

Approximately 5 g of the sample material was powderized with the aid of a *McCrone* micronizer, to achieve an average particle size of $< 10\,\mu m$. To the former swing mill ground material 7 ml of ethanol was added in a glass beaker, while stirring in a ultrasonic bath, to achieve a homogenic suspension. The suspension was then added to a plastic grinding container filled with small agate cylinders and ground for 10 minutes. The micronized dispersion was afterwards put for drying over night in an oven at 60 °C.

For the bulk sample analysis approximately 4 g of the micronized material was placed in aluminum holders, which were then run in the *Bruker* XRD-machine to gain a qualitative and semi-quantitative overview over the buk-mineralogical composition of the 34 chosen samples.

Qualitative analysis of the bulk samples Qualitative analysis of the bulk material has been conducted manually, by reading distinct peak positions in the diffractogram, using d-values as displayed in Table 2.2. In addition the analytical software *EVA* with its search and match function was used to distinguish minor mineral phases in the samples. The distribution of primary- and secondary mineral phases in the studied substrate was of main emphasis.

- Quartz (002)-peak at 4.25 Å was used, due to the mixed mineral association of quartz and illite at the (001)-peak at 3.34 Å.

- Biotite and illite, the 10 Å peak is utilized.
- Kaolinite the (003)- peak at 3.58 Å was utilized.
- Chlorite/smectite, the (001)-peak at 14 Å is used in bulk assemblage.

Table 2.2: Summary table of utilized d-values for the qualitative estimation of XRD-bulk samples.

	Mineral	d-value (Å)	Range	Reflection
Primary phases	Quartz	4.25	0.1	001
	Plagioclase	3.19	0.025	003
	K- Feldspar	3.24	0.025	003
	Biotite	10	0.1	001
	Hornblende	8.4	0.1	001
	Ilmenite	2.75	0.1	001
	Zircon	3.3	0.025	001
Secondary phases	Siderite	2.79	0.02	001
	Dolomite	2.89	0.02	001
	Calcite	3.04	0.02	001
	Hematite	2.69	0.02	001
	Illite	5.02	0.02	002
	Kaolinite	3.58	0.025	003
	Chlorite/Smectite	14	0.01	001
	Pyrite	2.71	0.025	001

Semi-quantitative analysis of bulk samples The bulk assemblage was performed by reading the count intensity of target peaks in the primarily refined diffraction curve by $K\alpha_2$-stripping (as recommended in the *Diffrac.EVA* user manual) to get a better fitting of the curve. The counting value for each present mineral phase was then recalculated into the percentage fraction of each sample. A summary table is given in Table C.1 and graphical illustrations are presented in chapter results Figure 3.40 and Figure 3.43 for profile B and D (summary graph for all XRD-bulk results is given in Figure C.1).

Mineral mobilization and fractionation during weathering The method suggested by Nesbitt (1979) compares the measurement of relative concentration changes of single, weathering prone mineral phases, compared with a weathering inert or resistant phase, such as zircon or quartz in the unweathered protolith, to the weathered material. For the purpose of this work, it has been decided, to estimate concentration changes, based on the comparison with quartz, since it seemed continuous enough in XRD-semi quantification [2]. The concentration changes

[2]This decision is also based on the results of Naqvi (2013), who performed the mineral change estimation in a similar approach.

are estimated in % and are calculated according:

$$\%Change = [(X^s/I^s)/(X^p/I^p) - 1]x100 \quad (2.2.1)$$

Where X, as any element in sample (s) compared to an immobile phase (I) is calculated in ratio to the same mineral calculation in the parent rock (p). Nesbitt (1979) suggested as immobile phase zircon, which will in this purpose be replaced by quartz, due to the fairly constant distribution in the studied samples[3]. Estimated changes are given in Table C.3 in the appendices and graphical approaches for selected mineral phases are represented in the chapter results.

2.2.3.2 Clay Fraction ($< 2\,\mu m$) preparation

1. **Gravity separation of particles** $< 2\,\mu m$. The swing mill powderized material was suspended in 50 ml of distilled water and disaggregated for about 10 min in a Bandelin Sonorex RK102 ultrasonic transistor to prevent particle flocculation and to accelerate dispersion. The suspension was then filled into cylindric beakers, which were all filled up with 250 ml of distilled water to an equal level under permanent stirring. The gravity separation of the particles < 2um was achieved by letting the samples settle for 24 hours in the cylinders. For separating the clay fraction from the coarse siliciclastic fraction a hose was injected into the column to extract the clay suspension equally above the same height in the cylinder and afterwards filled into laboratory beakers for preservation.

2. **The Millipore filter transfer method** The gravity separated suspension (fraction $< 2\,\mu m$) was filtered by the aid of a Millipore vacuum technique. The percolated samples were pasted from the filter paper onto glass substrates for XRD-clay analysis. As filter material, nitrate cellulose with an pore size of $0.45\,\mu m$ from the company *Satorius Stedim* was used. The filtering apparatus consists of a side-necked vacuum flask and a funnel reservoir clamped to a flat porous glass base. After filtering the sample was flushed with little 1M Magnesium-Chlorite ($MgCl_2$) to induce cation exchange within particular clay phases. Clay minerals holding either Mg^{2+} cations or Cl^- anions within their mineral lattice in exchangeable state. Smectites and vermiculites will by treatment of 1M $MgCl_2$ interchange ions with the solution and make clays around the 14 Å-peak better detectable in X-ray diffraction (Moore et al., 1989). Advantages of the filter transfer method are only fair crystal orientations produced trough filtering and little particle size segregation (Moore et al., 1989). Further Moore et al. (1989) stated, that if the filter material is inverted onto the glass substrate, most particle representative portion of the sample is detected by the X-ray beam, and the least representative (enriched in the finest size)

[3]As parent rock sample, Q2-12 was chosen for its higher quartz content.

becomes the bottom of the sample on the glass plate. The produced glass substrates were placed in aluminum holders for further analysis in the *Bruker* XRD machine.

Qualitative analysis of clay separated samples In the following all clay treatment proceedings and peak positions used for qualitative distinction are elucidated.[4]

Table 2.3: Summary table of d-values utilized for the qualitative XRD-clay mineral analysis.

Mineral	d-value (Å)	d(060) (Å)	2 θ (CuKα)
Smectite (Montmorillonite)	17	1.49-1.50	62.22-61.67
Illite	10	1.49	61.90
Biotite	10	1.54	60.16
Kaolinite	3.57	1.49	62.31
Chlorites	3.54	1.53-1.54	60.16-59.69
Smectite/Illite mixed-layers	5.0 - 5.61	-	-

- The first XRD-analytical approach of the clay samples was under *air dried* conditions of the substrate.
- After all *air dried* samples have been processed, the substrates were placed in a glass exsiccator, filled with *ethylene glycol* at its bottom and put in an oven for about 12 hours at a temperature of 60 °C. Swelling clays, i.e smectites, are detectable by the expansion of the 14 Å-peak at air dried conditions to approximately 17 Å in ethylene glycol solvated curve.
- In the next step the samples were heated to *350°C* for about 2 hours. This process is irreversible and destroys mineral lattice of smectite, which collapses after heating to 10 Å (see Figure 2.4).
- The *550°C* heating, as the *350°C* treatment is irreversible. Kaolinite becomes amorphous at this temperature and the curve collapses entirely (Moore et al., 1989) and Figure 2.4.

Semi-quantitative analysis of clay fraction The semi-quantification of the clay fraction has been performed using the ethylene glycolated curve of each analyzed sample. As for the bulk assemblage maximum peak intensities of target positions have been counted with the aid of the *Bruker software Diffrac EVA*. Noted count intensities of the formerly determined mineral phases were recalculated in percent with respect to the sum of the total counts in each sample. The semi-quantification of the clay samples will be treated strictly as internal ratio distribution

[4]The heating procedures for 350 °C and 550 °C were performed by Maarten Aerts (UIO).

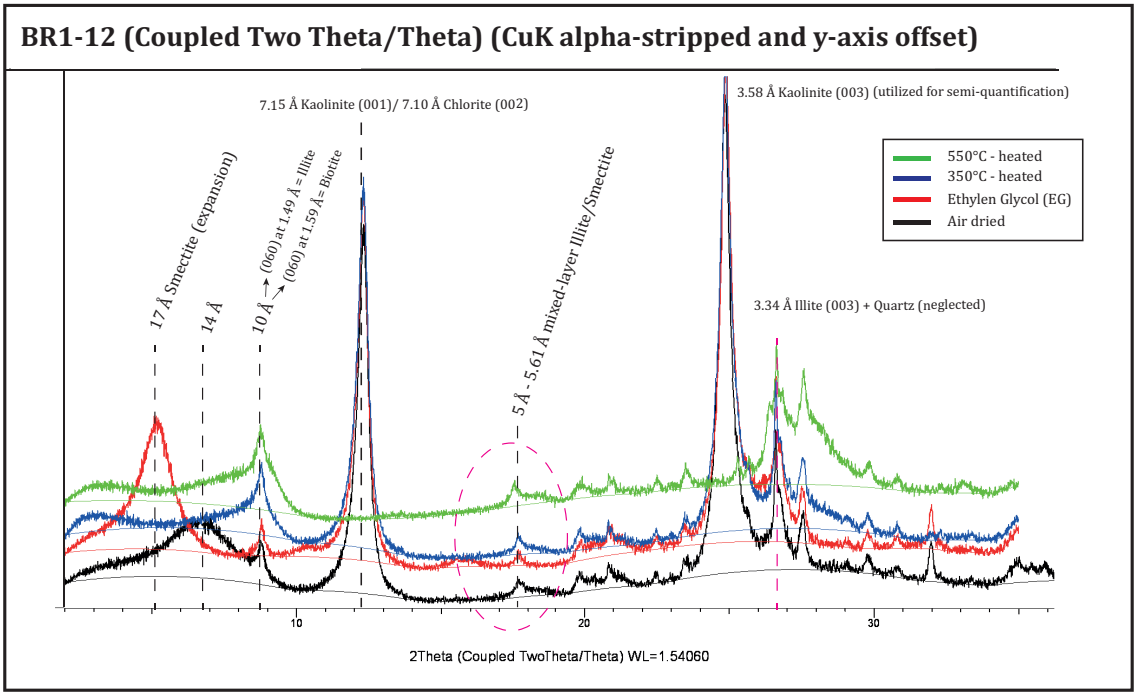

Figure 2.4: Example curve for qualitative and latter semi-quantitative distinction, by the aid of the XRD software *EVA*. The application shows a set of *air dried*, *ethylene glycol* , *350°C* and *550°C* treated clay curve. For simplification in this illustration are the curves y-offset, therefore count numbers along the y-axis were whitened out. Significant peak positions according Table 2.3 are illustrated. Note that the 060-positions are not illustrated in this graph, due to the main emphasis on the range between 0°2 θ and 30°2 θ. Semi-quantification was performed for the ethylene glycol solvated curve, before y-offset (see paragraph *semi-quantitative analysis*).

for the clay fraction, since the comparison with the bulk data would not be in correct relation. Approximately 10 g of sample material was used for XRD analysis, whereof 50% was used for the bulk analysis and the other half was used for clay analysis. The material loss during the clay sample preparation was indeterminable, therefore the ratio of clay material, compared to the total volume used is unknown and the results are incomparable.

3 | Results

The results presented in this chapter are based on fieldwork and -observations, where sedimentary logging and regular interval sampling of the weathering profile at Nygård kaolin pit was performed, as explained in Chapter Methods. Detailed photographs of the studied site and comprehensive microscopical thin section descriptions contribute to the petrographical and mineralogical analysis (XRD, SEM) of the sample material. In the first step the results of the unweathered Rønne granite are presented to define the unweathered petrographical properties of the weathering educt.

The following section comprises the detailed description of two profiles logged at the Nygård weathering succession. In total five sections were logged in intervals of approximately 2 m distance at the 12.5 m long and 5 m high outcrop, out of which profile B and D will be discussed complementary in detail (see subsequent Figure 2.1). Samples of profile A,C and E are not encountered in the following, only 9 samples have been processed out of the three sections. The focus will therefore be on the more densely sampled profiles B and D.

The petrographical investigations were conducted to distinguish dissolution of primary mineral minerals, like plagioclase, biotite and hornblende as driving weathering agents and the precipitation of secondary minerals, e.g. kaolinite, smectite, chlorite and illite. The weathering sequence of the profile at Nygård, wether evolved through a single cycle of weathering or by multiple crystallization generations? Indications for mineral formation under sub-aerial, diagenetic temperature conditions during burial or late diagenetic reactions associated with re-exposure of the profile (e.g. formation of iron oxide) were fundamental settings for the following chapter and driving motives for this work.

3.1 The Rønne granite at Klippeløkken

The Rønne granite constitutes a heterogeneous, medium to coarse grained plutonite, characterized by numerous carbonaceous pegmatite intrusions of cm to m range in width. Hand specimens display mafic appearance (Figure 3.1 b)). The exiguous presence of biotite, hornblende and ilmenite as dark mineral components, and the high transparency of the felsic mineral assemblages, such as quartz, K-feldspar and plagioclase contribute to the melanocratic character of the fresh granite (Jørgart, 2000).

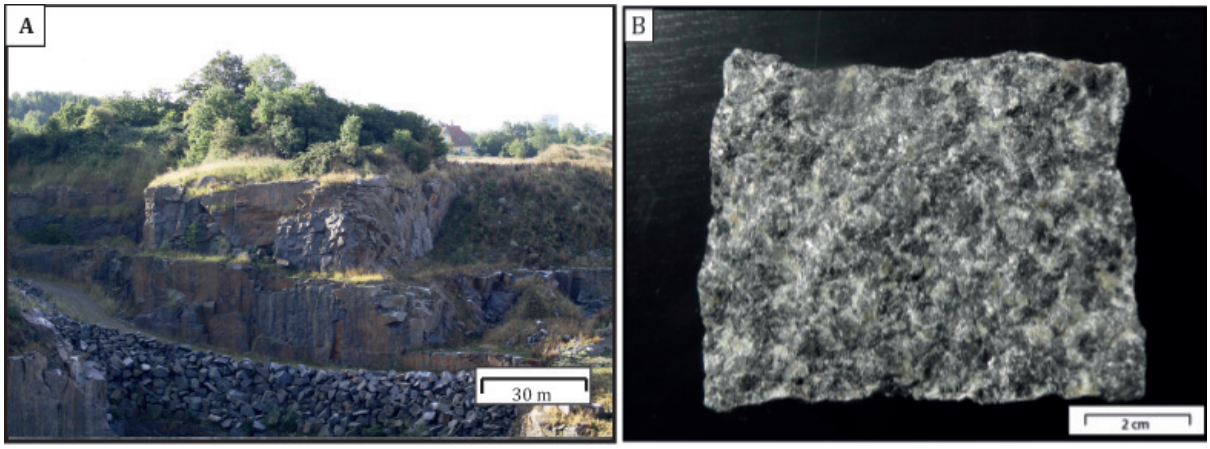

Figure 3.1: a) Klippeløkken granite quarry b) fresh Rønne Granite cobblestone.

3.1.1 Petrographical and mineralogical description of the Rønne Granite

3.1.1.1 Petrological classification of the parent rock

The Rønne granite was classified according the IUGS Subcommision on the Systematics of Igneous Rocks (Streckeisen, 1976). Point counting analysis presented in Table 3.1 and Table B.1 constituted the main quantitative approach for the classification and were complimented with semi-quantitative XRD estimations from bulk analysis. According to this classification the Rønne granite is in "senu stricto" an monzo-granite with tendency towards the quartz-monzonite stability field (Figure 3.2), due to its relatively low quartz concentration of approximately 17% after point counting analysis.

Table 3.1: Mineral composition of the Rønne Granite in percent, estimated from point counting, as described in Chapter 2. For summary of point counting results see Table B.1, in the appendices.

Method	Sample	Quartz	Plagioclase	K-Feldspar	Mica	Hornblende	Accessories
Point counting	Q1-12	16	38	26	4	14	2
	Q2-12	19	34	23	8	14	2

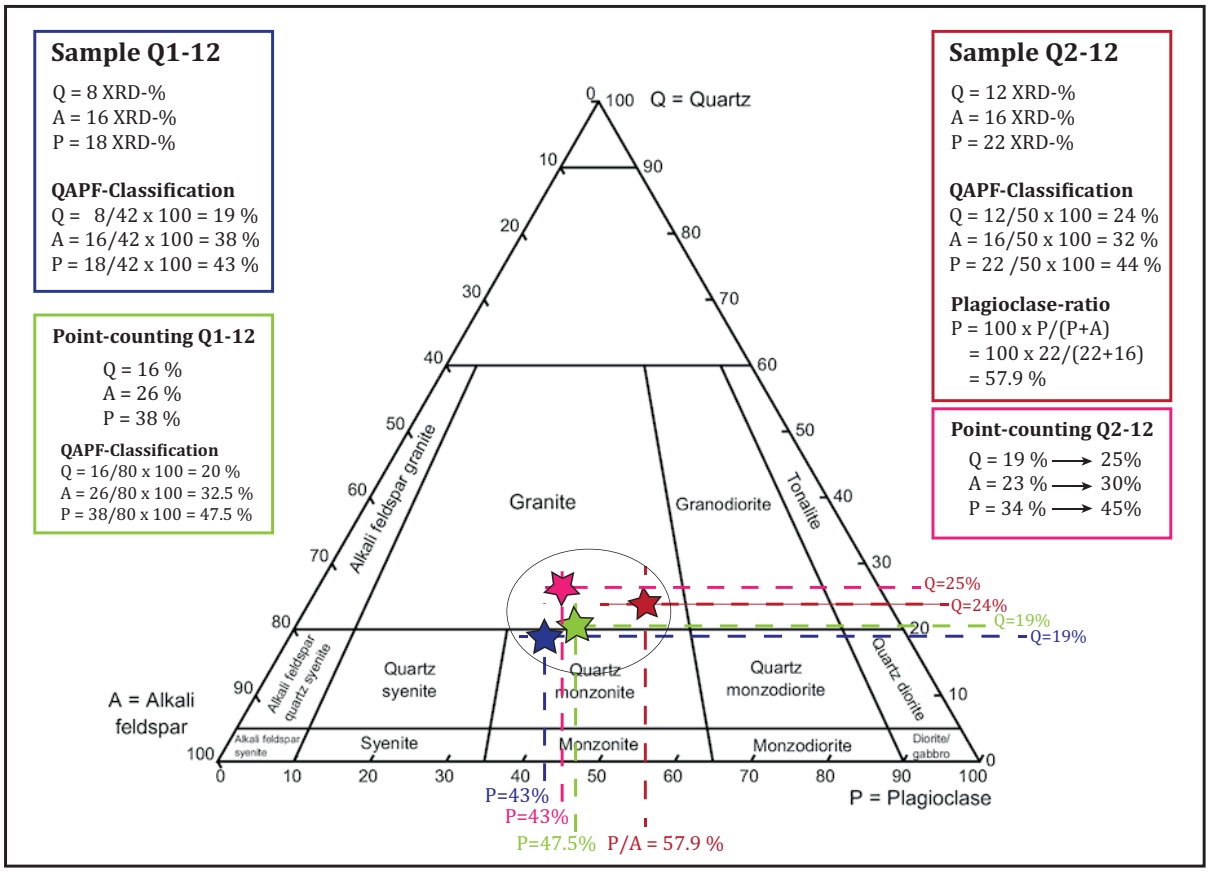

Figure 3.2: Streckeisen classification of the Rønne Granite. XRD semi-quantification and point counting results from sample Q1-12 and Q2-12 are illustrated. The four estimations represented, display a general tendency towards the granite paragenetic field. Plagioclase exceeds the K-feldspar content marginally, the feldspar content in the paragenesis is evidently not high enough to lay within the granodioritic field and is therefore in 'sensu stricto' a granite.

3.1.1.2 Thin section observations (Samples Q1-12 and Q2-12)

Thin section observations of two samples from the Rønne granite revealed holocrystalline, phaneritic textural features in the weathering source rock. The thin sections disclosed under plain polarized light (ppl) an abundance of felsic compartments, compared to mafic minerals. Mafic phenocrysts, were mainly constituted of inter-growing hornblende (amphibole) and biotite (mica). Common overgrowth by an isotropic, opaque mineral phase could be studied within mafic minerals, which by means of its frequently cubic appearance was distinguished as pyrite.

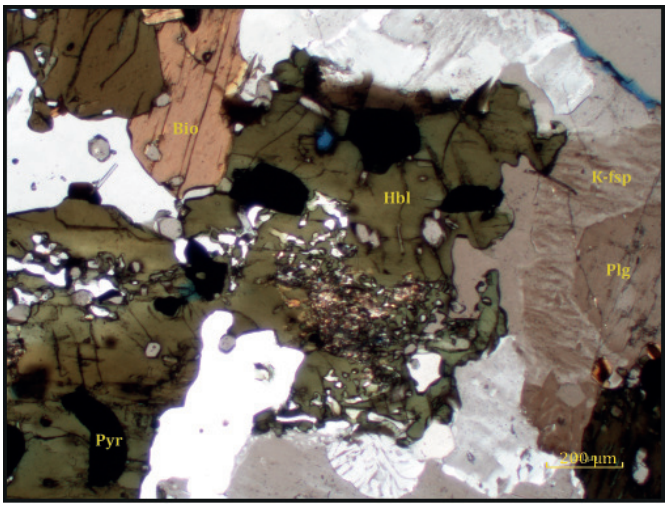

Figure 3.3: Hornblende, biotite and feldspar association in sample Q1-12.

Hornblende could easily be distinguished according its pleochroism in ppl, which in E-W position of the crystals along (110) displays dark green and in N-S position shows light green color (Figure 3.3). Absence of bird's eye extinction, in addition to two cleavage directions in these minerals, intersecting approximately at angles of 60°/120°, are main characterization and differentiation features of the amphiboles against the often adjacent biotite. Polycrystalline quartz was found embayed in hornblende phenocrysts, which is associated with primary crystallization of quartz. The growth of much larger minerals in the crystal interspace characterizes typical interstitial quartz formation during the last stage of magma cooling of the rock paragenesis and thus determines a secondary crystallization phase. Point counting of the fresh slides of the parent rock (see Table 3.1 and Table B.1) revealed 14% of hornblende estimated in both sections.

Biotite, often displays first signs of alteration by broken or even splayed layers along its preferred cleavage direction (001) (Figure 3.3). Main distinguishing features beside the pleochroism are very well determined pleochroic halos. Zircon inclusions are often remarkable and may achieve 1 mm or even 1.5 mm in size. Grain shapes resembled a frequent marginal rounding, which might indicate dislocation. Biotite concentrations in the studied sections, measured by point counting are fairly low represented by 4 % in Q1-12 and 8% in Q2-12. Mica amounts of muscovite could only be observed in minor phase as scattered, fine grained and under-determined association around hornblende and as cryptocrystalline sericite inclusion in plagioclase.

Felsic compounds, mostly transparent with slight tinge of yellow-brown color along mesofractures under ppl were distinguished under xpl, using conoscopic images for determination.

Interstitial, eu- to subhedral quartz grains are commonly between 2-4 mm in size and comprise with 16 % in Q1-12 and 19% in Q2-12 an important, more weathering resistant, felsic component in the Rønne granite (Table 3.1). Detailed studies of the quartz association revealed different preferred orientations of the quartz crystals. Some of the grains represent text book examples of the uniaxial mineral, showing white to gray birefringence colors (Figure 3.4a)), straight extinction (Figure 3.4a)), well determined uniaxial images and rutile needle inclusions,

whereas others display birefringence colors of light- to honey-yellow (Figure 3.4b)), undulose extinction (Figure 3.4b')) and flash figure appearance in conoscopic view (see paragraph flash figure appearance in interstitial quartz grains below). Sericite inclusions could be observed commonly in both orientation types.

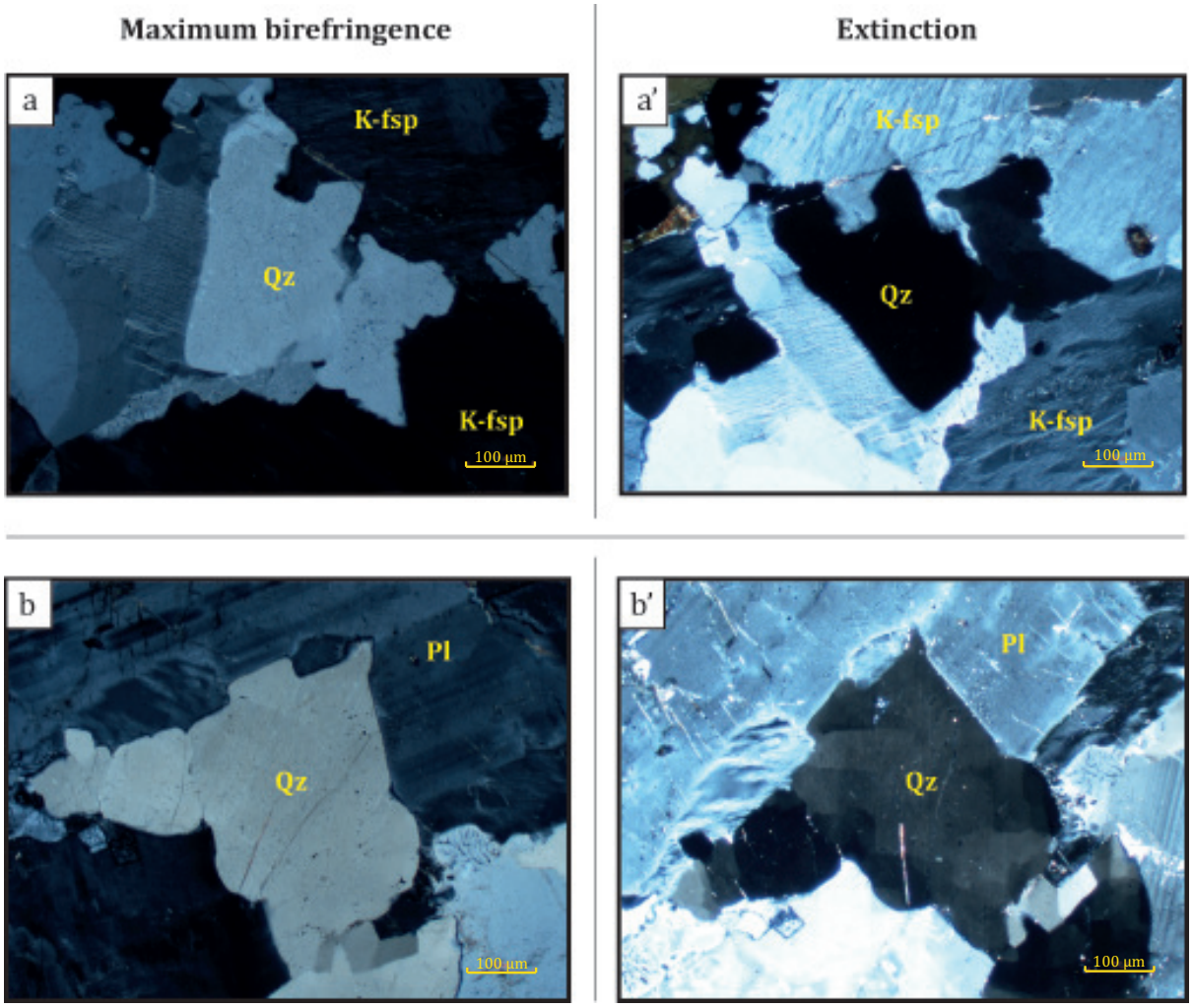

Figure 3.4: Quartz associations in sample Q2-12, xpl-images showing a) quartz mineral oriented with crystallographic A-axis perpendicular to the microscopy table, displaying light gray birefringence color and a') straight extinction. Whereas image b) represents typical quartz grain found displaying flash figure appearance, due to its orientation. Photo b') illustrates a grain with undulose extinction.

Feldspar comprises the main felsic mineral association in the fresh granite samples. Plagioclase, with grain sizes up to 5 mm, is represented by 38% in Q1 and by 34 % in Q2 based on point counting observations (Table 3.1). The solid solution series of Ca-rich end member anorthite and the Na-rich end member albite constitute alongside with mafic components hornblende and biotite the most prone minerals to weathering in the studied rock paragenesis. The plagioclase is transparent under plain polarized light and shows continuous extinction under xpl. Polysynthetic twinning, used for the estimation of the plagioclase composition

according the *Michel Levy method* (Table 3.2 and Figure 3.5), is rarely well enough determined in sharp albite twins and often of patchy character, with blurry appearance along the twin edges. Carlsbad twining could be observed in some grains, but polysynthetic twinning was more common. Most of the plagioclase grains displayed sericitization, often along twinning planes but also along micro-fractures, within the mineral interior. Most remarkable is a common growth rim around plagioclase, constituted of K-feldspar where no sericitization was found. The plagioclase minerals seem less altered and twinning better preserved in this inter-growing constellation, but sericitization is still very common. No distinct transition line could be observed from K-feldspar rim, to the polysynthetic twinned plagioclase. The K-feldspar rim is characterized by two sets of polysynthetic twins, indicating the low temperature K-feldspar variant microcline. Tartan-twinning is abundant and lamellar twining could be observed frequently, which adds to the former suggestion, due to the triclinic character of the microcline K-feldspar. Large magnification observation (10p, 0.25- 40p, 0.65p) revealed pertithic exolution within the potassium-rich feldspar, especially within the mentioned growth rims around plagioclase (see Figure 3.6). Lenticular shaped albite exolution may appear due to decreasing temperatures, while retrograde cooling of the magma. This correlates well with the assumption that the main K-feldspar polymorph in the observed samples is the low temperature variety microcline (approximately 200 °C to 450 °C), based on the twinning character and the rather wide 2V angle $>50°$ appearing in conoscopic view. However, minor presence of the mid-temperature polymorph orthoclase (approximately 450 °C to 600 °C) was found according characteristic carlsbad twins and a comparably higher 2V of approximately 40in these crystals.

Table 3.2: Summary table displaying the average anorthite mol-% in plagioclase, estimated from samples Q1-12 and Q2-12 of the unweathered granite.

Mineral	$\alpha 1$	$\alpha 2$	$(\alpha 1+\alpha 2)/2$	Mol% An	Biaxial character (+ or -)
1	36	40	38	63	
2	24	25	24.5	45	
3	33	33	33	58	
4	21	20	20.5	36	
5	8	9	8.5	23	(-)
6	9	13	11	27	(-)
7	16	15	15.5	30	
8	12	15	13.5	28	
9	19	16	17.5	32	
10	5	5	5	22	(-)
11	9	10	9.5	25	(-)
12	8	11	9.5	25	(-)
		Average mol-% An		**35 Mol%**	

The plagioclase crystals show determined sericitization in the central mineral area, indicating reasonable existence of anorthite, as fine grained sericitic mica is often derived as alteration

product of the Ca- end member of plagioclase. Sericite and the initial alteration were rather disturbing for the microscopic determination technique, where the presence of sharp and well defined polysynthetic twins control the quality of the results tremendously. Multiple sets of polysynthetic twins could be formerly found in minerals surrounded by a rim of K-feldspar. The results presented in Table 3.2 for the fresh, unaltered plagioclase in sample Q1-12 and Q2-12 display an average mol-% An of 35. The observed crystal minerals show consistent values estimated throughout both samples of the fresh Rønne granite.

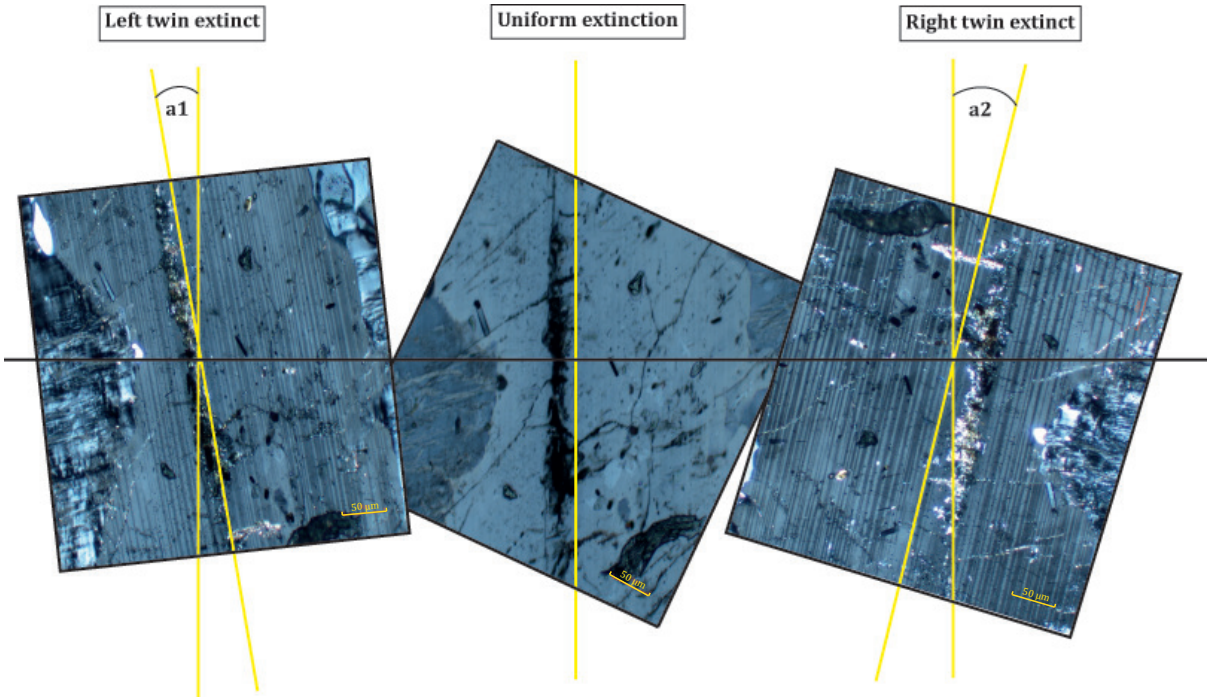

Figure 3.5: Polysynthetic twinning set, observed in Q2-12, for plagioclase composition determination. Position α_1 and α_2 changes of extinction angles in the observed plagioclase crystal are displayed in Table 3.1. Plagioclase shows sericitization along the anorthite/albite twins.

3.1.1.3 SEM-analysis of the source rock

Results of the scanning electron microscope analysis were utilized, using backscattering electron images (BSE) on carbon coated thin sections, as displayed in Figure 3.6 and Figure 3.7 a), for qualitative analysis, and secondary electron image (SEI) microscopy was conducted for surface morphological observations of stub samples coated in gold (Figure 3.7 b)).

Backscattering electron image of sample Q2-12 (Figure 3.6) illustrates, slightly sericitized plagioclase in fresh, unaltered Rønne granite. Plagioclase composition in the protolith, was as mentioned previously, distinguished by the aid of *Michel Levy's* method, which revealed an approximate anorthite concentration of 35%. Inter-growth of hornblende and biotite displayed in Figure 3.7 a), is common in samples Q1-12 and Q2-12. Hornblende (light gray in image)

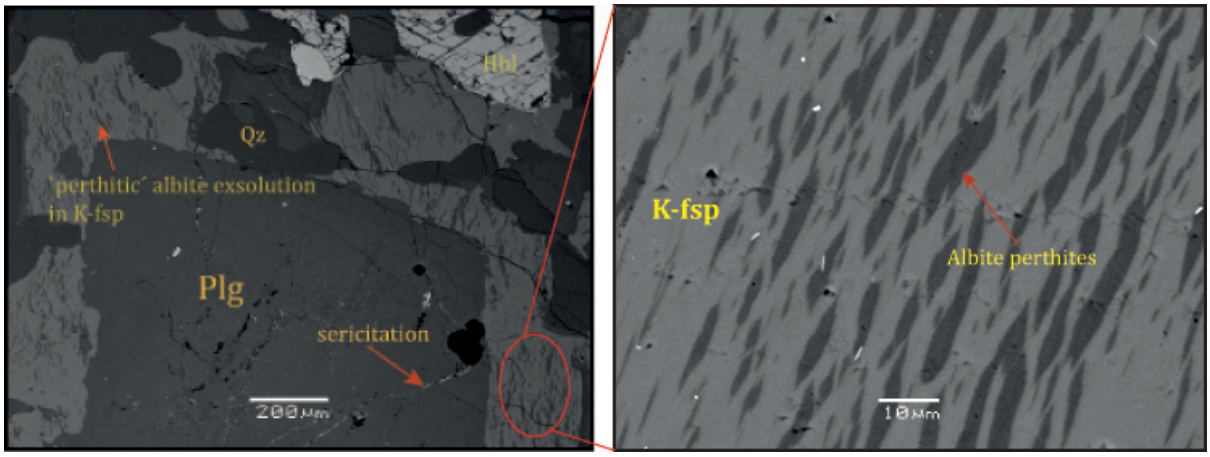

Figure 3.6: Sericitized plagioclase (plg), surrounded by K-felspar with perthitic albite exolution lamellas and left, close up image of perthitic albite exsolution (darkest minerals in right image is quartz).

shows typical cleavage inter-secting at an angle of 60°-120°. Primer embayed, crystalline quartz growth can be defined by the dark gray colored patches within the hornblende crystal, differing in size from usually larger interstitial quartz grains surrounding the hornblende/biotite crystal. Biotite shows widened inter-layering space, mineral borders are sharp along the 001 plane and BSE revealed initial kaolinitization within the inter layers.

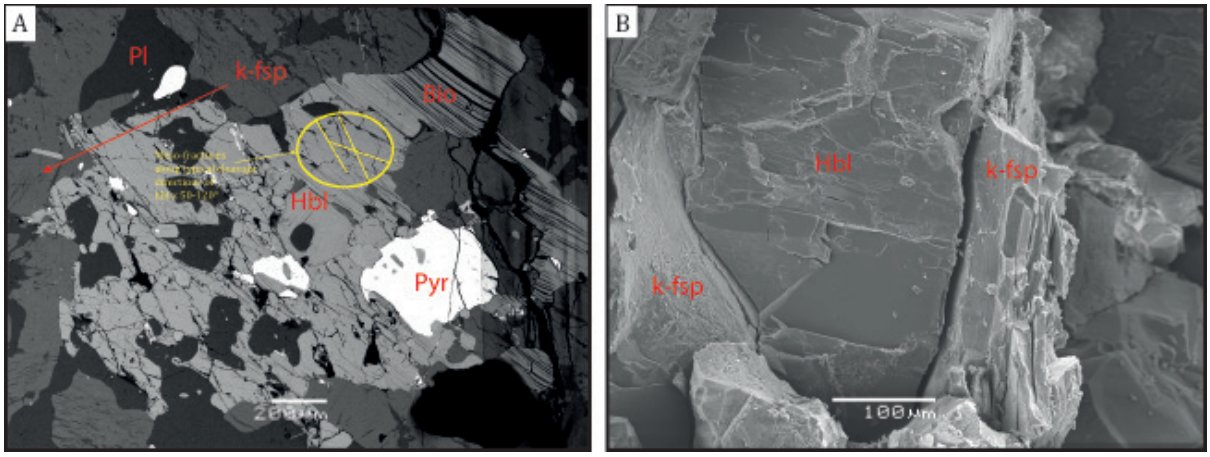

Figure 3.7: a) Back scatter electron image (BSE) of inter-grown hornblende with biotite, joint by K-feldspar, plagioclase and pyrite, displayed by the white mineral, due its high reflectance (Q2-12). Hornblende shows characteristic cleavage, crossing at 60-120°, along which first signs of denudation can be observed. b) Secondary electron image of a gold coated stub sample (Q2-12) showing hornblende, surrounded by K-feldspar, minimal etching at its surface can be observed.

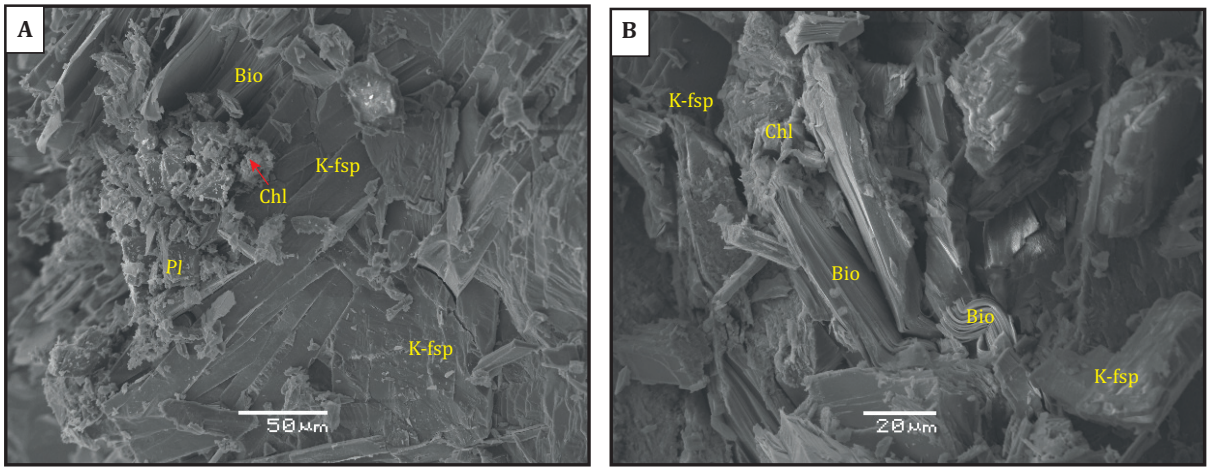

Figure 3.8: Secondary electron image of Q1-12 sowing a) biotite layers standing out of surrounding K-feldspar, the biotite and the plagioclase are slightly chloritized. b) displaying well determined biotite layers, slightly bended and chlorite could be observed along the mineral margins.

3.1.1.4 XRD-analysis of the source rock

In this section qualitative and semi-quantitative results of the XRD-bulk analysis of the unweathered bedrock samples Q1-12 and Q2-12 from the Klippeløkken granite quarry are presented.

Qualitative XRD observations of sample Q1-12 (displayed in Figure 3.9) complemented the microscopical analysis, presented in section *thin-section analysis*. Semi-quantitative estimations of the sample (see summary table Table C.1) confirmed the predominance of plagioclase over K-feldspar, 18 XRD% plagioclase and 16 XRD% microcline, which gives an estimated amount of 8 XRD% and a quartz/total feldspar ratio of 0.19 in sample Q1-12. The plagioclase composition was estimated according a technique suggested by Moore et al. (1989), using in well developed curves the XRD peak position appearing between 29.28° 2θ and 29.68° 2θ to distinguish the anorthite percentage. The of course, rough estimation of the plagioclase composition in Q1-12 has shown a peak at approximately 29.90° 2θ [1], in Q1-12 (see Figure 3.9) which indicates an anorthite content of approximately < 40% in the mostly unweathered plagioclase. This observation coincides with the microscopical estimation of the plagioclase composition according to *Michel Levy*, where an average anorthite content of 35% could be distinguished. The 10 Å- peak in the fresh, unweathered material represents the biotite peak [2], 18 XRD% were estimated in this sample, together with 17 XRD% Hornblende. As accessory mineral associations 6 XRD% zircon and 4 XRD% pyrite were observed.

Semi-quantitative observations of sample Q2-12 revealed higher abundance of plagioclase

[1] Moore et al. (1989) stated that 29.28° 2θ equals Ab_{67} and 29.68° 2θ equals Ab_{33}

[2] In clay fraction 10Å-peak was used as illite and biotite peak, due to the mixed mineral appearance of biotite and illite at this position, minerals where differentiatiated according the 060-peak appearance at 1.49 (illite) and 1.54 (biotite) in clay samples.

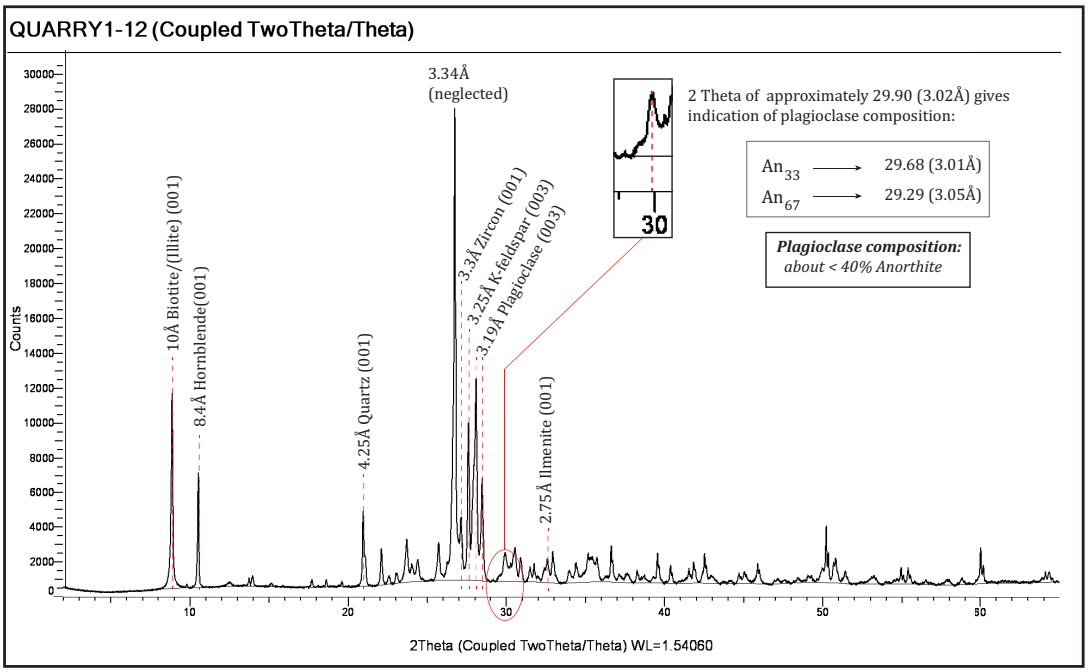

Figure 3.9: XRD bulk diagram of sample substrate Q1-12. Primary constituents are illustrated according their d-value position (see Table 2.2). The 3.34 Å- peak was neglected, due to its mixed mineral phase appearance. A quantification approach of the plagioclase composition according the 29.90° 2θ peak is illustrated, based on the technique discussed in Moore et al. (1989). $An_{<40}$ and $Ab_{>60}$ content in plagioclase accordingly, could be distinguished in sample Q1-12.

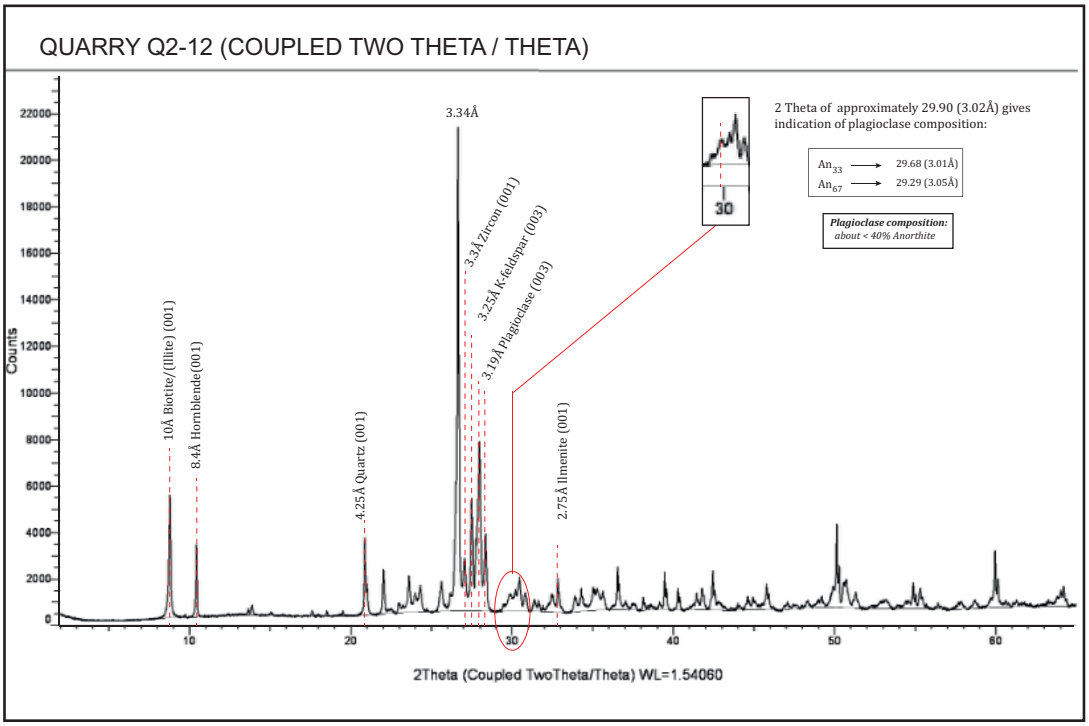

Figure 3.10: XRD bulk diagram of sample substrate Q2-12, for explanation see Figure 3.9 accordingly.

feldspar of 22 XRD% compared to K-feldspar, in which equally 16 XRD% as in sample Q1-12 were determined. The plagioclase composition (Figure 3.10) indicates similar distribution values of approximately $An_{<40}$ in both samples. Lower concentration of biotite and hornblende can be easily notified by lower peak intensities of the 10 Å- and the 8.4 Å-peaks (Figure 3.10), compared to Q1-12 (Figure 3.9). Biotite abundance of 15 XRD% was estimated and the hornblende concentration, according this semi-quantification was significantly lower with 10 XRD% in Q2-12 compared to 17 XRD% in Q1-12.

3.2 The saprolite profile at Nygård kaolin pit

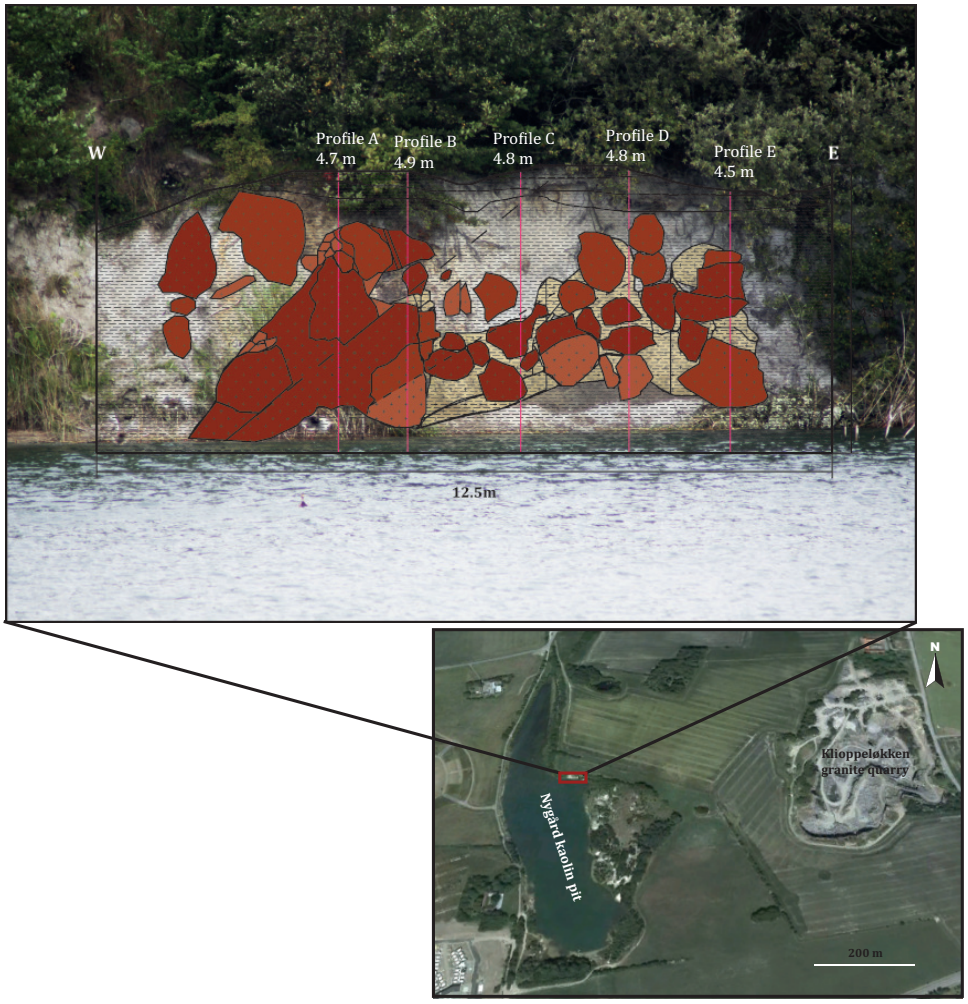

Figure 3.11: Image of the saprolite section at Nygård, the lower map displays the location of the outcrop. The upper image combines the sedimentary logging with a field photograph. The image is derived from a field sketch, drawn in 1:10 (see Figure D.1).

3.2.1 Weathering classification and sedimentary log association

In this section first attempts for the classification of five different weathering classifications, based on field observations will be presented (see Figure 3.13 for explanation). In further reference the term weathering facies is used as a equivalent for weathering class, derived from its sediment geological origin. Moore et al. stated in Boggs (2006), that facies can be defined as ”any restricted part of a designated stratigraphical unit which exhibits characters significantly different from those of other parts of the unit”. According to field observations of the saprolite lithology at Nyård kaolin pit, based on properties like physical resistance, color appearance and macroscopical mineral observations in hand specimen (studied with hand lenses), five classes or weathering facies are suggested (after Ollier et al. (1984)) (see Figure 3.13). In the following these first attempts (see Figure 3.14 to Figure 3.18), are compared and refined by petrographical and mineralogical observations. The subsequently printed log images illustrate the position of corestones in the studied profile and propose a weathering facies for the different weathering lithologies based on the acquired observations.

3.2.1.1 Corestone associations

Previously introduced concepts of spheroidal corestone weathering were studied at Nygård by means of the fracture appearance, general orientation within the profile and macroscopical association of the boulders. Lateral trends from west to east (left hand side to right hand side of the profile) could be distinguished (Figure 3.11) and are illustrated subsequently in the schematic log images. The corestone association found in the weathering section at Nygård displayed a very heterogeneous character, weathering rindlets were commonly underdeveloped as thin, scattered exfoliations or entirely destroyed (Figure 3.12). Often elliptical shaped boulders could be determined where the elongated axis coincided with distinguished fracture directions (see Figure 3.12 a)). Randomly scattered corestones could be studied frequently, displaying no preferential fracture direction (Figure 3.12 b)) and might thereby constitute higher classes of denudation. Sharp borders around better preserved corestone margins from less weathered granite to highly altered clay-rich residual denote rather small scale reactions in cm range and illustrate the effectiveness of exfoliating processes, fracturing and drainage to alteration.

3.2.1.2 Weathering classification

Figure 3.13 illustrate and describe the attempted weathering classification of the observed facies according lithological characteristics of the weathering strata in field. The weathering classes from I, defining the unweathered Rønne granite to V specifying the completely weathered friable soil (Figure 3.13), were distinguished according previously elucidated

parameters.

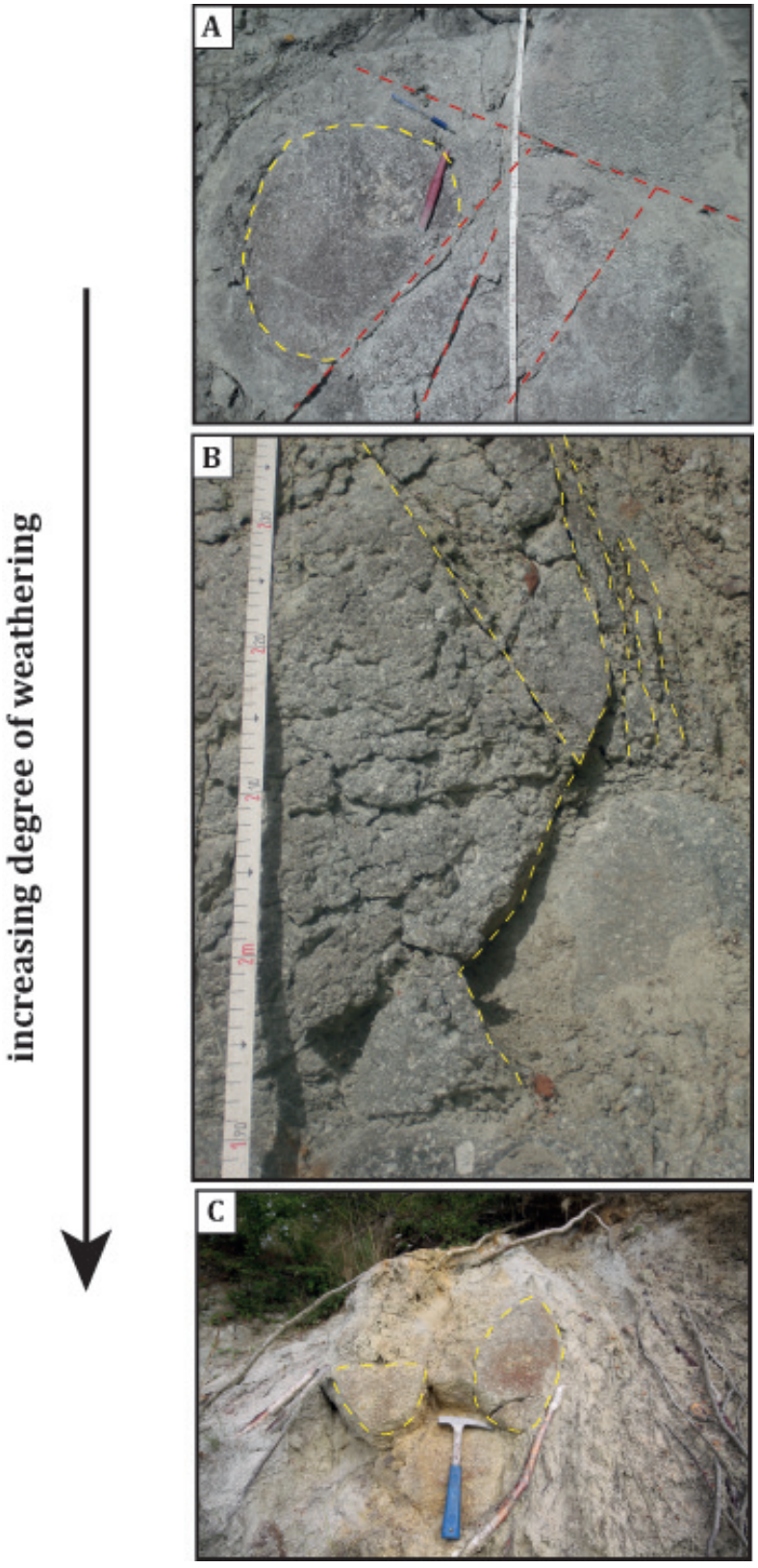

Figure 3.12: a) Enbedded corestone (yellow dashed line) with two main strike directions of fractures (red dashed line) (profile A). b) Scattered corestone with rudimentary ringlets (profile B). c) well developed, oxidized corestone embedded in residual soil (from outside the studied weathering section).

Class	Grade of weathering	Description of material and mass
Fresh	I	No visible sign of rock material weathering. Near boundary with Grade II slight discoloration on major defects.
Slightly weathered	II	Discoloration indicates weathering of rock material and defect surfaces.
Moderatly weathered	III	Less than 50% of material decomposed and disintegrated to a weakly cohesive, friable intact soil. Core Rock discolored, weakened
Highly weathered	IV	More than 50% of material decomposed and disintegrated to a weakly cohesive, friable intact soil. Rock Cores discolored and weakened.
Completely weathered	V	Intact friable soil which may be weakly cohesive. Soil has fabric of parent rock.

Figure 3.13: Definition of the five weathering classes, as applied in field for the macroscopical appearance of hand specimen, according the grain sizes, friability and color determination. (modified after Ollier et al. (1996))

3.2.1.3 Sedimentary log association

The sedimentary log images in this thesis are displayed as a hybrid-solution of the classical, sediment geological approach for the overlaying residual soil layer, combined with detailed sketches of the saprolite horizon (displayed in Figure D.1 in the Appendix).[3] Profile A located at the western margin of the saprolite profile (left hand side) is composed of a rather massive corestone complex mostly associated with weathering class II and III. Fracture sets are well determined in two main directions (presented in following section) and commonly intersect in typical angles of 60 °and 120°. The massive corestone complex is commonly intervened with highly weathered, clay-rich residual along fractures. The lower most 50 cm and upper most part (2.70 m-3.40 m) constitute, strongly altered, friable saprolitic material of weathering class V (Figure 3.14). The medium part of the section is defined by red to red-brown oxidation, highly resistant granite. This massive corestone complex becomes progressively fractured and the corestone associations more rounded in eastern direction (to the right hand side, with 2 m distance from profile to profile). Profile B illustrates increasing heterogeneity in the lithology, where increasingly weathered facies becomes more interfering along size enhanced fractures and more scattered corestones. Profile C, D and E show well-rounded to elliptically shaped, distributed corestone associations surrounded by increased altered facies of weathering class IV and V. The lateral trend from west to east (left to right) seem to coincide with increasing degree of weathering, which opposes the general hydraulic gradient of the area in the recent situation. The elevation difference from the approximately 800 m distant granite quarry at Klippeløkken in ENE direction to the Nygård kaolin pit was estimated using GPS measuring points to be 38 m (see Figure D.2 in the appendices).

[3]Despite the main emphasis on profile B and D (see Figure 2.1) for the petrographical and mineralogical description, all profile logs are included in this section, as lateral developments are easier displayed and it seemed more convenient for the reader to compare the results with the summary sketch (Figure 3.11) by consecutively ordered log images.

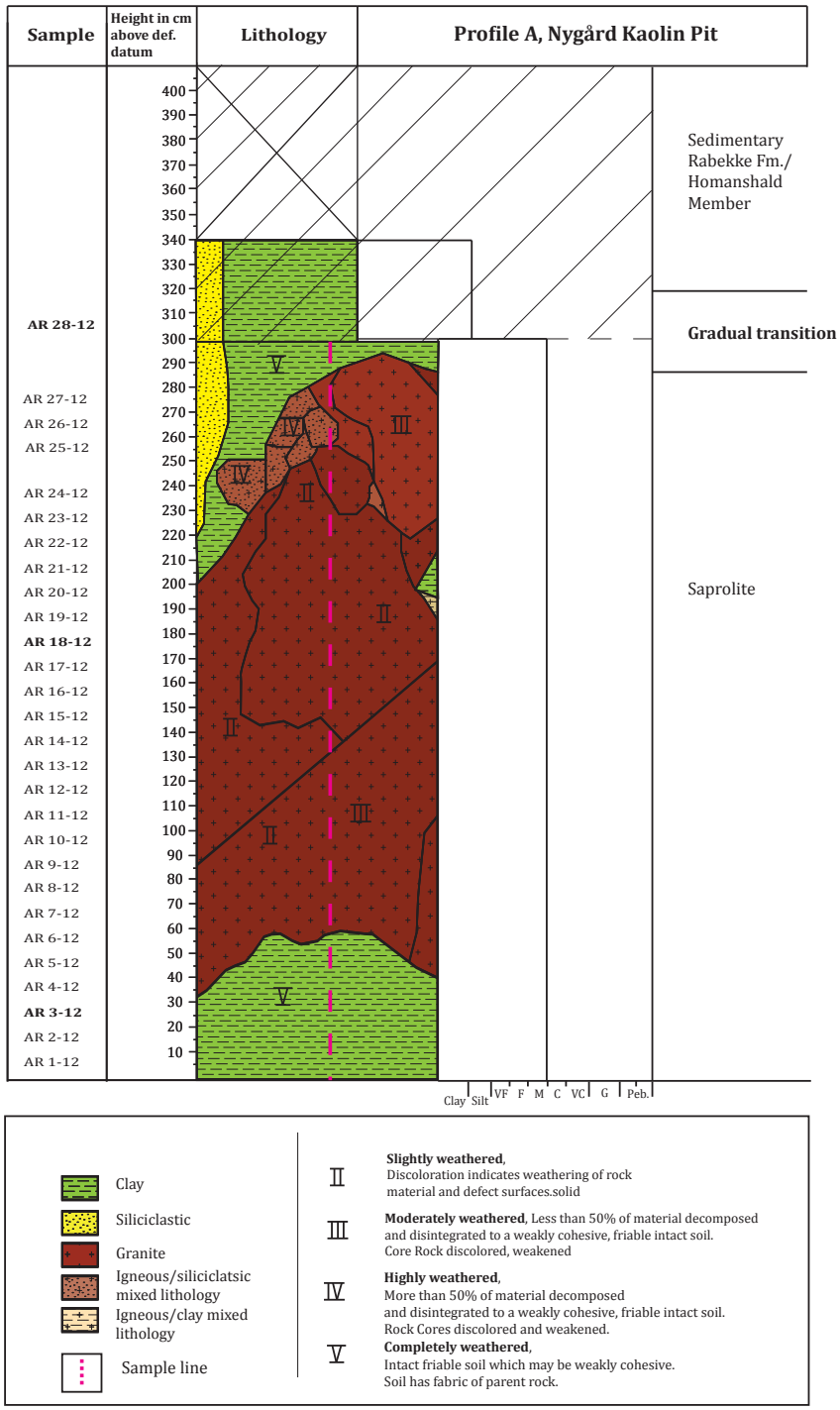

Figure 3.14: Profile log section A. Weathering classification based on field observations of the heterogeneous, weathered protolith is illustrated by roman numbers (see Figure 3.13). Pink, dashed line indicates the path along samples have been extracted. The samples gathered in this section are illustrated on the left side. Note that samples printed in bold font distinguish the samples selected for petrographical and mineralogical observations. The profile was divided based on field observations into the lower saprolite horizon and the uncomformably overlaying lower Rabekke Formation, the Homanshald Member. The lithological border is marked by a gradual change from the weathering unit to the residual soil. For the upper sedimentary cover a classical logging approach was conducted. The upper part was neglected, due to the strong gradual transition and the main emphasis on the weathering section in this illustration.

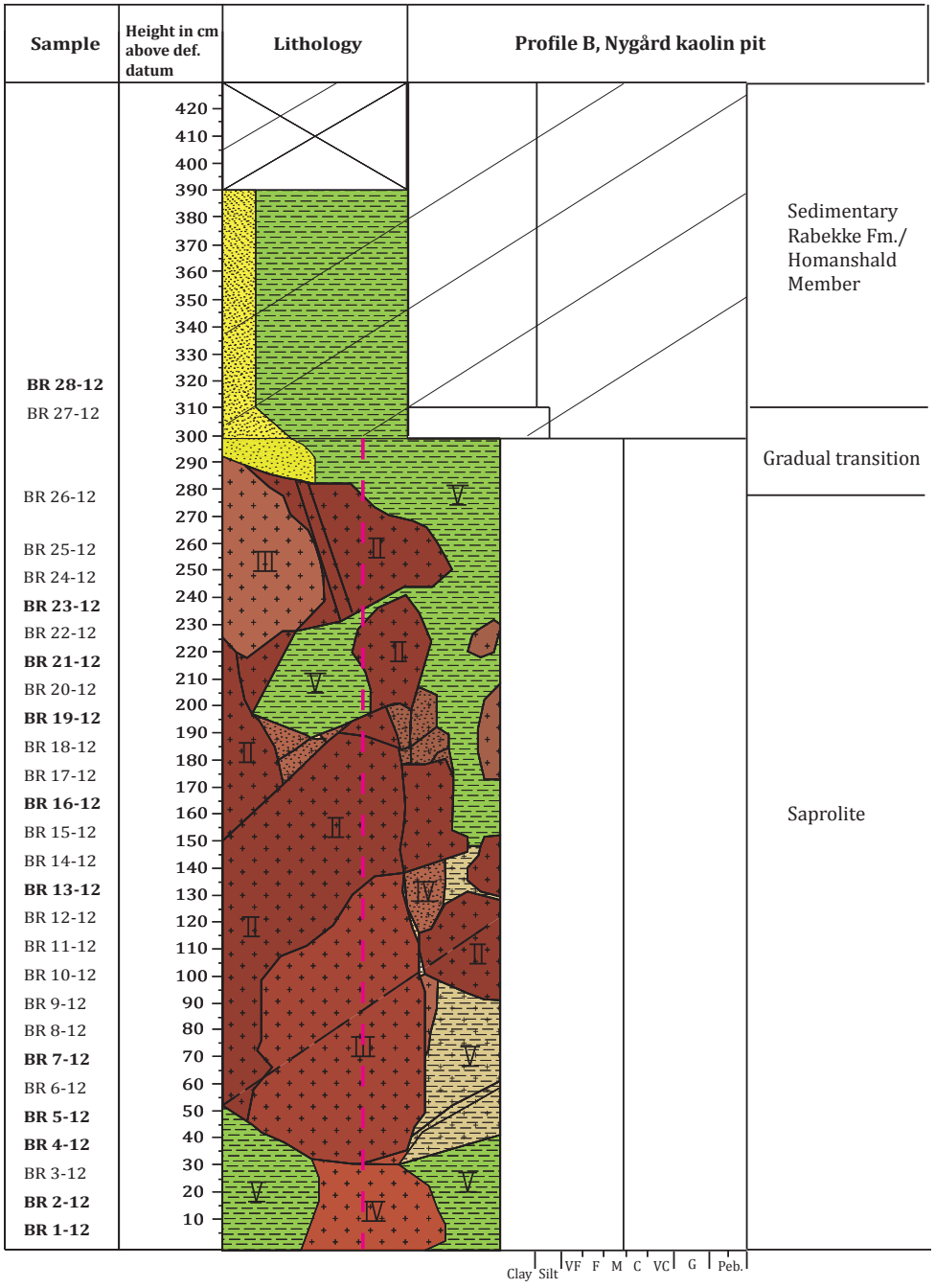

Figure 3.15: Profile log section B, legend see Figure 3.14. Weathering classification based on field observations of the heterogeneous, weathered protolith is illustrated by roman numbers (see Figure 3.13). Pink, dashed line indicates the path along samples have been extracted. The samples gathered in this section are illustrated on the left side. Note that samples printed in bold font distinguish the samples selected for petrographical and mineralogical observations. The profile was divided based on field observations into the lower saprolite horizon and the uncomformably overlaying lower Rabekke Formation, the Homanshald Member. The lithological border is marked by a gradual change from the weathering unit to the residual soil. For the upper sedimentary cover a classical logging approach was conducted. The upper part was neglected, due to the strong gradual transition and the main emphasis on the weathering section in this illustration.

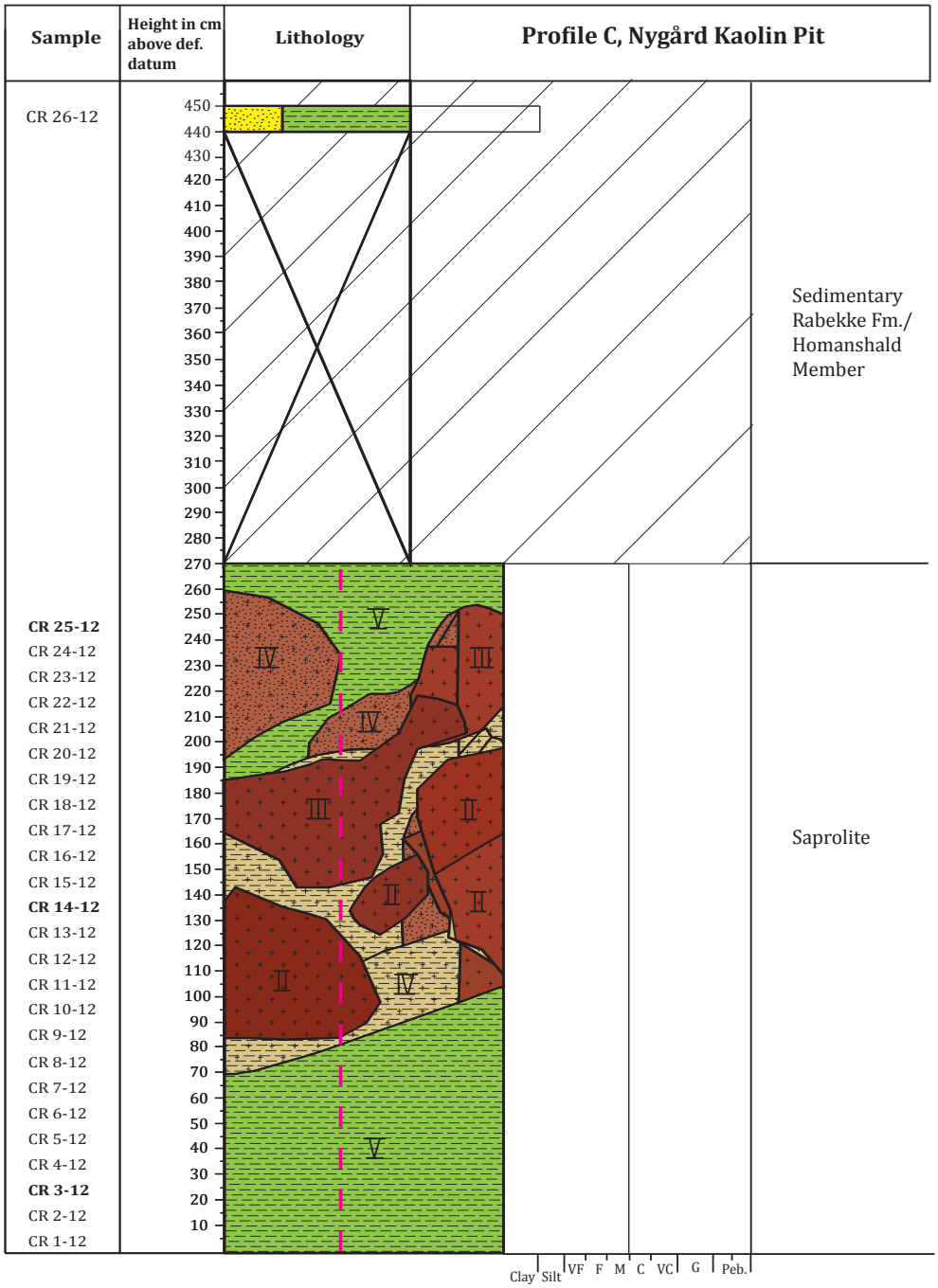

Figure 3.16: Profile log section C, legend see Figure 3.14. Weathering classification based on field observations of the heterogeneous, weathered protolith is illustrated by roman numbers (see Figure 3.13). Pink, dashed line indicates the path along samples have been extracted. The samples gathered in this section are illustrated on the left side. Note that samples printed in bold font distinguish the samples selected for petrographical and mineralogical observations. The profile was divided based on field observations into the lower saprolite horizon and the uncomformably overlaying lower Rabekke Formation, the Homanshald Member. The lithological border is marked by a gradual change from the weathering unit to the residual soil. For the upper sedimentary cover a classical logging approach was conducted. The upper part was neglected, due to the strong gradual transition and the main emphasis on the weathering section in this illustration.

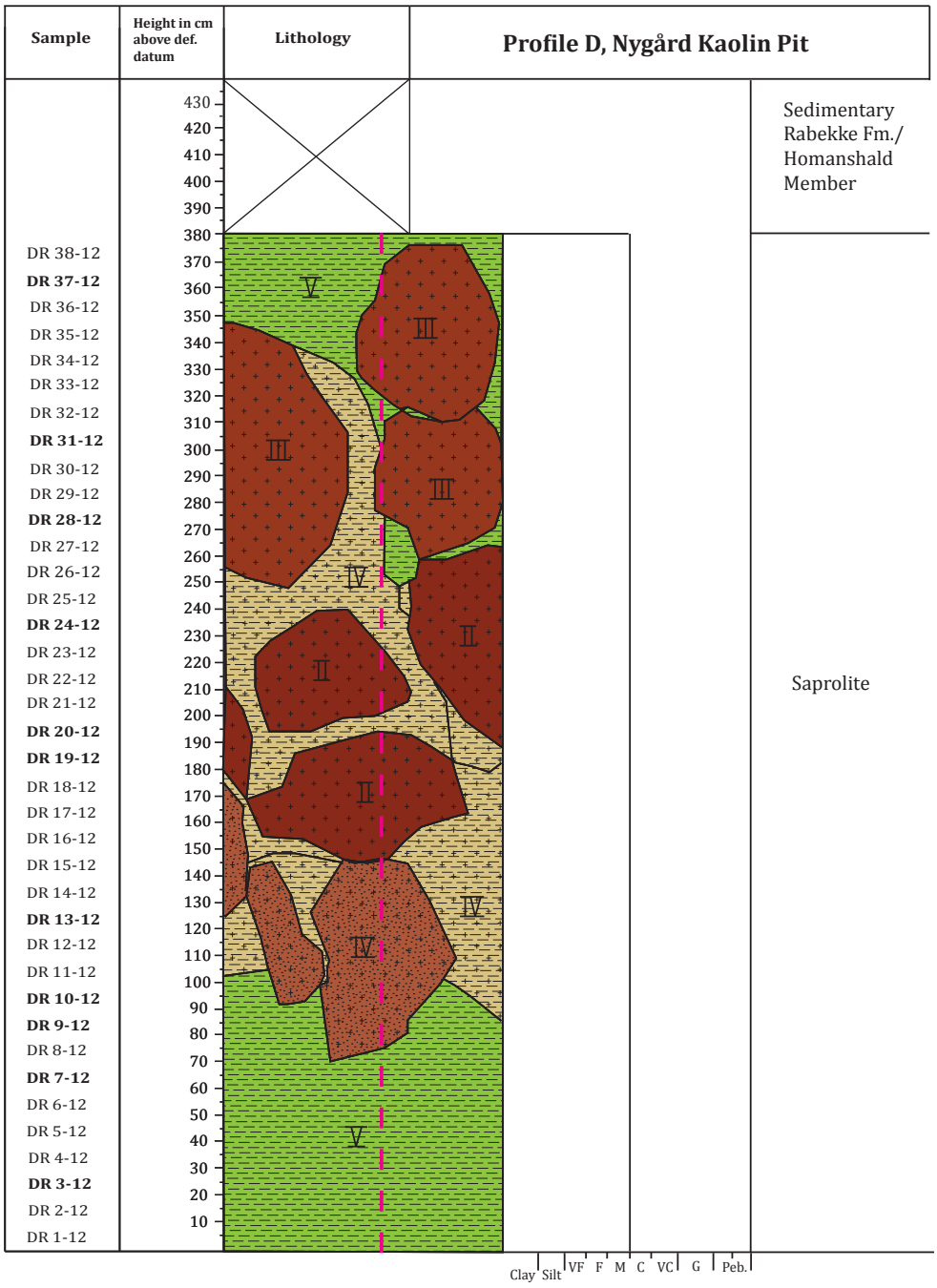

Figure 3.17: Profile log section D, legend see Figure 3.14. Weathering classification based on field observations of the heterogeneous, weathered protolith is illustrated by roman numbers (see Figure 3.13). Pink, dashed line indicates the path along samples have been extracted. The samples gathered in this section are illustrated on the left side. Note that samples printed in bold font distinguish the samples selected for petrographical and mineralogical observations. The profile was divided based on field observations into the lower saprolite horizon and the uncomformably overlaying lower Rabekke Formation, the Homanshald Member. The lithological border is marked by a gradual change from the weathering unit to the residual soil. For the upper sedimentary cover a classical logging approach was conducted. The upper part was neglected, due to the strong gradual transition and the main emphasis on the weathering section in this illustration.

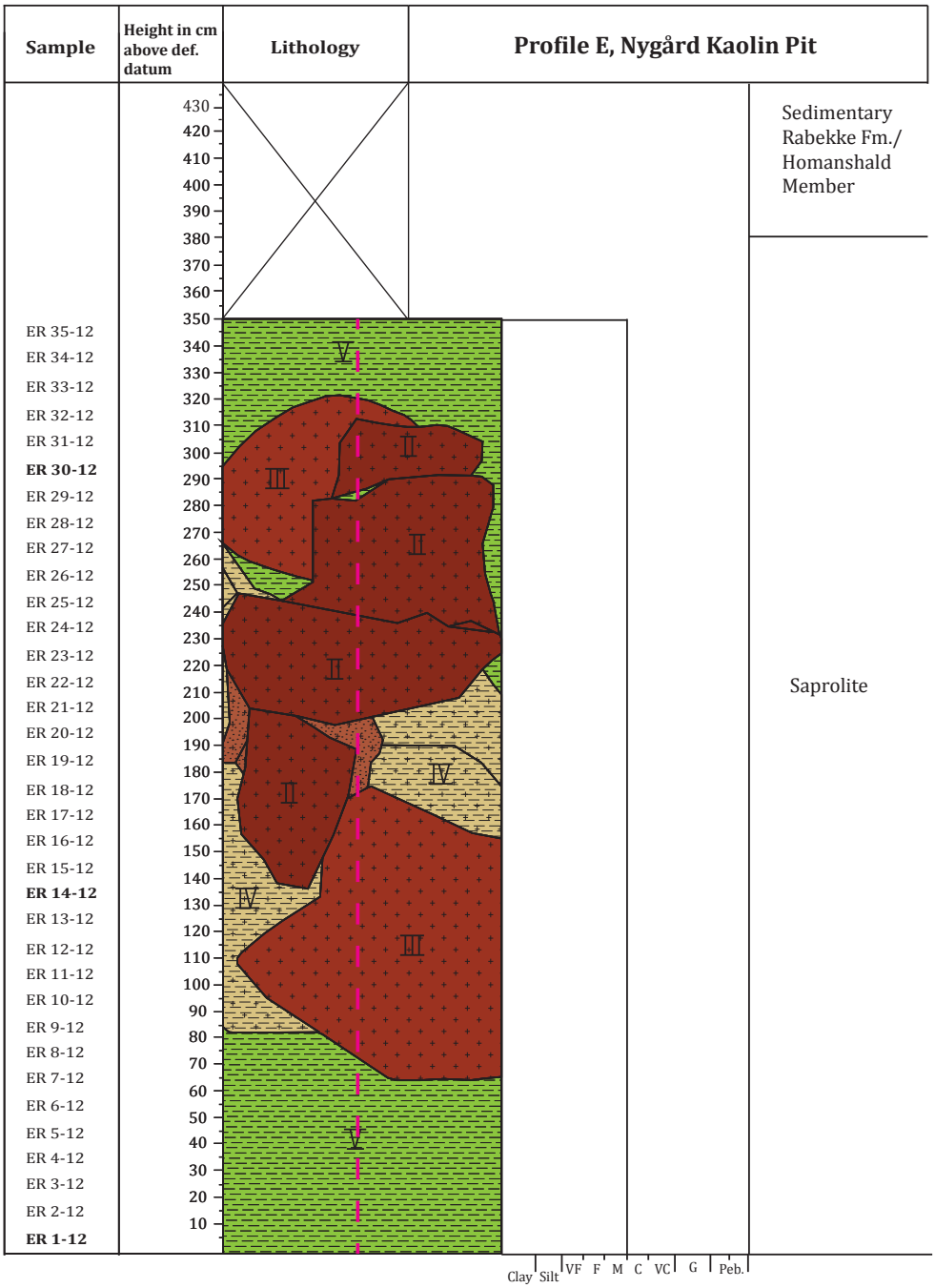

Figure 3.18: Profile log section E, legend see Figure 3.14. Weathering classification based on field observations of the heterogeneous, weathered protolith is illustrated by roman numbers (see Figure 3.13). Pink, dashed line indicates the path along samples have been extracted. The samples gathered in this section are illustrated on the left side. Note that samples printed in bold font distinguish the samples selected for petrographical and mineralogical observations. The profile was divided based on field observations into the lower saprolite horizon and the uncomformably overlaying lower Rabekke Formation, the Homanshald Member. The lithological border is marked by a gradual change from the weathering unit to the residual soil. For the upper sedimentary cover a classical logging approach was conducted. The upper part was neglected, due to the strong gradual transition and the main emphasis on the weathering section in this illustration.

3.2.2 Fracture measurements

Fracture sets were registered using a simple compass, for estimating the general strike direction, with integrated clinometer for detecting the dip angle of the measured fracture or joint. The right hand rule was applied for all measurements, to gain consistent results. All acquired values were then plot in rose diagrams presented in Table 3.3 for the Klippeløkken granite quarry and Figure 3.20 for the Nygård kaolin pit.

3.2.2.1 Klippeløkken granite quarry

The fracture measurements at Klippløkken granite quarry (Figure 3.19), approximately 800 m ENE of the studied saprolite section at Nygård, resulted in the determination of two dominant strike directions of the fractures and fault encountered. The ascendant strike orientation was NNW to SSE (350°) and ENE to WSW (70°), which coincides with the macro-scale fault orientations of the south-western margin of the island, as displayed in Figure 1.1. Intersection angles of fractures on a minor scale were often determined in characteristical 60°and 120°.

Table 3.3: Sumary table for fracture measurements at Klippeløkken granite quarry

Klippeløkken Quarry		
No. of measurement	Strike	Dip
1)	344	24
2)	134	44
3)	064	84
4)	159	76
5)	360	24
6)	162	24
7)	296	17
8)	252	88
9)	346	23
10)	061	86
11)	360	24
12)	083	33
13)	063	90
14)	360	84
15)	344	18
16)	210	40
17)	010	25

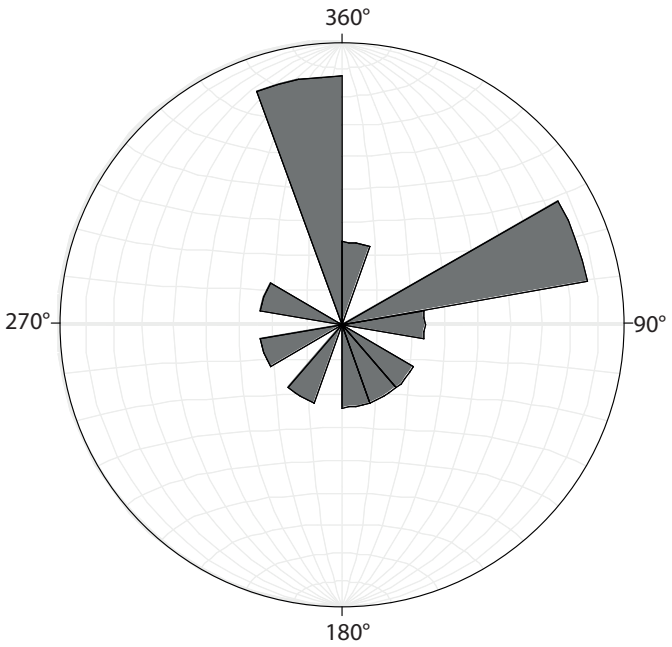

Figure 3.19: Klippeløkken quarry, dominant strike directions of 350°(NNW) and 70°(ENE) are displayed. A mean dip angle was calculated of 47.3°

3.2.2.2 Nygård kaolin pit

Fracture measurements in the weathered section at Nygård, are less distinct according the overall trend than in the source rock, but still compute well with the dominant strike directions measured in the protolith. The majority (about 80%) of fractures strike within 335°and 10°(NNW-SSE and NNE-SSW), and < 20% of the fractures were recorded to strike in WNW to ESE (70°). Remarkable is the strong resemblance of fractures striking towards 10°, may indicating minimal tectonic influence.

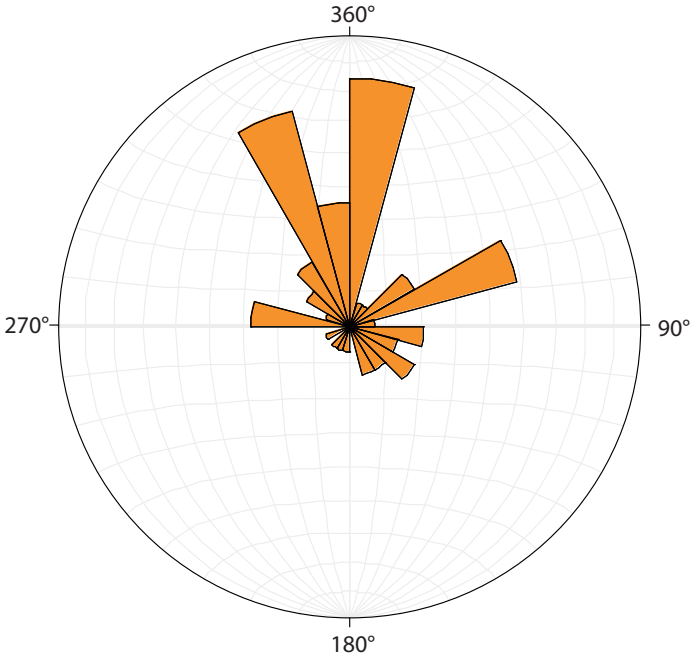

Figure 3.20: Nygård kaolin pit, dominant strike direction was estimated of > 80% between 335°and 10°. < 20% strike towards 70°and a mean dip angle of 38°was estimated.

Table 3.4: Summary table for fracture measurements at the Nygård kaolin pit

Nygård Kaolin Quarry								
No. of measurement	Strike	Dip	No. of measurement	Strike	Dip	No. of measurement	Strike	Dip
1)	330	18	18)	052	25	35)	056	44
2)	360	38	19)	060	70	36)	330	26
3)	006	20	20)	344	36	37)	017	40
4)	006	20	21)	320	18	38)	037	53
5)	006	20	22)	320	18	39)	008	52
6)	190	74	23)	348	48	40)	360	72
7)	348	52	24)	098	30	41)	336	36
8)	344	8	25)	070	46	42)	338	62
9)	200	58	26)	050	40	43)	012	24
10)	090	12	27)	006	72	44)	010	40
11)	090	12	28)	347	60	45)	144	80
12)	120	13	29)	062	30	46)	332	28
13)	360	46	30)	283	4	47)	310	22
14)	010	26	31)	283	4	48)	280	18
15)	120	28	32)	350	62	49)	110	80
16)	134	36	33)	014	54			
17)	064	50	34)	326	38			

3.2.3 Gamma ray measurements

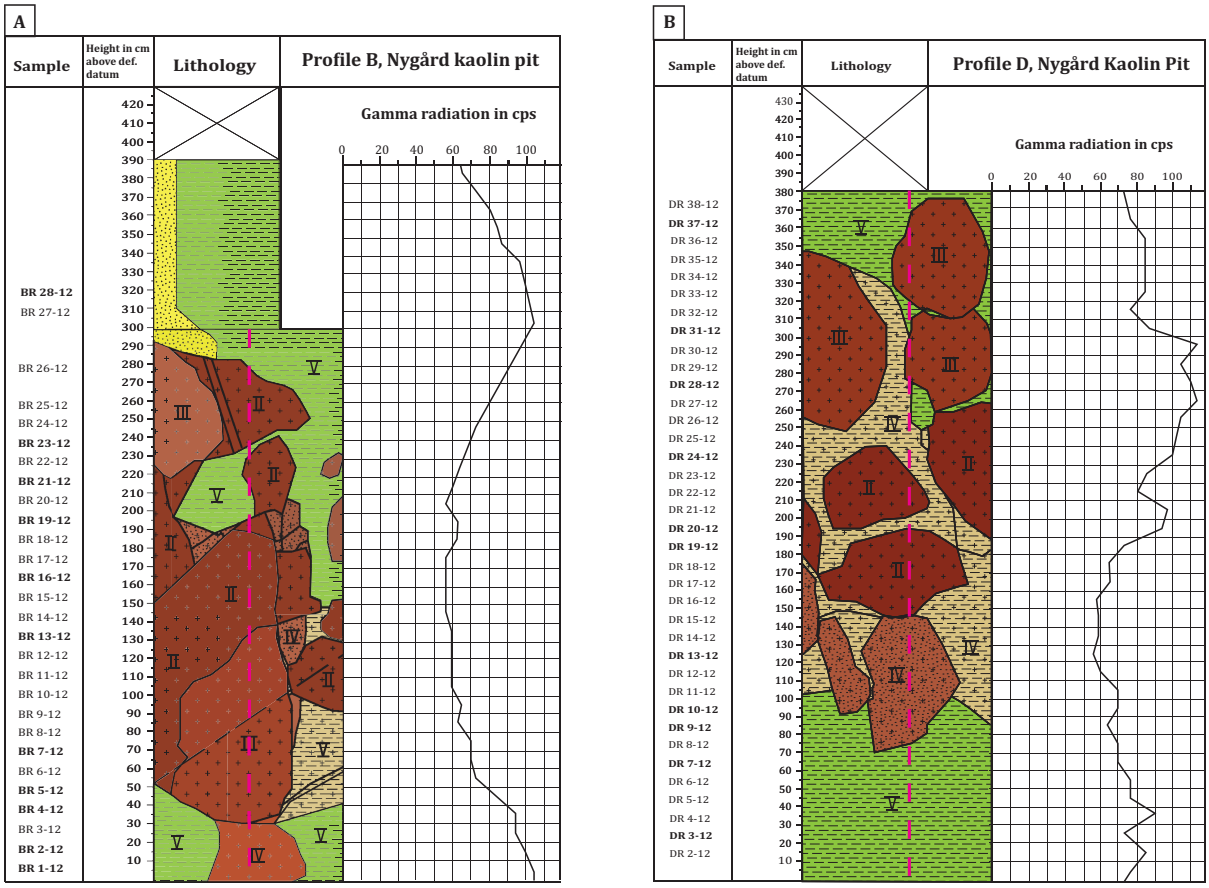

Figure 3.21: Gamma ray logs of the measured a) profile B and b) profile D.

The natural emitted gamma radiation of Th, U and K measured in the saprolite of profile B and D are presented in Figure 3.21. Relatively low cps (counts per second) values (40 cps to 120 cps) are recorded in both profiles with marginally higher maximum values of 115 cps in profile D compared to profile B. The rock assemblage in profile B comprises lower emittance of about 60 cps in the medium part of the section, where less weathered, more massive corestone associations were observed. In the lower most 50 cm and the upper most parts of profile B, higher weathered material was studied, which may lead to enhanced radiation. Approximately 100 cps were recorded in highly weathered parts of section B. This trend corresponds to the more heterogeneous profile D, in which more distinct and rounded corestone boulders are embedded in the saprolitic strata, which exhibit a higher variation of the γ-radiation curve. The mean radiation increases in section D, which may be associated with the higher portion of increased weathering facies interfering with decreased corestone assemblage.

3.2.4 Petrographical and mineralogical description of the weathering section

3.2.4.1 Thin section analysis

The thin section description includes detailed analysis of sample slides from profile B and profile D. Each section confines 11 samples respectively, of which most representative slides were selected and compared, to enhance and refine the introduced weathering classification of the field observations. Previously presented weathering facies associations, derived from field-observations are complemented by thin section observations. Weathering processes, and their products, are highly heterogeneous in 3-dimensional manner, emphasis was rather put on finding comparable petrogenic characteristics in profiles B and D, than following each profile line in consecutive order. The results of mineral trend estimations within each specific profile will be printed in the following section (XRD results).

Thin sections were categorized according the increasing denudation of plagioclase feldspar, estimated from point counting (for summary of point counting see Table B.1; the results of the classification are given in Table 3.5). The point counting quantification revealed characteristic borders which led to the approximated categorization of the slides as illustrated in Table 3.5. The primarily classified sections were then optically analyzed in detail to observe wether the distinguishing approach of weathering facies according quantitative amounts of the primary mineral minerals, such as plagioclase, is applicable or more detailed elemental analysis are necessary.

Table 3.5: Weathering class categorization of thin sections, according plagioclase abundance in samples, derived from point counting. Note, that plagioclase decreases vertically within each column and horizontally with increasing weathering class.

I (> 20% plag.)	II (> 11% plag.)	III (< 11% plag)	IV (< (8.5% plag)	V (< 3% plag.)
Q1-12	DR20-12	BR7-12	BR2-12	DR10-12
Q2-12	DR28-12	BR19-12	DR24-12	BR21-12
		DR19-12	BR19-12	
		DR37-12	BR16-12	
		BR4-12	DR3-12	
			DR7-12	
			DR13-12	
			BR5-12	
			DR9-12	
			BR1-12	
			DR31-12	
			BR28-12	
			BR23-12	

3.2.4.2 Thin section analysis Profile B and D

Due to the distance of about 800 m to the fresh granite quarry at Klippeøkken, which was categorized as weathering facies I, the classification of higher order weathering facies at Nygård kaolin pit had to be chosen carefully. First categorization, as mentioned above, was conducted according the amount of plagioclase, based on point counting analysis. In the next strep, logical location of the sample within the corestone complex was encountered, meaning that field classification based on hand specimen characteristics combined with the overall, quantitative, petrogenic appearance are compared with the subsequent thin section analysis.

Weathering facies II (Corestone association) Corestone members of weathering facies II were classified according one thin section of each profile B and profile D. Sample BR16-12 from a height of 1.60 m- 1.70 m in Profile B and DR20-12 from 1.90 m- 2.00 m in profile D (see Figure 3.15 and Figure 3.17) were evaluated being most representative slides for this facies. Sample BR16-12 (Figure 3.22) is under-represented in the amount of plagioclase feldspar, only 7.2% could be distinguished. Additionally 5.2% biotite were estimated, section BR16-12 was rather classified based on its optical appearance in thin section, than with respect to the mineral abundance estimated from point counting analysis.

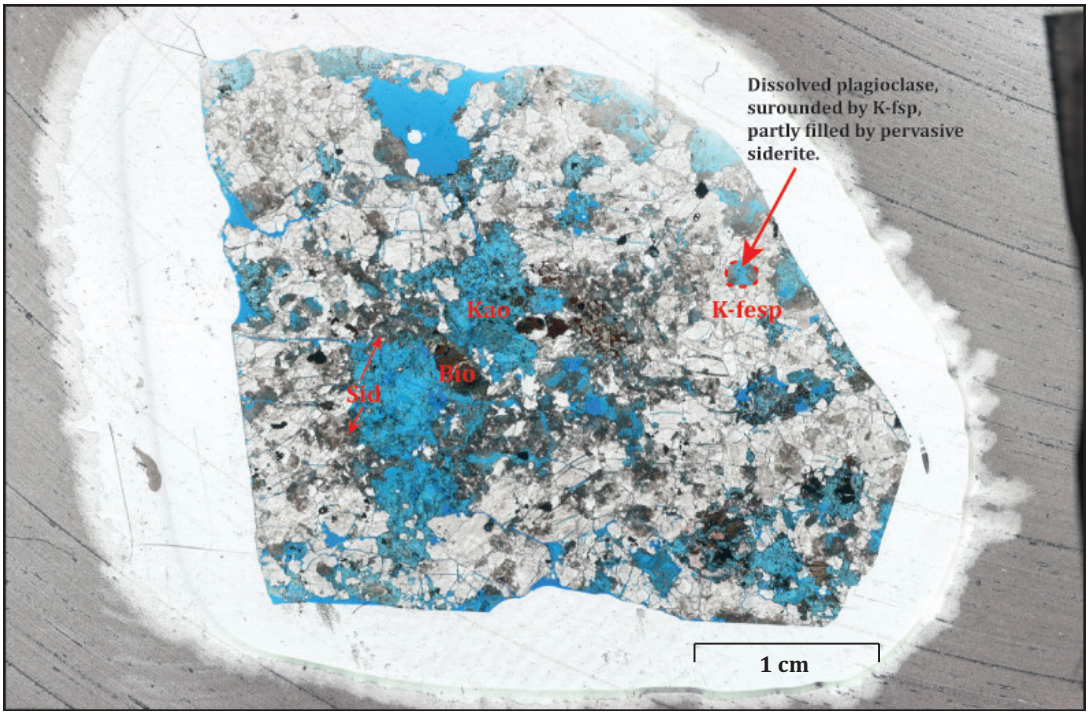

Figure 3.22: Thin section scan BR16-12 of weathering facies II, showing already strong weathering pronunciation. Plagioclase is mostly dissolved and party replaced by sideritic carbonates. Quartz and K-feldspar remained mostly unaltered. The blue epoxy displays pore-space, but also may cover kaolinite, usually displayed as white to gray booklets within the inter-mineral voids

Mafic components in thin section BR16-12 are mostly absent, hornblende represented only by 0.5% is just sparsely remained in minor splays. Biotite, in the fresh rock represented with up to 10 % (point counting Table B.1) can only be observed in scattered layers, often splayed along the 001 plane. Pleochroic color formerly deer-brown (E-W) and light brown (N-S) in fresh samples, displays now more disperse coloring and a strong greenish stain, often found along the mineral margins. High magnification analysis indicate transformation of biotite to illite. Zircons, previously observed as pleochroic inclusions in biotite, are often dislocated from its primary host.

Felsic compartments, such as quartz and feldspar show strong meso-fracturing in ppl, no cleavage trend could be observed. The fractures, formerly opened pathways for percolating solutions are now mostly filled by pervasive overgrowing carbonates. Fe-rich siderite is the foremost carbonate component with 21% estimated from point counting. However, calcite recognized by its extremely high birefringence color of an higher order in xpl is found frequently within pore spaces. Regular overgrowth of carbonate might indicate late diagenetic precipitation.

Quartz was observed as second most dominant phase with approximately 15%. Grain sizes appear decreased, compared to the fresh samples and grain boundaries are often more rounded. Mineral surfaces were microscopically unaltered. Grain orientations are similar to those of the fresh granite and flash figure appearance could be observed as well.

K-feldspar, represented with approximately 27% in sample BR16-12 appears highly heterogeneous. Some grains display anhedral mineral-mineral margins, optically unaltered, whereas others seemed more prone to weathering along their margins. Remaining K-feldspar rims, surrounding now mostly dissolved plagioclase, occur more prone to alteration on the interior side, where plagioclase was replaced by kaolinite and now over-grown by siderite. Polysynthetic twinning and typical tartan twinning in microcline minerals, distinguished according its biaxial negative character under conoscopic view, is clearly less determined as in fresh samples.

The pore space of this sample is commonly filled by fine crystalline kaolinite, displaying in highest magnification (40x10) characteristic booklet stacking of the clay mineral. Illite clay minerals could be anticipated, but not clearly distinguished, as the minerals in the pore space were too small for microscopic analysis.

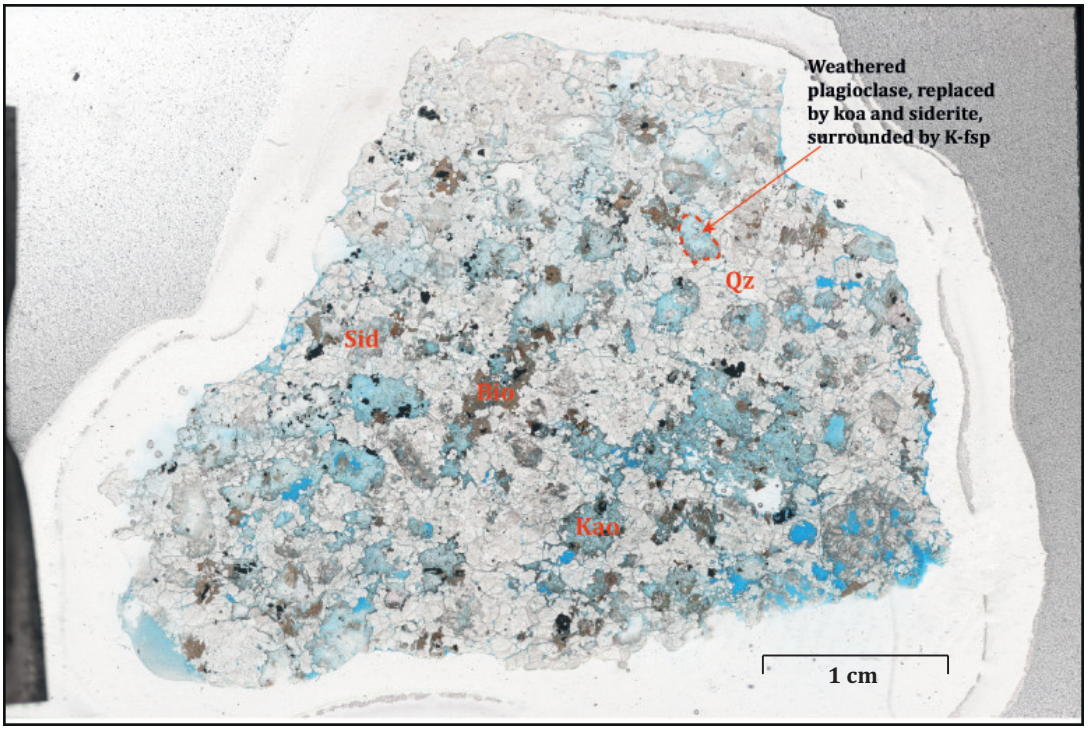

Figure 3.23: Thin section scan DR20-12 of weathering facies II, showing already strong weathering pronunciation. Plagioclase is mostly dissolved and party replaced by sideritic carbonates. Quartz and K-feldspar remained mostly unaltered. The pore space demarcated by blue epoxi is less pronounced than in BR16-16.

Sample DR20-12 (Figure 3.23) exhibits similar characteristics as observed in BR16-12. The mafic mineral biotite is more abundant in thin section DR20-12 with 10.5%, than in BR16-12 (5.2%). Scattering along the 001-plane, pleochroic discoloration and absence of pleochroic inclusions are common features with sample BR16-12. Meso-fracturing of the felsic components, such as feldspar and quartz seems less pronounced as in the sample from profile B. Quartz mineral shapes are commonly subhedral and grains display enhanced rounding as observed in the previous sample. K-feldspar, as in the formerly presented section appears mostly inert to weathering, but shows initial dissolution along mineral interior margins, where plagioclase was replaced by kaolinite and later carbonate. The siderite content in DR20-12 is lower, with 13.2%, compared to BR16-12. Calcite seems to exceed the amount of siderite, based on optical judgement. Inter-mineral void spaces are more homogeneously filled with kaolinite.

Based on microscopical analysis, weathering facies II is mostly characterized by reduced abundance of plagioclase. More fragmented minerals could be observed mostly surrounded by K-feldspar. Hornblende seems highly affected by alteration, partly remained fragments were studied adjacent to chlorite and might be associated with mixed-layer clay minerals.

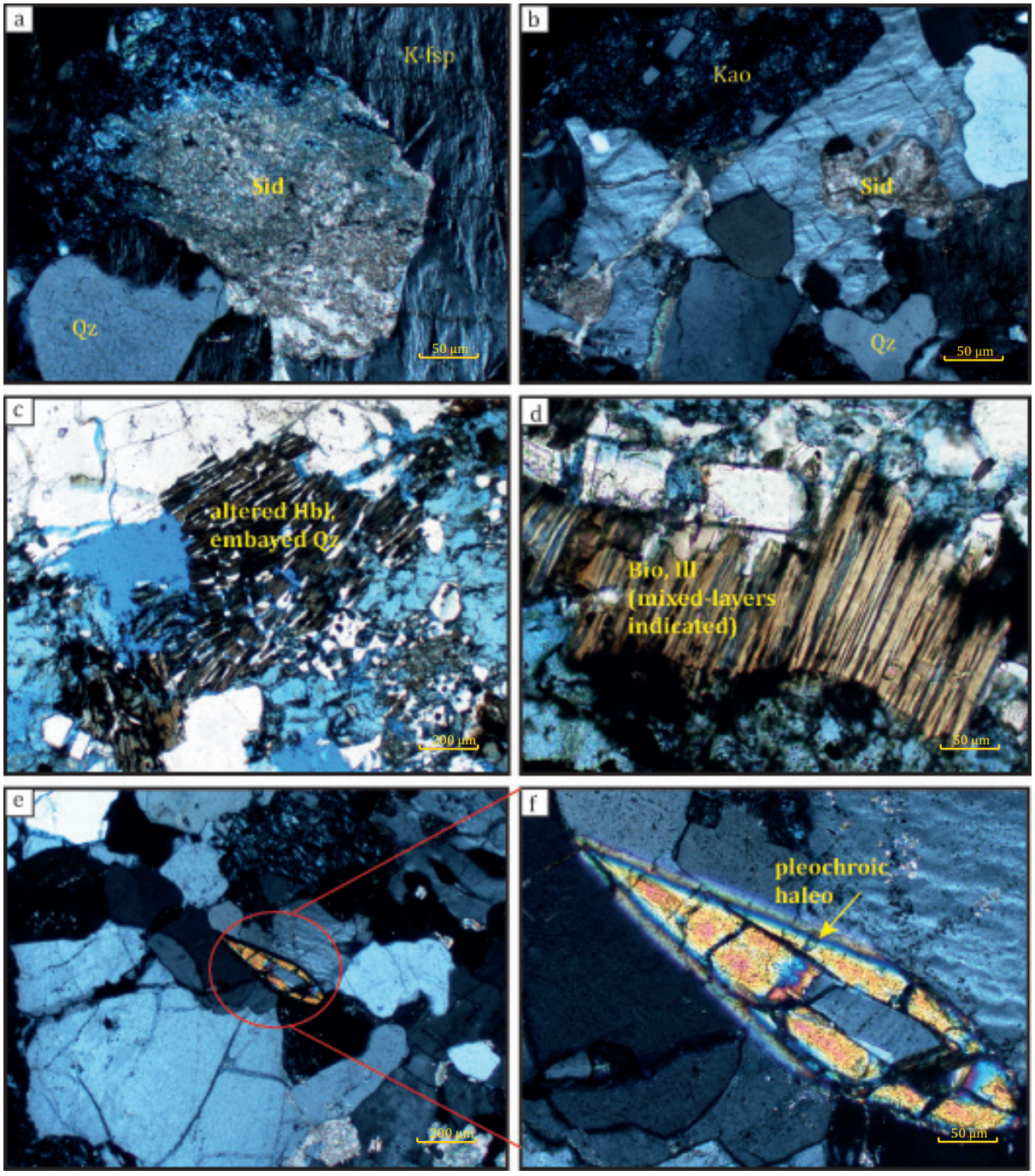

Figure 3.24: Cross polarized light (xpl) images, taken with a *Microphot SA* microscope, with a *NIKON DS-Fi1* camera of mineral associations of weathering class II. a) Pervasive growth of siderite, microcline seems effected by weathering (BR16-12). b) Overview photo over microcline pervaded by siderite and embayed quartz grain. c) Altered hornblende mineral, scattered, with embayed polycrystalline quartz (DR20-12). d) Altered biotite crystal, increasing alteration along 001 plane fringes. e) Drop shaped pleochrioc halo of zircon and f) close up photo showing dispersion colors along the zircon mineral margins, embedded in K-feldspar and quartz.

Weathering facies III Weathering association class III is represented in thin section according sample BR13-12 of profile B, taken from a height between 1.30 m to 1.40 m and sample DR37-12 extracted between 3.60 m and 3.70 m.

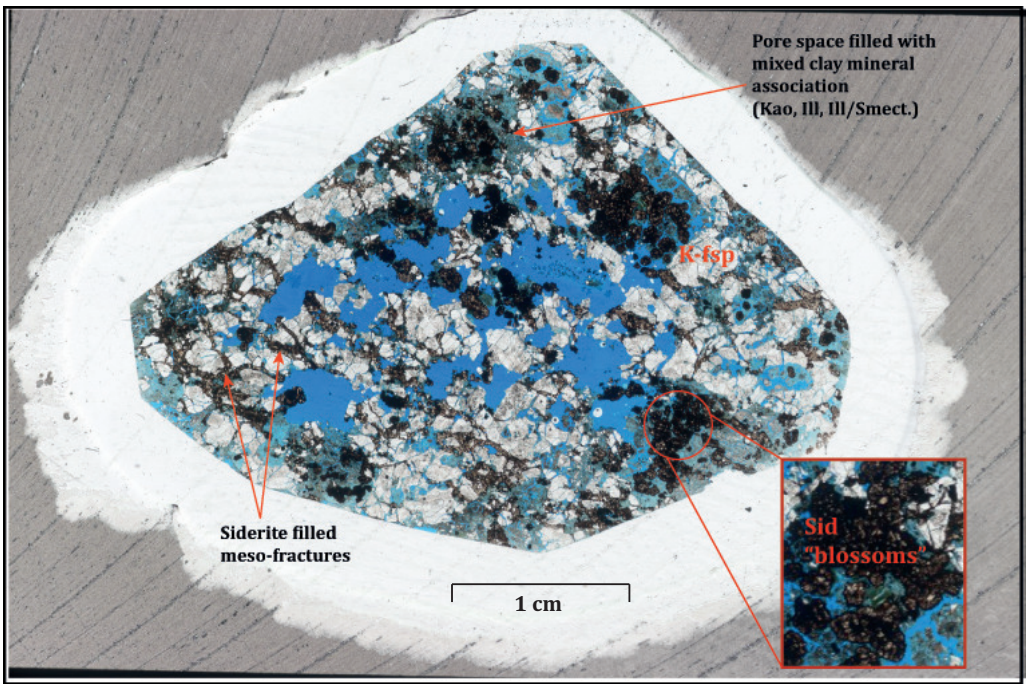

Figure 3.25: Thin section scan BR13-12 of weathering facies III. Siderite blossoms (red circle) are well defined and oxidized along the rims, especially in open void space. Sideritic fracture filling was commonly observed in felsic components.

Main characteristics found in BR13-12 (Figure 3.25) compared to weathering facies II appear to be a strong increase of clay associations. The dominantly felsic phenocrysts of optically unaltered quartz (4.7%) and significantly more altered microcline (20%) can be hardly described as subhedral. Clearly size reduced quartz and microcline minerals are often intergrown and, thus give more room for the authigenic, pervasive overgrowth of siderite, which commonly forms ”blossom” like crystallization features and is represented by 20% in this section. Higher degree of oxidized iron staining of corona shape can be observed along the mineral margins of such ”blossom”.

Mafic minerals appear mostly destroyed and replaced by different clay minerals. Preserved structures of the layer silica biotite, now transformed into green-brown minerals, still showing pleochroic behavior. Kaolinite may be described as cryptocrystalline, since the blue appearing minerals (due to the epoxy) could only be distinguished according their weak birefringence color with crossed polarizers. Microcline, K-feldspar surfaces exhibit much higher effected surface alteration, compared to weathering facies II and polysynthetic twinning becomes increasingly blurried.

Sample DR37-12 (Figure 3.26) was used as example for weathering facies III. Microscopical results for this section are for the most incidences comparable to the previous slide

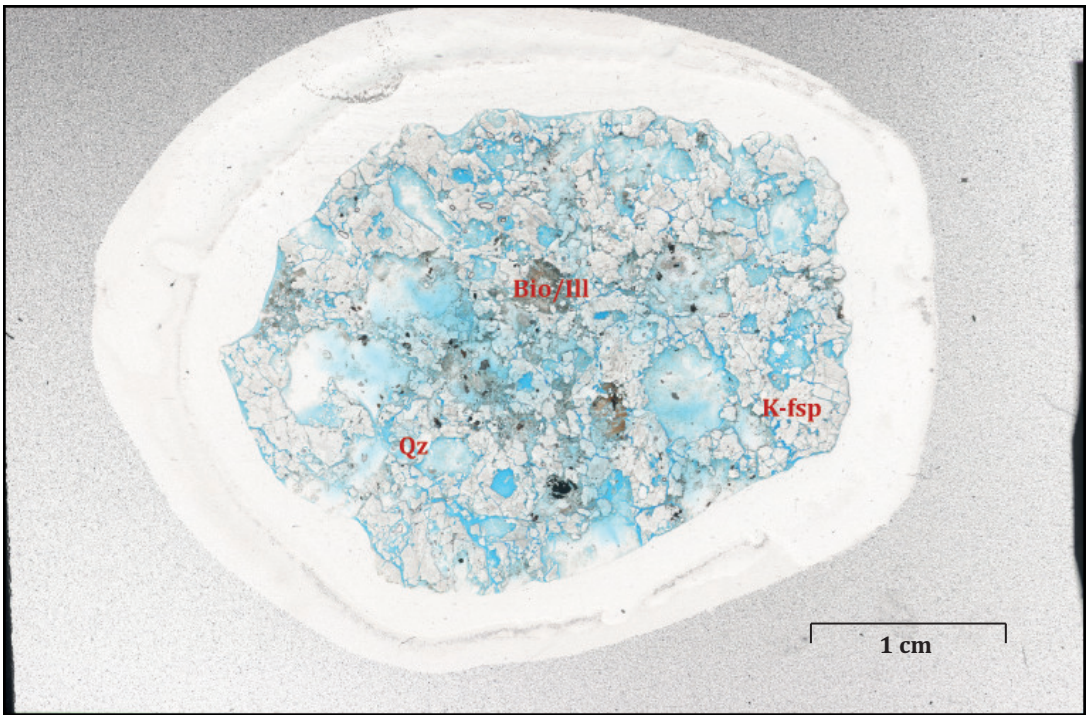

Figure 3.26: Thin section scan DR37-12 of weathering facies III.

(Figure 3.25), with the difference that clay associations of the proto-crystaline biotite are not as maturely defined as in BR13-12. Brown pleochroic color is still preserved and mineral transformation seem more mature. Further, the quartz phenocrysts appear more rounded compared to BR13-12. Siderite is completely absent in this slide.

As summary for weathering facies III, it might be summarized that weathering resistant microcline seems effected at its surface, grain sizes are increasingly reduced and clay mineral association become more dominant and more common.

Weathering facies IV Weathering facies IV will be presented according sample BR2-12 (0.1 m-0.2 m) (Figure 3.27)and sample DR24-12 (2.30 m to 2.40 m) (Figure 3.28)of the two respective profiles. It comprises a consecutive decomposition of the less prone K-feldspars. Mineral margins appear increasingly etched and quartz grain surfaces seem more fractured, compared to weathering facies III.

Mid temperature polymorph of K-feldspar, orthoclase can be more easily distinguished in this stage of alteration, according its low relief and weak pleochroism in ppl, compared to less weathered samples. Characteristic carlsbad twinning, such as its conoscopic image revealed negative biaxial character, with a small 2V of about 10°. Orthoclase appears less altered than the low temperature variant microcline. Perthitic exsolution in microcline crystals becomes determined in lesser amounts and sericitic inclusions are more clearly determined indicating higher weathering resistance of the cryptocrystalline micas. Sericite is only abundant with

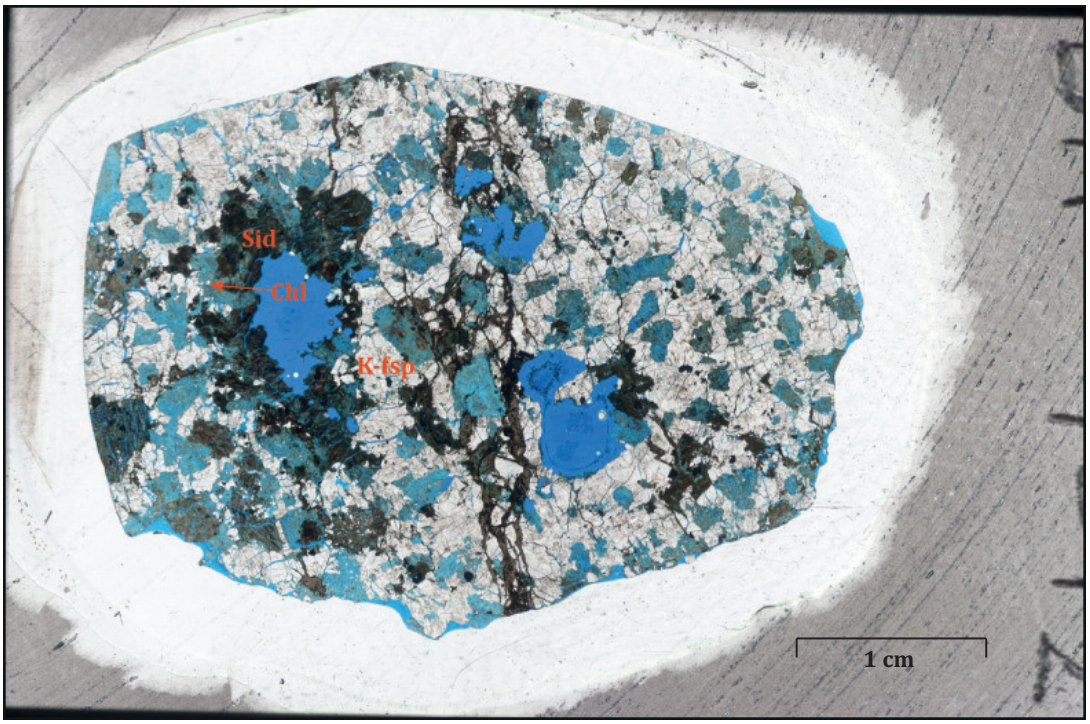

Figure 3.27: Thin section scan BR2-12 of weathering facies IV.

11% and rather associated with pervasive fracture filling.

Biotite, just vaguely distributed as scattered layer pieces in III is now completely transformed into apparently multiple clay minerals, of which ill it may be defined under the microscope. Hornblende, barely distinguishable in class III displays now more obviously the source for chloritoid clay minerals, characterized by its significant pleochroism (light green to dark green, from N-s to E-W).

Siderite ”blossom”-structures are absent. Commonly, siderite shows dark red, corona like staining along its mineral margins, indicating oxidation conditions. Kaolinite, such as other clay associations appear in patches within the intra- and inter-mineral void spaces.

In section DR24-12 illustrated in Figure 3.28, observed under plain polarized light (ppl), the mafic components are nearly absent only small pieces remained, as highly altered fractures. Under xpl the mineral assemblage of DR24-12 seems very scattered and mineral margin relations may rather be described as xenomorphic and adjacent to cryptocrystalline kaolinitic clay. In difference to slide BR2-12, siderite is absent (5%) and the kaolinite concentration is fairly high with 27%. General mineral features are comparable to BR2-12.

In weathering facies IV, K-feldspar varieties become more easily to distinguish, orthoclase seems less prone to alteration, than microcline. Clay associations are increasingly determined

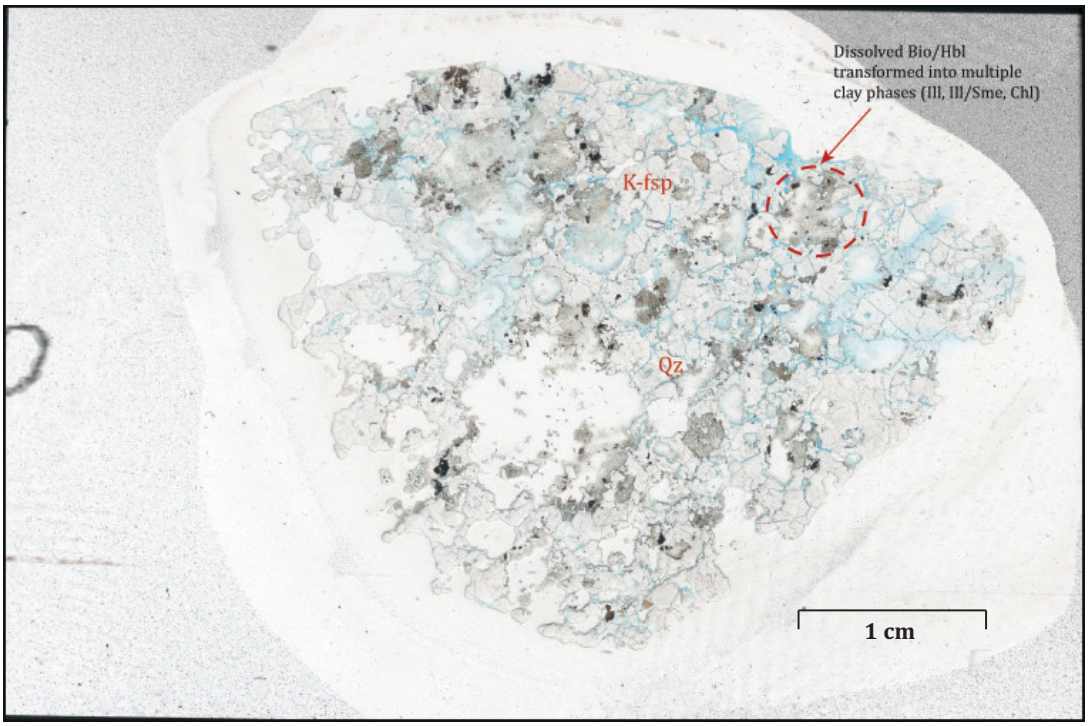

Figure 3.28: Thin section scan DR24-12 of weathering facies IV.

and encounter more space.

Weathering facies V Weathering facies V is characterized by sample RaF 3B-1985, taken from the upper most part of the kaolinite succession, when the kaolinite quarry was still active back in 1985 (Figure 3.29) [4]. The sample comprises mostly cryptocrystalline kaolinite booklets, forming the ground mass for edge-rounded to rounded quartz phenocrysts. Kaolinite booklets are frequently distinguishable under the microsope. Primer mineral associations of K-feldspar are entirely altered. Despite the main clay association with kaolinite, sparse traces of illite according color difference may be devined.

Microscopical weathering classification of single mineral associations After classifying hand specimen, based on field observations and bulk rock assemblages in thin section, an attempt has been conducted to find weathering stages restricted for single mineral association. Figure 3.30 displays the anticipated weathering sequence of plagioclase (a, c, e, g and i), mafic assemblages of biotite and hornblende (often inter-grown) in images b, d, f, h and j.

- I: plagioclase, initially showing characteristic sericitization in two orientations. First along cleavage-, polysynthetic- twinning planes and second along mesofractures, displayed in image a). The suggested weathering sequence for mafic mineral components

[4]Prof. Henning Dypvik contributed this sample slide, since such pure kaolinite was not accessible any longer, after the pit was filled with water.

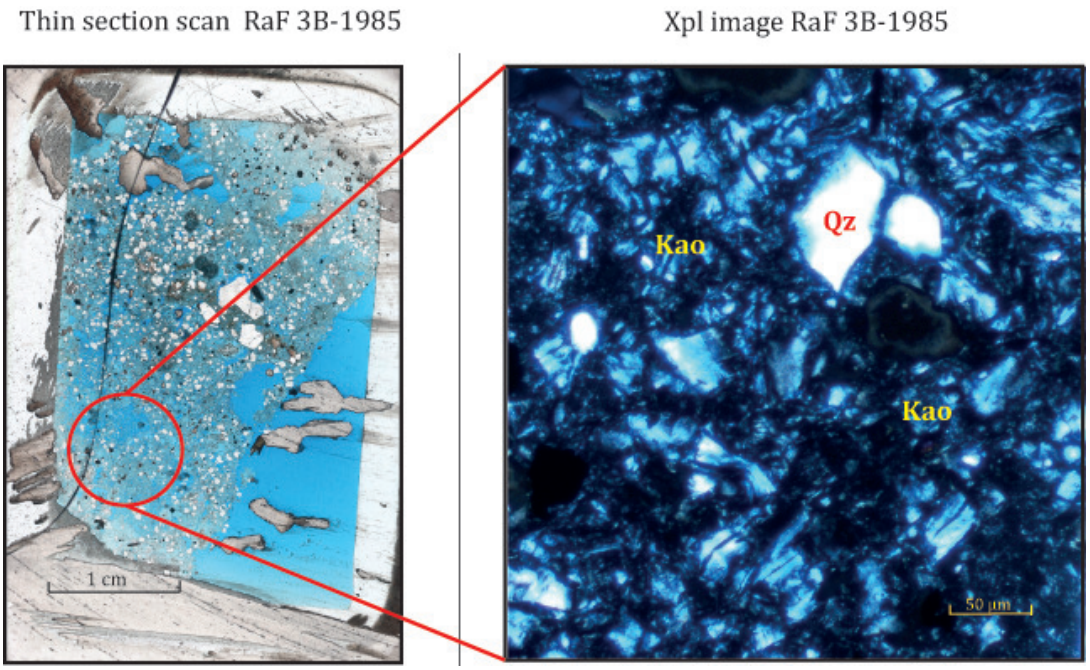

Figure 3.29: Thin section scan of sample RaF3B-1985 showing high abundance of kaolinite compared to size diminished quartz clasts. Right hand side image shows the section under cross polarized light, with micro- to cryptocrystalline kaolinitic matrix. Single booklet structures can be observed. Quartz clasts in this sample are a view mm to cm in size and often edge-rounded.

is displayed on the right hand side of the template (Figure 3.30). Image b) comprises a unweathered hornblende crystal (olive green, two cleavage directions), inter-grown with light brown biotite.

- II to IV: show increasing dissolution of plagioclase along meso-fractures (image c) and g)). White ”dissolution-paths” and myrmektitic-like dissolution of the feldspar may constitute prolonged weathering, as displayed in image e). This stage determines the initial break up of plagioclase in flakes and the transformation into kaolinite. Hornblende dissolves faster compared to biotite, as displayed in image d). Biotite remains more stable, but weakened along 001 cleavage. Prograding disillusion of biotite can be seen in image f) where remnant wafers of biotite illustrate increasing transparency and alteration of the layer silica. Pervasive overgrowth of siderite is observed, which due to the overgrowth is associated with later diagenetic or authigenic processes. Remarkable for the dissolution of biotite with prolonged weathering is the variation in the weathering mode. Partly biotite dissolves and becomes as mentioned more transparent, or the minerals become more scattered and splayed, as displayed in Figure 3.30 h).
- V: is characterized by almost entirely dissolved plagioclase feldspar and rudimentary remains of sericite (image i)) this might display the latest stage of plagioclase dissolution. The cryptocrystalline muscovite appears more weathering resistant, compared to biotite or hornblende.

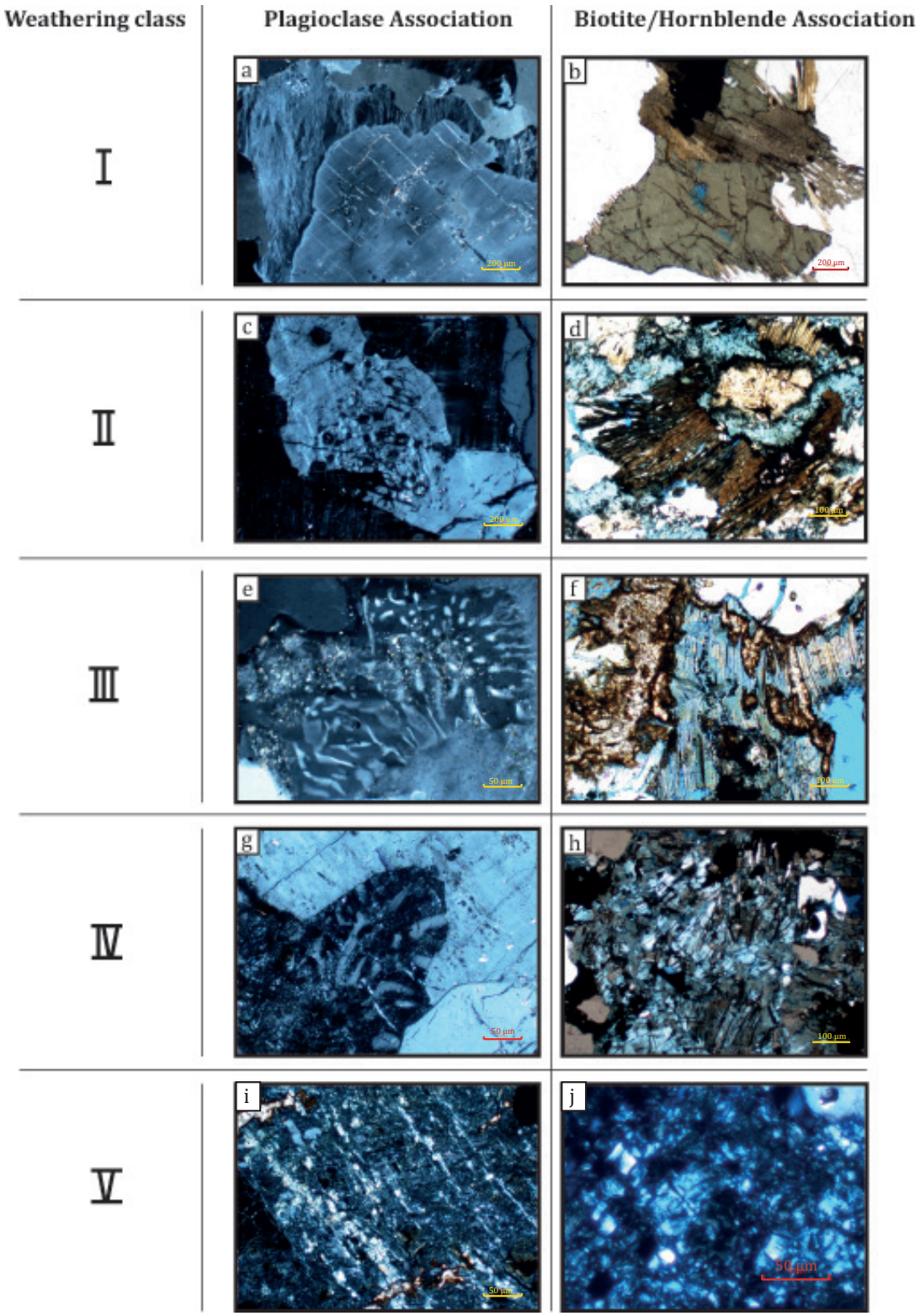

Figure 3.30: Overview image of all facies associations, for plagioclase and mafic components.

3.2.4.3 SEM analysis

This section comprises the SEM-results of the weathered section at Nygård kaolin pit, analyzed as thin section and stub samples.

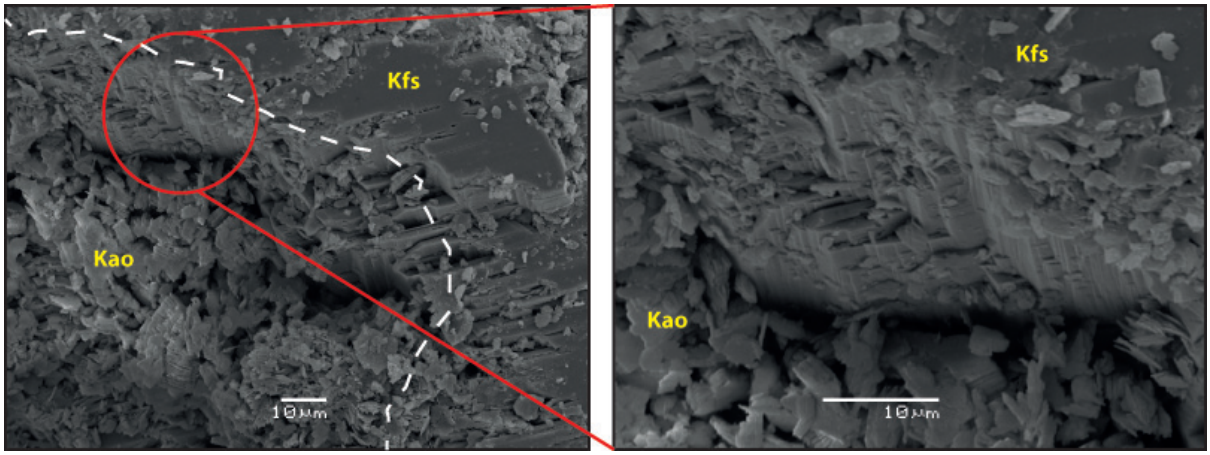

Figure 3.31: Remaining K-feldspar rim around dissolved and transformed plagioclase into kaolinite flakes in sample DR9-12.

Figure 3.31 displays the secondary electron image of feldspar in sample DR9-12. K-feldspar is better preserved and only weathered on the surface surface. The transition between K-feldspar to plagioclase is illustrated as a white, dashed line in the left hand side image (Figure 3.31). Plagioclase is entirely replaced by kaolinite flakelets. The transition line demarcates the growth border around the formerly intact plagioclase (for comparison see Figure 3.6). The right hand side image displays a close up, where random kaolinite flakes and booklets can be found laying upon the K-feldspar and accumulated kaolinite can be observed in the lower part of the image. Kaolinite assemblage in direct adjacency to the K-feldspar (along the transition line) appears less ordered (single flakes no booklets) and the formation of clay booklets more random as compared to the kaolinite cover, displayed in Figure 3.33. Sharp border edges characterize the dissolution surface along the K-feldspar margin and the inner margin of the K-feldspar rim seem only fairly affected by alteration and the remnant of the K-feldspar rim is well preserved.

Biotite crystals in weathering class III are frequently observed strongly splayed, deformed and surrounded by kaolinite. Pervasive overgrowing siderite, as illustrated in Figure 3.32 was a prevalent feature in sample BR19-12. Remarkable for the kaolinitic intrusion along the 001 crystal planes of the biotite, is the intruding growth of kaolinite within the biotite lattice as displayed in the close up image Figure 3.32 (right). Along the mineral margins of such biotite crystal often no signs of dissolution or interaction could be observed, according the extremely sharp appearance of the mineral borders between biotite and kaolinite. Other areas of the crystal, mostly along the 001 crystal planes, showed strongly size diminished wafers of biotite, which indicate the presence of illite in SEM. Neogenetic, possibly authigenic derived

K-feldspar could be found frequently at the splayed ends of biotite minerals, distinguished by its unaffected, freshly appearing surfaces (see also Figure 3.36).

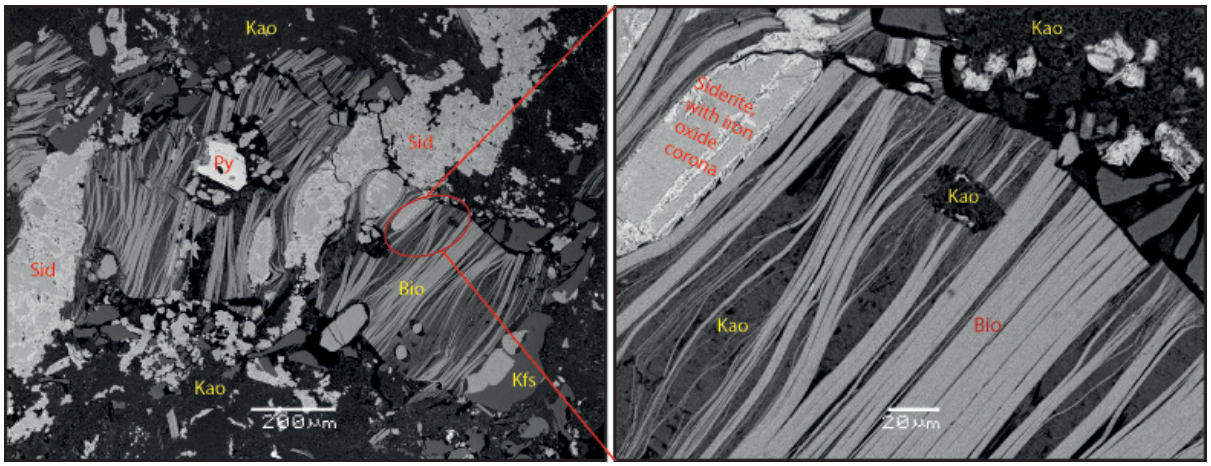

Figure 3.32: BSE image of biotite crystal from sample BR19-12.

The kaolinite association studied by the aid of a secondary electron images of sample DR9-12 revealed a dense kaolinitic cover, overlaying the remaining mineral assemblages (Figure 3.33). Detailed imaging of the sample area illustrated in Figure 3.33 (right side image) displays the regular formation of kaolinite booklets, which indicated an higher degree of ordering and indicates the in situ formation of the mineral in this image. Kaolin blankets were studied appearing in patches over the stub sampled grain.

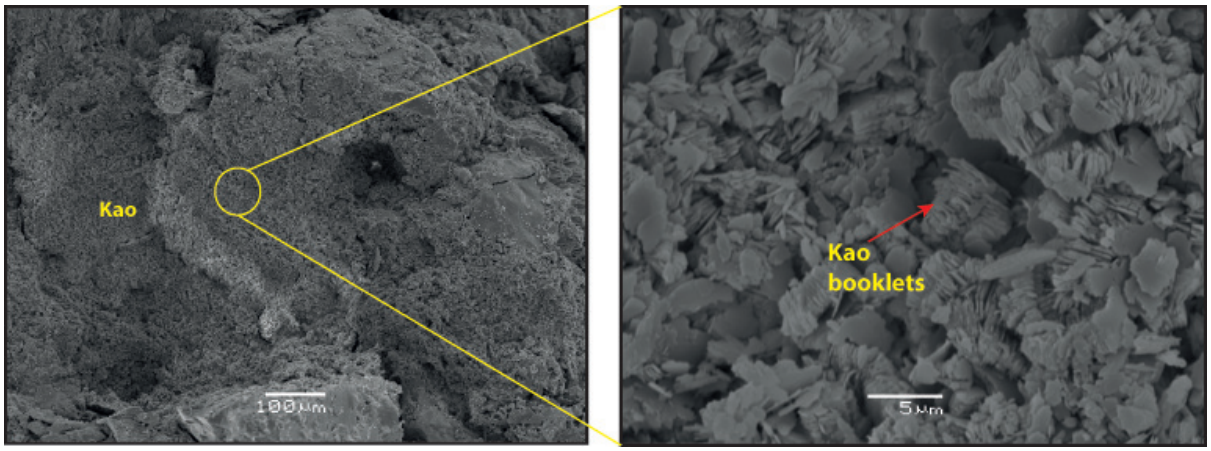

Figure 3.33: SEI image of sample DR9-12 displaying area of almost pure kaolinite.

Surface dissolution of K-feldspar could be studied by obviously etch pitted and alteration affected feldspar crystals. SEM analysis of this example revealed that the etch pits partly contained albite. This suits the overall pattern of the pits, which reassemble the pattern of exsolution lamellas, studied in fresh K-feldspar (see Figure 3.6).

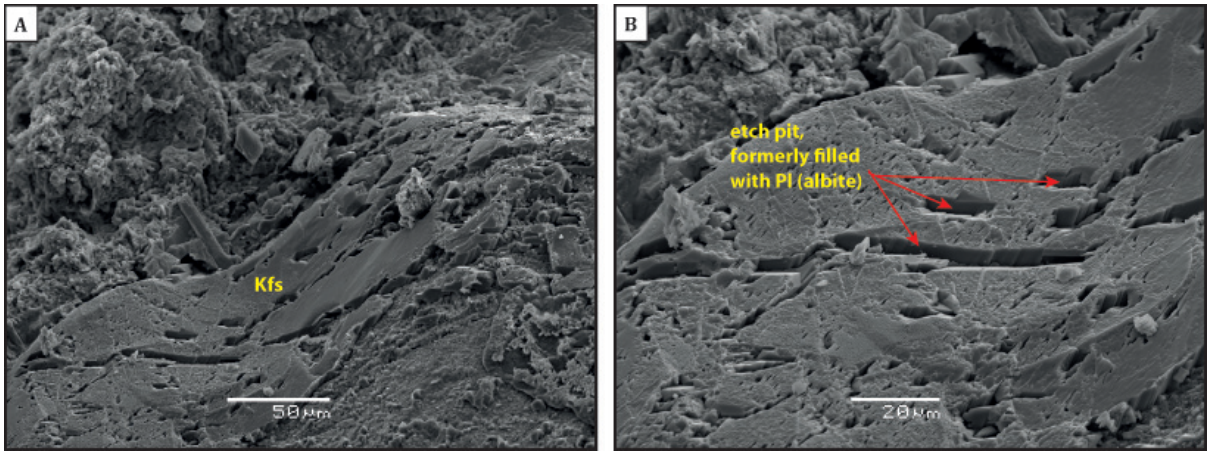

Figure 3.34: BSE image of weathering effected, etch pitted K-feldspar (compare with fresh feldspar Figure 3.6).

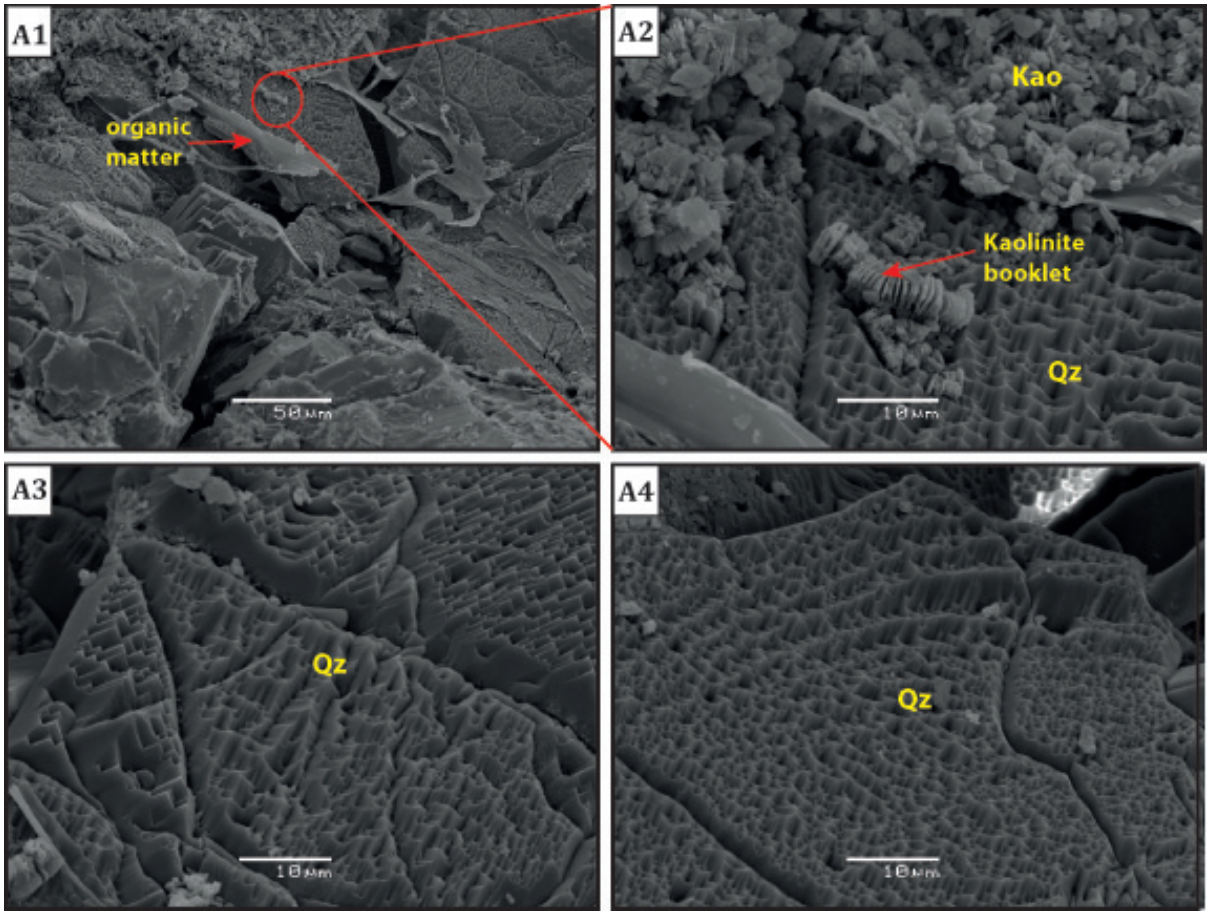

Figure 3.35: Quartz association in sample DR9-12 display in a1) strongly etched surfaces. Common organic overgrowth (rootlets) could be found. a2) illustrated a more detailed image were singe kaolinite booklets lay on top of the etched quartz. Images a3) and a4) show further detailed images of the apparently strong etched quartz surface.

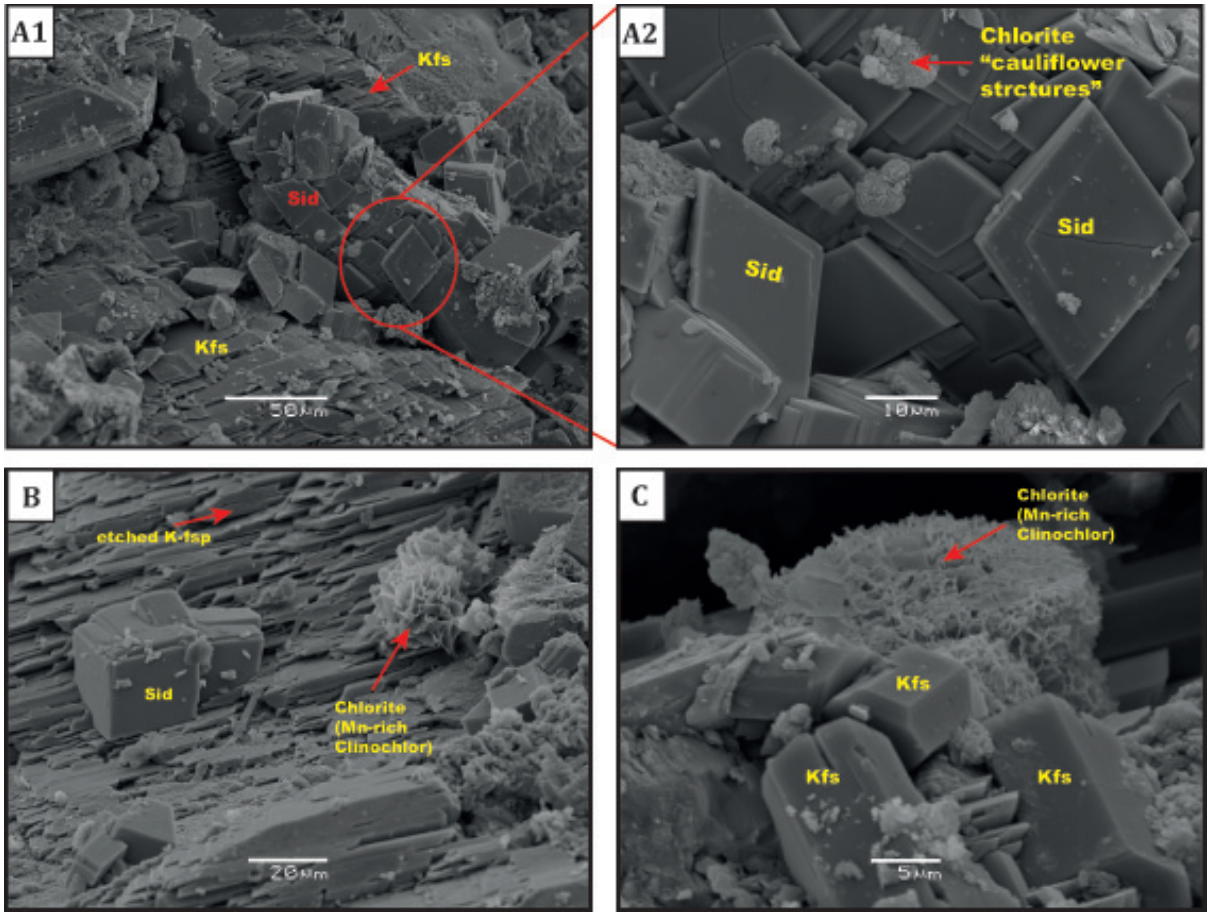

Figure 3.36: BSE image of gold coated stub sample DR9-12. a1) Rhombohedral siderite crystals overgrowing weathered, etch pitted K-fsp displaying degraded weathering surfaces along (001) axis. a2) Close up image of rhombohedral siderite crystals with partly overgrown Mn-rich chloritoid (Clinochlor), showing cauliflower growth structures. b) Illustrating siderite rhomboeder growing authigenicly upon weathering etched K-feldspar and adjacent clino chlor. c) close up image of chlorite cauliflower growing on neogenetic, aughigenic K-feldspar. (Images b and c from sample DR7-12)

3.2.5 XRD analysis

In the following section graphical approaches of XRD-bulk and -clay fraction analysis are presented together with the detailed description of the acquired results. During the process of the thesis work, different types of graphical illustrations have been attempted. Since correlation-coefficience plotted as scatter plots revealed certain disadvantages in the vertical correlation within the studied profiles and trends were not applicable, it was decided to use histograms.

3.2.5.1 Bulk analysis

The bulk assemblage comprises the sample analysis of 22 samples out of 34 utilized samples. Representative 11 samples of each profile B and D (see Figure 3.40 and Figure 3.43) are used

for the determination of general mineral distribution trends, i.e. plagioclase vs. kaolinite, with the scope to establish and distinguish the origin of secondary minerals within each profile. Vertical distribution trends of primary and secondary minerals are studied, to compare wether vertical trends might be distinguishable from one profile to the other, or if the rather small scale weathering processes leading to highly heterogeneous lithology make lateral correlation impossible.

Profile B The mineralogy revealed abnormally high abundance of carbonates in profile B, with a siderite to calcite ratio of 0.76 (Figure 3.37 a)). The internal carbonate ratio was chosen to illustrate, due to the high concentration and distribution of calcite and siderite in thin section observations. Carbonate is, as previously mentioned, foremost represented by siderite. As illustrated in Figure 3.40, the siderite content increases within the medium section of the profile, which is associated with less weathered, highly fractured corestones. This could as well be observed in thin section analysis, where siderite precipitation in less weathered samples was restricted as pervasive overgrowth in meso-fratures and void spaces. Samples of higher weathering facies, with increased pore space showed ”blossom”-like growth of siderite and SEM imaging revealed rhomboedric growth of siderite over surface etched K-feldspar and kaolinite (see Figure 3.36). Ratio calculations of kaolinite and siderite, printed in Figure 3.37 b), display an average value of 0.30 where sample BR4-12 might be over represented with a ratio of 0.70.

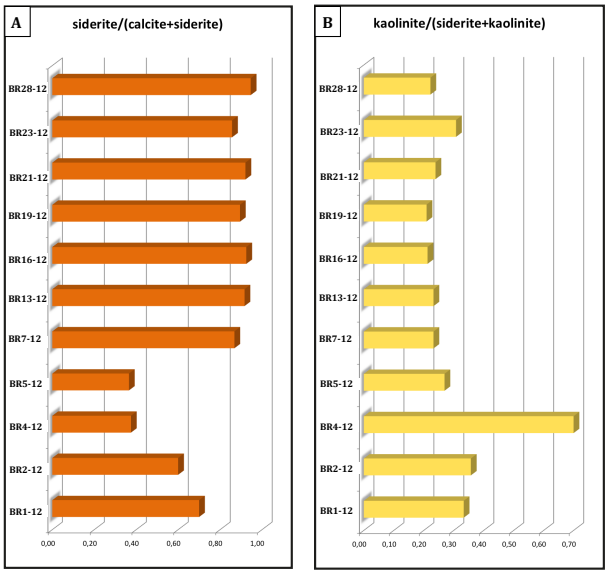

Figure 3.37: a) internal ratio of the main carbonaceous compounds siderite vs. calcite. b) in contrary kaolinite vs. siderite, due to the common overgrowth studied in thin section. The histograms show an inversely proportional trend and indicate a relation of the kaolinite and siderite concentration in profile B.

The in thin sections studied overgrowth of sideritic carbonate over kaolinite (seeFigure 3.24) indicated in XRD analysis an inversely proportional relation of siderite and kaolinite (Figure 3.37). Average siderite concentration of 25 XRD% in all profile B samples, comprises its minimum value of 3 XRD% in sample BR4-12 and its maximum value of 38 XRD% in sample BR16-12. The highest abundance could be found from sample BR5-12, at a height of 0.4 - 0.5 m, to BR28-12 at a height of 3.20 m. Calcite is abundant with an average concentration of 7 XRD% in profile B and seems over represented in sample BR5-12 with 33 XRD%, mostly present as fracture and pore-spaces filling.

Mineral associations, like quartz and K-feldspar with an expected higher weathering resistance, than plagioclase and mafic components were estimated in equilibrium, compared to semi-quantifications of the unweathered protolith. 16 XRD% of K-feldspar in average in profile B, is in equivalent with the values of the unaltered granite. Sample analysis of samples BR5-12 and BR7-12 showed significantly lower K-feldspar values with 9 XRD% in contrast to the remaining samples in profile B with at least 16 XRD%. For the quartz/feldspar ratio in profile B, 0.38 was estimated comprising an internal feldspar ratio of 0.16, which is slightly lower compared to the unweathered granite with 0.22.

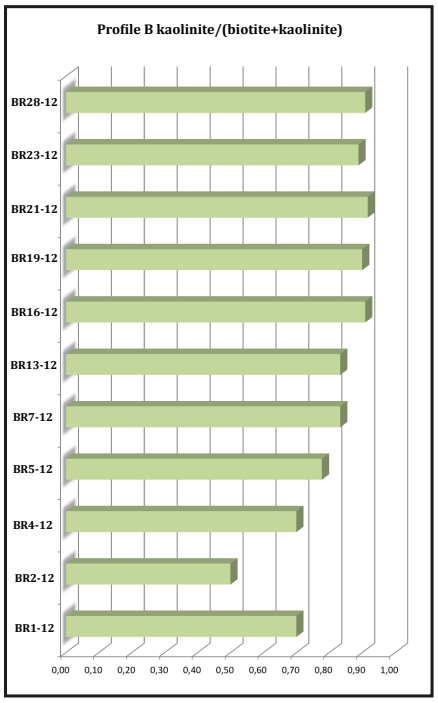

Figure 3.38: Histogram displaying the ratio calculations of kaolinite vs. biotite in profile B. Kaolinite increases with profile height, biotite is mostly absent. The increase of kaolinite is unproportional to the concentration decrease of biotite.

Mafic components, like biotite and hornblende are in the unweathered source rock represented with 16 XRD% and 14 XRD%, and now diminished to only 2 XRD% of biotite and 1 XRD% hornblende in weathering profile B. The alteration of biotite to illite formerly studied in thin section, revealed in later XRD clay fraction analysis the presence of illite/smectite mixed-layered clays. Hornblende, as one of the most weathering prone minerals in this paragenesis is associated with chlorite as its alteration educt. Zircon, as original accessory mineral could be distinguished with 6 XRD% in these samples. The high abundance of zircon was also recorded qualitatively by Waight et al. (2012), but no comparable XRD results are known. Minor accessories are the iron-titanium oxide, ilmenite and the iron sulfide, pyrite.

The ratio estimations for kaolinite and biotite in profile B are illustrated in Figure 3.38. An average ratio of 0.81 was computed and seem to exhibit a strong increase of kaolinite on the expense of biotite especially in the upper part of the profile. XRD Semi-quantification of biotite in the section revealed an marginally higher abundance of the mafic mineral within the lower most 50 cm in the profile. The highest detected concentration of biotite was found in sample BR2-12 with 5 XRD%. The concentration drops with increasing height down to 1 XRD%. In contrast, the kaolinite abundance increases inversely proportional to a maximum estimation of 10 XRD% in the bulk samples.

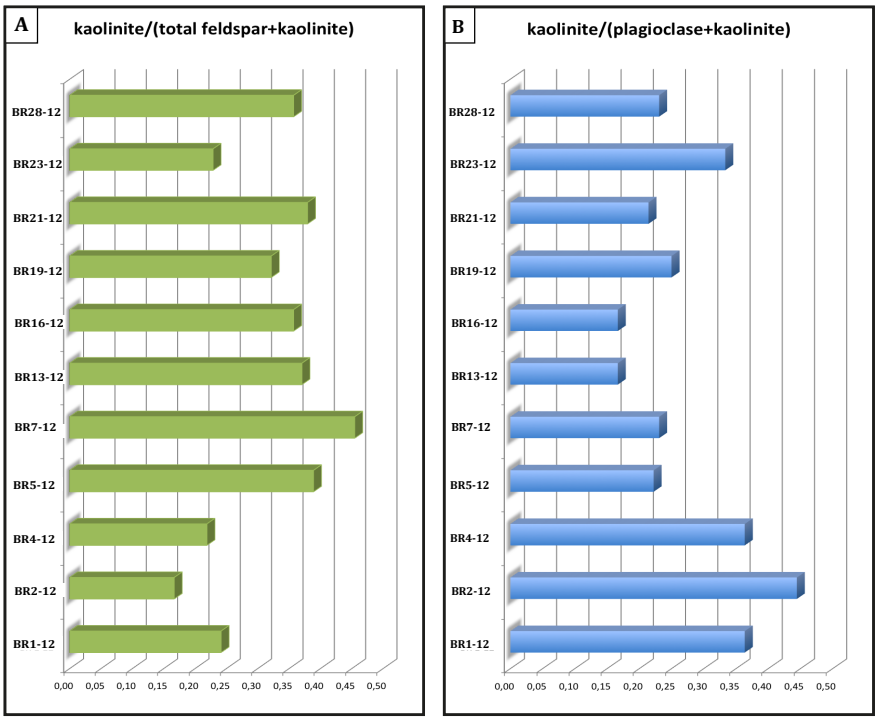

Figure 3.39: a) Kaolinite/total feldspar ratio compared to b) kaolinite/plagioclase ratio. Negative correlation can be observed between the two diagrams, indicating the relation between feldspar dissolution and kaolinite precipitation.

The qualitative and semi-quantitative determination of kaolinite in bulk samples was

performed on the (002)-peak at 3.58 Å. Chlorite and the swelling clay smectite was determined according the shared 14 Å-peak in bum sample analysis. The 14 Å-peak revealed expectedly low values in semi-quantification of the bulk samples and had to be specified after ethylene glycol solvation and heating treatment in later clay separated analysis (see section XRD-clay fraction). The estimation for kaolinite, appearing at 3.58 Å was more promising in the bulk assemblage, and exhibited a mean value of 7 XRD% in profile B.

The corestone distribution in profile B (Figure 3.15), as pointed out previously, displays a rather massive character of a fractured, but apparently less weathered corestone complex. The overall mineral distribution based on the semi-quantification does not clearly reflect lithological trends of the profile. The only increasing content with height in profile B was observed for siderite. The plagioclase/kaolinite ratio (Figure 3.39a)) compared to the kaolinite/total feldspar (plagioclsase+K-feldspar) ratio (Figure 3.39b)) does coincide inversely proportional and might thereafter indicate the origin of kaolinite from plagioclase. Decreased values of plagioclase in specific samples coincide with increasing amounts of kaolinite, which is a reasonable trend in perspective to the previously discussed petrographical analysis, where the ultimate transformation of kaolinite of plagioclase could be found (compare, e.g. Figure 3.31).

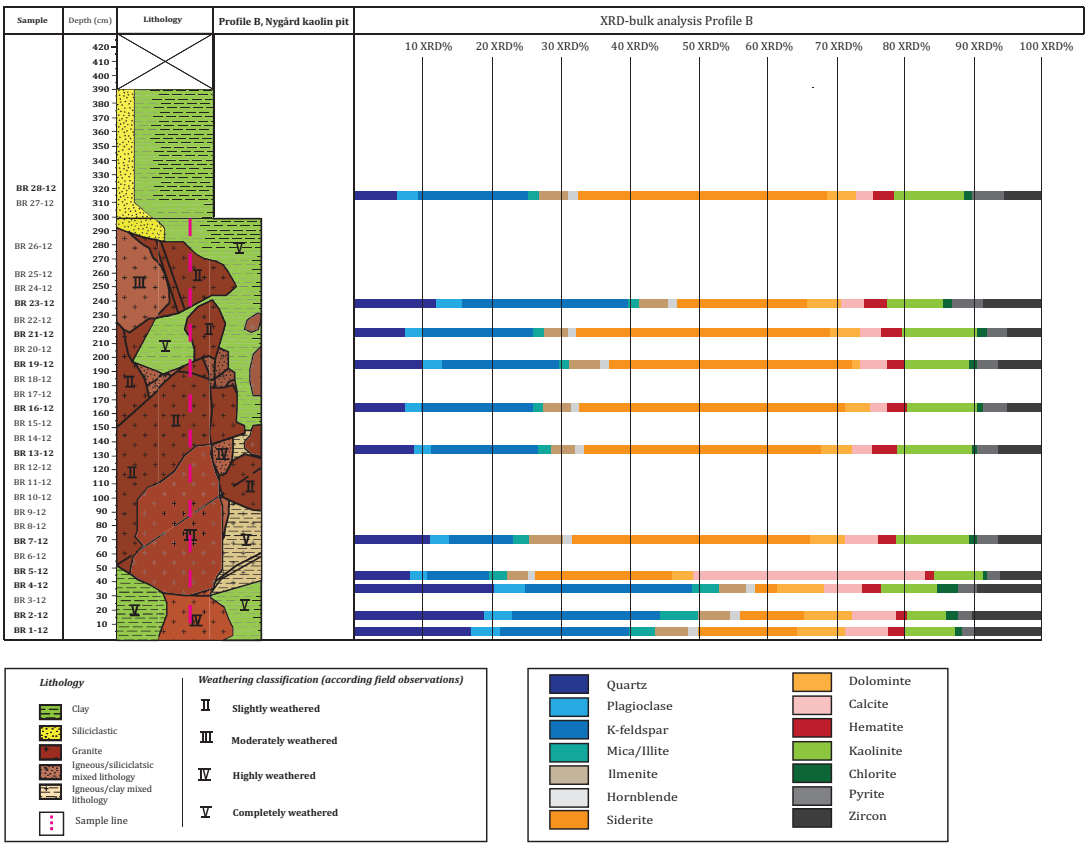

Figure 3.40: Graphical representation of the XRD-bulk analysis, histogram displays the mineral content of the analyses samples inXRD-%. For data reference see Table C.1.

Profile D The XRD-bulk analysis of profile D illustrates compared to profile B a strong decrease in siderite concentration. In average, only 7 XRD% could be distinguished, whereas the calcite concentration is higher than in profile B with a mean of 9 XRD%, giving a siderite/calcite ratio of 0.47 in difference to the formerly examined 0.76 in section B. Thin section analysis of the calcite crystallization showed clear abundance of carbonate along meso-fractures and pore spaces, as fine crystalline association.

Calcite, fairly easy to distinguish under the microscope by its extremely high birefringence color under xpl, showed no detectable oxidation staining in microscope observations. Profile D is characterized by relative abundance of siderite in the lower part of the profile steadily decreasing with height and increasing calcite concentration within the middle part of the section. 20 XRD% of siderite were estimated in sample DR3-12 and only 7 XRD% of calcite. In sample DR19-12 siderite concentration suddenly drops to 2 XRD%, where in contrary the calcite concentration increases to 21 XRD%.

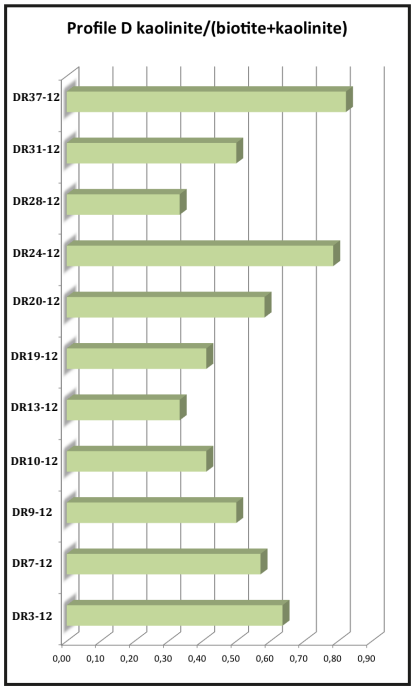

Figure 3.41: Figure illustrating the internal ratio estimation of kaolinite vs. biotite. The kaolinite concentration is more variable in profile D, as compared to profile B. Biotite concentrations are higher in this section, which may lead to the increased variation. Increasing corestone heterogeneity and enhanced interspacing between the boulders are reassembled by the graph.

The biotite concentration in profile D is enhanced with an average value of 7 XRD%. The maximum concentration of biotite could be distinguished in sample DR10-12 with 10 XRD% and DR13-12 with 12 XRD%. Both samples are relatively low in kaolinite but no overall

correlation between the two minerals (biotite-kaolinite) could be seen. Hornblende is almost completely dissolved and the mean value of 1 XRD% coincides with that determined in profile B (1 XRD%). The remaining concentration of hornblende in the weathering section can be ascribed to random, minorly distributed fragments of the mineral in samples, as observed in thin section. The feldspar paragenesis seem more abundant compared to section B. Plagioclase/K-feldspar ratios were estimated to be about 0.22, in contrast to 0.16 in the 4 m distant profile B. Investigations of the feldspar relationship compared to the major clay phase kaolinite comprises lower values for the kaolinite/total feldspar ratio of 0.23, due to the higher abundancy of K-feldspar (20 XRD%) in the section. In contrary, the kaolinite/plagioclase ratio increased to 0.46, as illustrated in Figure 3.42. The highest estimated abundance of kaolinite in this section occurs in sample DR37-12, which by thin section observation was classified to be weathering facies III.

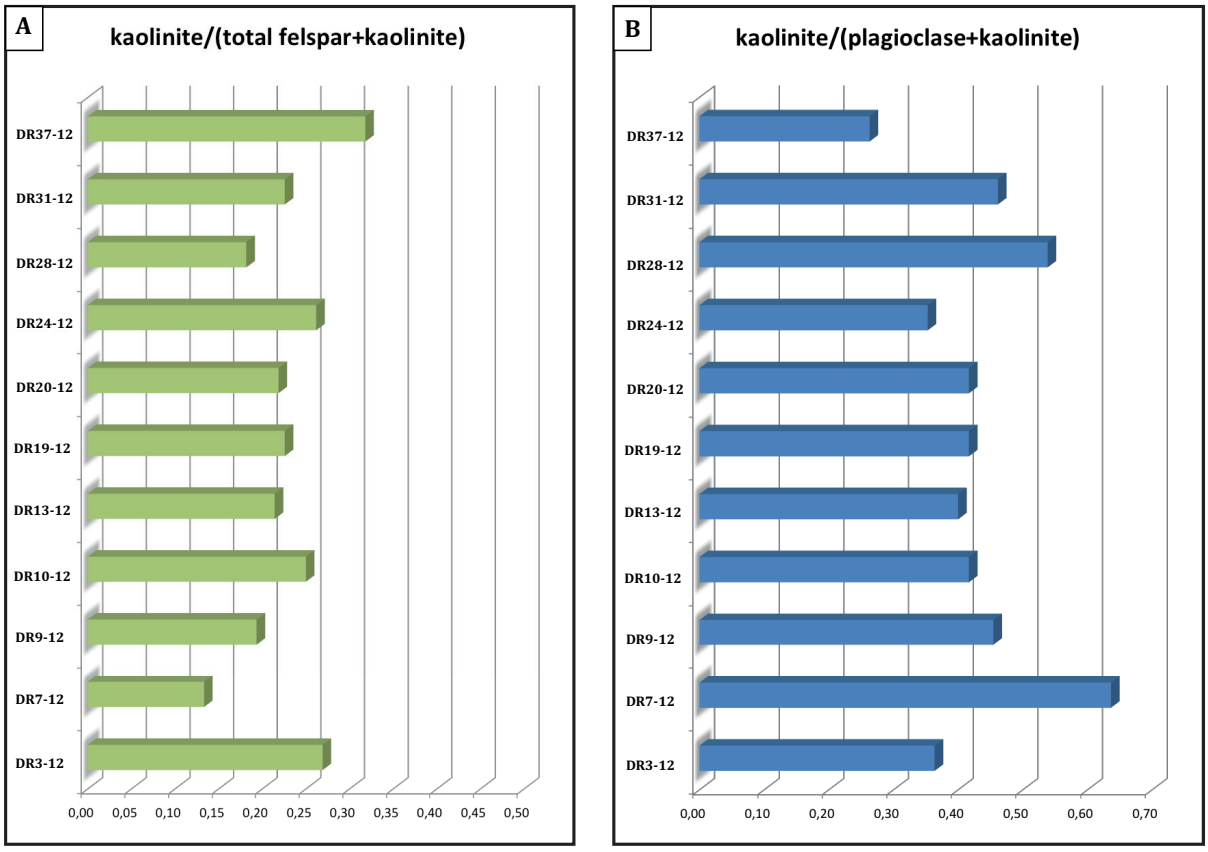

Figure 3.42: Histogram illustrating the mineral ratio distributions of a) kaolinite/total feldspar and b)kaolinite/plagioclase. The diagrams exhibit a partly inverted correlation where a relative abundance of kaolinite is present, the feldspar (foremost plagioclase) concentration decreases.

The concentration of the common accessory mineral zircon was observed in reverse abundance in profile D compared to profile B. Whereas in profile B the concentration of zircon was highest in the lower parts of the profile, it seems to increase with height in section D.

Zircon is mostly unaffected by weathering, by vast independency of weathering controlling parameters, such as climatic controls and geochemical agents, it might constitute the most weathering inert phase known. Therefore, it is more prone to transport and dislocation and could in this case contribute to later discussions about hydrological transportation factors, since the estimated concentrations of zircon in the saprolite were unaltered compared to the fresh parent rock. In both sample types the concentration was distinguished within a range of 5-10 XRD%, which reflects extremely high values. Thin section analysis of random zircon minerals in weathered strata revealed relatively large sizes of the crystals, often reaching up to 2 mm. The in fresh samples of the Rønne granite studied zircon associations commonly were found embedded in biotite or hornblende. Weathered sections displayed dislocated, edge rounded zircon crystals, indicating transportation.

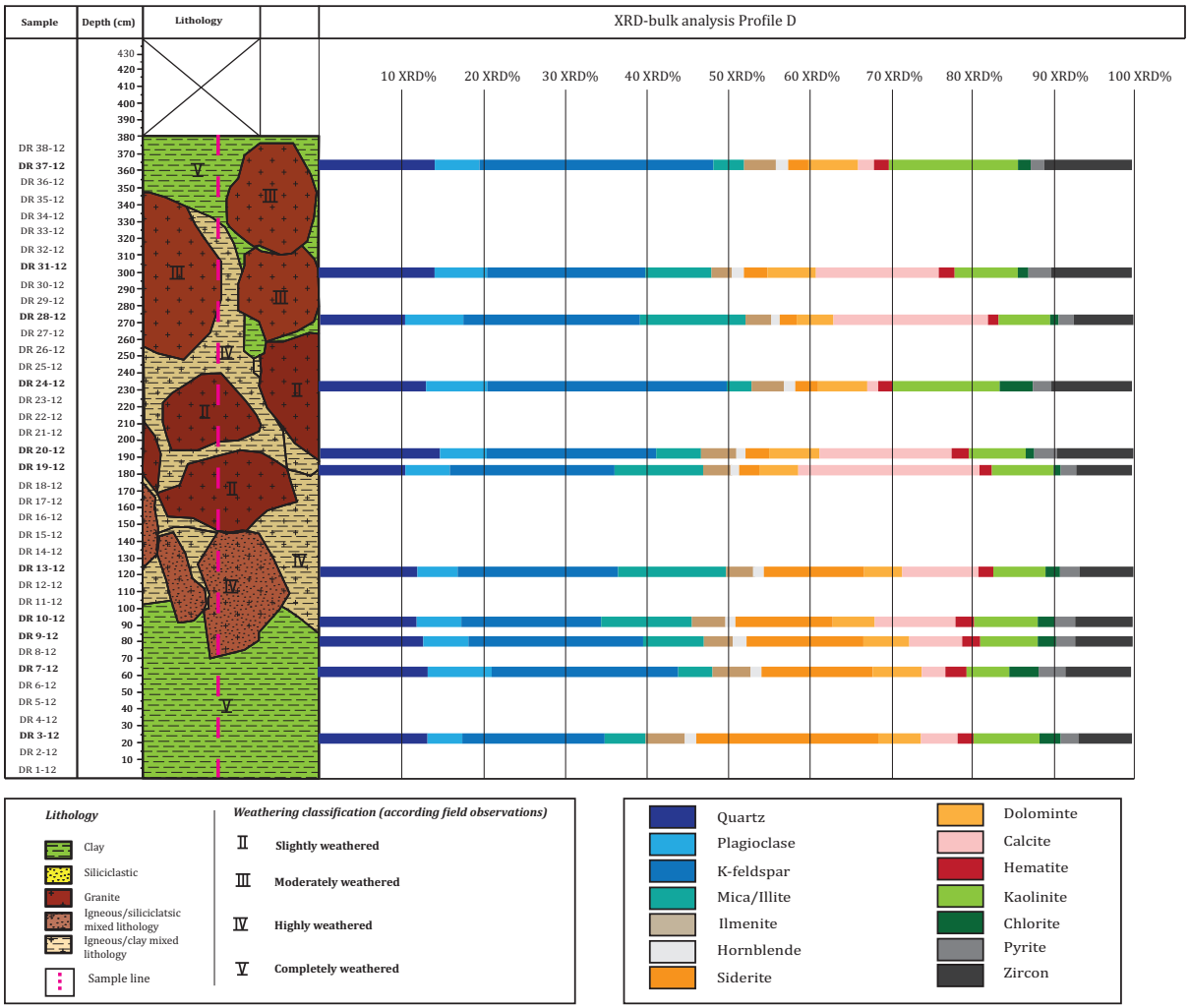

Figure 3.43: Graphical representation of the XRD-bulk analysis, histogram displays the mineral content of the analyses samples inXRD-%. For data reference see Table C.1.

Mineral mobilization and fractionation during weathering

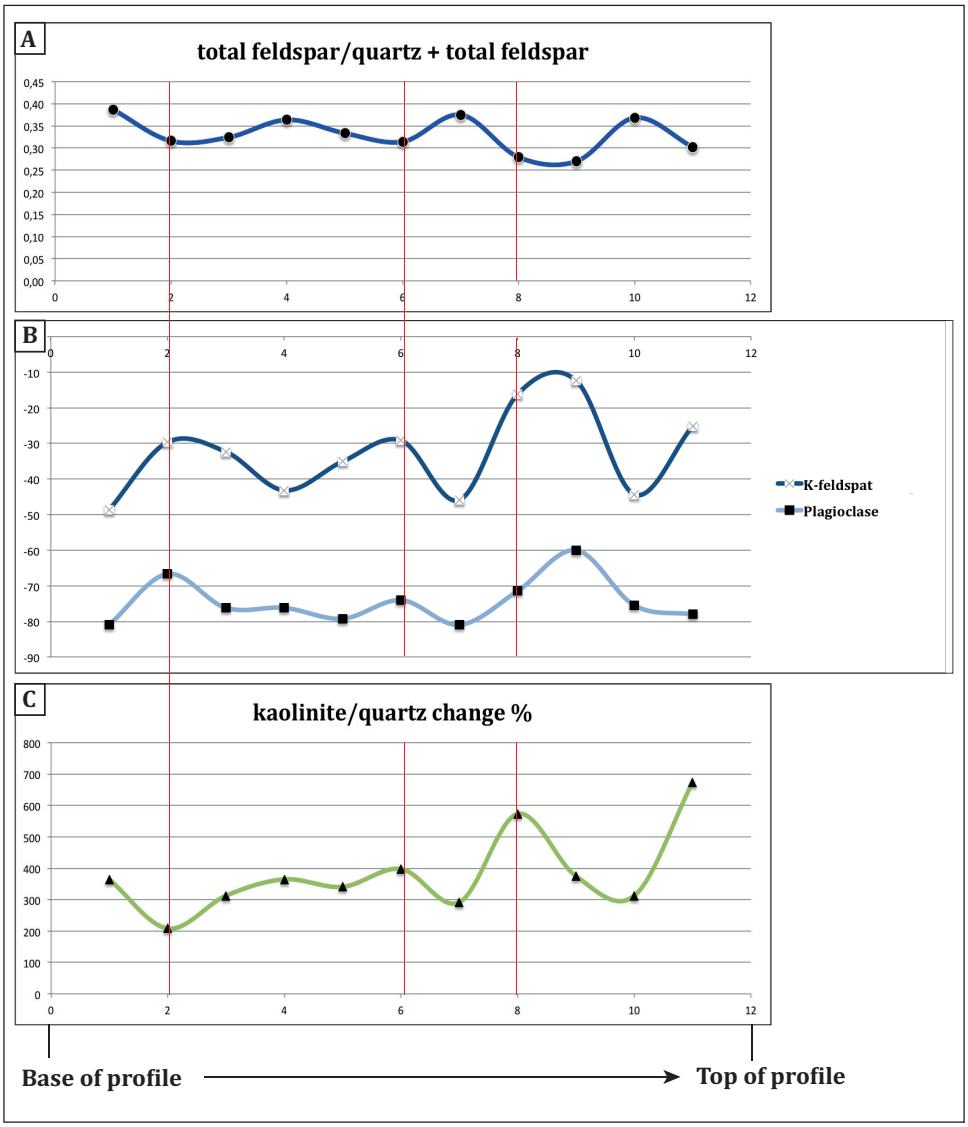

Figure 3.44: Example illustration for the calculated mineral loss in profile D after, compared to the unweathred Rønne granite (after Nesbitt (1979), calculated as presented in chapter results, (2.2.1)). The x-axis (1-12) represents the samples taken from bottom to top. a) shows the ratio curve for total feldspar vs. quartz, where fairly constant ratio values could have been distinguished in the lower part of the profile (0-6) and some minor variations of slight increase and decrease can be seen in the middle to the upper part of the profile. Figure b) displays the mineral changes estimated for the feldspar separated curves of of K-feldspar (upper) and plagioclase (lower). Higher variation, at less denudation rates can be observed for the K-felspar curve, whereas the plagioclase curve shows similar variation pattern at a higher dissolution rate. c) Illustrates the change in kaolinite in % within profile D, note that the change rates are extremely high, up to a surplus of 700%, compared to kaolinite concentrations in the parent rock. The extreme loss rates of plagioclase up to 80% coincide with the strong increase in kaolinite precipitation within these samples.

3.2.5.2 Clay fraction analysis

For qualitative and semi-quantitative determination of the clay fraction (< 2 µm), all 34 samples have been analyzed. Subsequently the main focus will be on previously discussed profiles B and D. The results presented in Table C.4 display a strictly clay associated distribution of the minerals and will not be compared, due to reasons explained earlier, with results of the bulk analysis.

The qualitative analysis of the air dried, the ethylene glycol solvated, the 350°C and 550°C heating samples was conducted according the techniques described in Moore et al. (1989) and with the aid of the USGS-flow chart for clay mineral identification.

Qualitative association of clay minerals in the saprolite profile In the weathering succession, five different groups of clay minerals were distinguished, the following approach appeared important to include in this section:

1. **Smectite**, as observed in sample BR19-12, the air dried curve showed a 14.24 Å-peak, expanding to 17.24 Å after ethylen glycolation with additional weak 5 Å-peak. The curve collapses to 10 Å after heating to 350°C and 550°C. The (060)-peak at 1.54 Å indicates the smectite polymorph montmorillonite (according USGS-flow chart).

2. **Illite**, the air dried curve showed a clear, symmetrical 10 Å-peak, with no change after ethylene treatment, 350°C and 550°C heating. The 060-peak was observed at1.54 Å, which determines illite with indication to biotite (according USGS-flow chart).

3. **Kaolinite**, was distinguished in sample BR19-12 according the air dried peak at 7.15 Å, which shows no change after ethylene glycolation and 350°C, but collapses entirely after 550°C heating, because kaolinite becomes amorphous at this temperature.

4. **Chlorite**, could not definitely be distinguished in this sample. The air dried peak position at 14 Å, expanding after ethylene glycol solvation to 17 Å (as explained above) by the presence of smectite, shows no change for the EG curve, but slightly collapses after 350°C and 550°C heating. An additional 060-peak at 1.54 indicates the presence of chlorite (according USGS-flow chart).

5. **Mixed-layered clay minerals**, are explained subsequently in paragraph *Mixed-layer clay mineral association*.

Profile B As illustrated in Figure 3.45, the most abundant clay mineral in profile B is kaolinite. Represented with an average concentration of 60 XRD%. Chlorite is the second most clay mineral, about 1/3 of kaolinite. Smectite and illite are comparably under represented in the section. Smectite, indicating in qualitative analysis the polymorph montmorillonite,

constitutes 11 XRD% while illite is only present with 4 XRD%. The vertical distribution of the clay minerals, foremost of kaolinite and smectite seem to have an inverse trend. The concentration of smectite, which is higher in the bottom part of the section (18 XRD% in BR1-12 and 21 XRD% in BR2-12) reduces in the medium part of the succession to 5 XRD%. Sample BR21-12 represents an apparent shift, where smectite increases and kaolinite decreases in the upper most samples (18 XRD% in BR28-12). Inversely proportional values are illustrated by the kaolinite curve, compared to the smectite concentrations. Reduced kaolinite values in the lower most samples, with 52 XRD% in sample BR1-12, such as in the upper most section with 55 XRD % in BR28-12 are in contrary to the middle section, where higher values with 62 XRD% in BR13-12 and the acme of 70 XRD% in sample BR16-12 could be found.

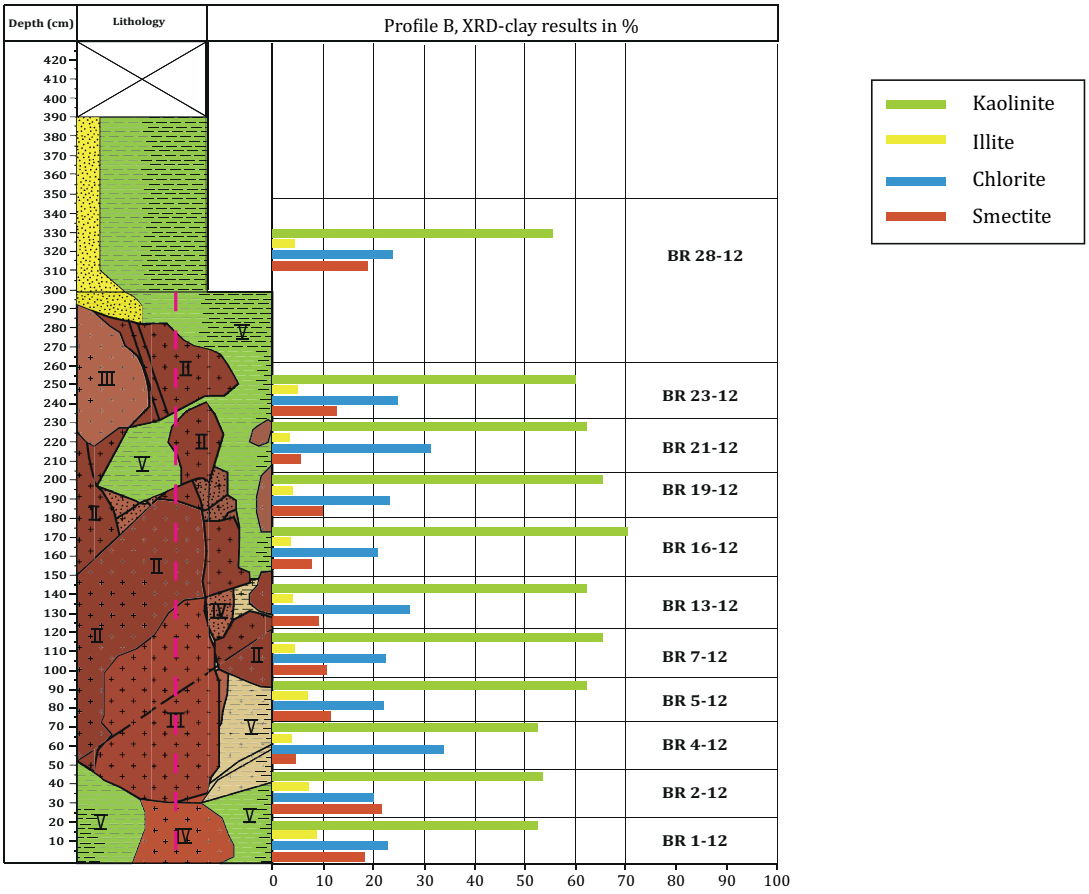

Figure 3.45: Clay mineral summary of profile B. Distribution of the main clay minerals present in the saprolite section are illustrated according the sample height. Vertical trends kaolinite display abundant concentrations in the middle part of the section. Chlorite, as the second most abundant phase seem over represented according the anticipated mineralogy and might be associated with a authigenic overprint (see also Figure 3.36).

Clay mineral ratio calculations displayed in Figure 3.46, were conducted with respect to the most abundant mineral associations of kaolinite, chlorite and smectite. The chlorite/kaolinite and the smectite/kaoliinite ratio (Figure 3.46 a)) seem to have no internal trend, whereas the

kaolinite/chlorite+smectite ratio compared to the chlorite, smectite ratios seem to coincide according the histogram (Figure 3.46). Smectite is associated with an early precipitation phase in granitoid weathering under humid, tropical conditions, in contrary, chlorite is rather associated as authigenically formed mineral association.

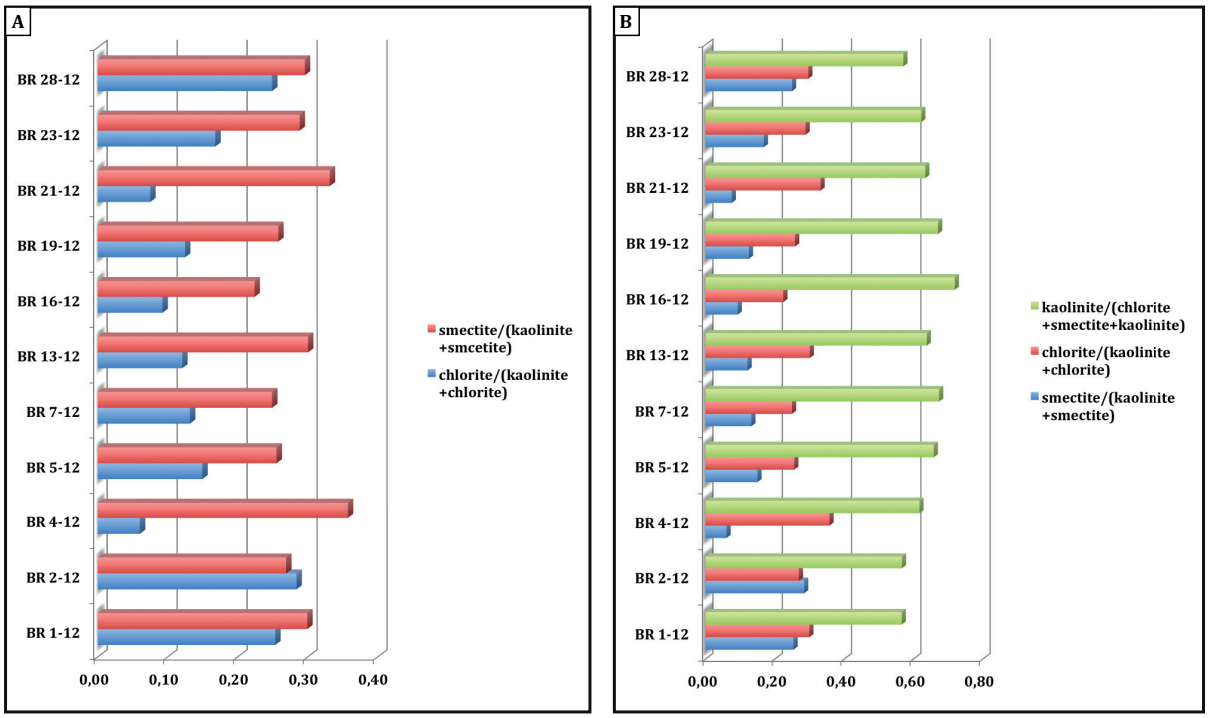

Figure 3.46: Ratio estimations of a) smectite and chlorite vs. kaolinite and b) in addition of kaolinite/(chlorite+smectite+kaolinite) to illustrate clay internal behavior within profile B.

Profile D Profile D comprises higher abundance of kaolinite, with an average of 79 XRD%, compared to the 60 XRD% in profile B. The physical shift of corestone association, from more massive and apparently less weathered in profile B, to more weathered heterogeneous and more rounded corestones in profile D is also reflected by the clay mineralogy. Vertical trends are more variant and the highest abundance of kaolinite, compared to reduced concentrations of foremost smectite and chlorite appear more restricted to corestone inter-spaces. The strongest decrease in concentration was observed for smectite, which in average is only present with an concentration of 3 XRD%, with an maximum value of 8 XRD% in sample DR31-12. The chlorite concentration lays in average at 15 XRD%. The relative decrease of chlorite and smectite, compared to the increase of kaolinite seems to be proportional. Illite, with a concentration of 3 XRD% occurs neglect-able.

Mixed-layer clay mineral association For the qualitative determination of mixed-layer clays, techniques suggested by Burst (1969) and Moore et al. (1989) have been followed. In

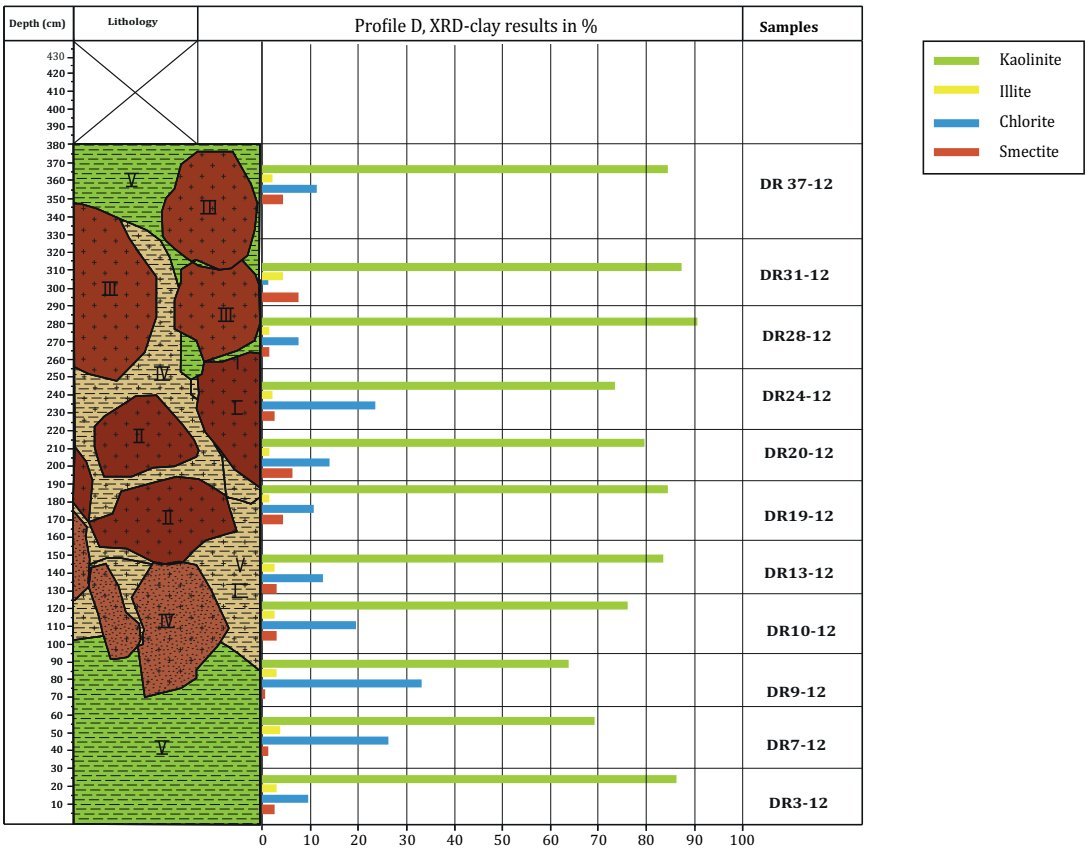

Figure 3.47: Clay mineral summary of profile D. Distribution of the main clay mineral phases present in the saprolite section are illustrated according the sample height. Vertical trends kaolinite display abundant concentrations in the middle part of the section. Chlorite, as the second most abundant phase seem over represented according the anticipated mineralogy and might be associated with a authigenic overprint (see also Figure 3.36).

the first step, peak positions shown by the air dried curve have been studied and compared with the ethylene glycol (EG) solvated curve. Commonly a significant change of the ethylene glycol solvated curve occurred at the 14 Å-peak, which expanded to 17 Å (see Figure 3.48). This expansion of the EG curve is evidence for the presence of a smectite component. In further procedure, peak positions of the EG curve within a range of 16°2 θ and 17.7°2 θ have been encountered to distinguish, wether the smectite mixed-layer is inter-layered by an illicit component. 002/003-peaks around 5.5 Å (±0.2) confirmed the presence of illite and revealed a illite concentration of about 50-90%. Illite/smectite mixed-layer minerals were not included into the semi-quantitative approach, since the intensity of the 5.5 Å-peak was too weak in the most samples. Weak intensities increase the error rate of the semi-quantitative method and it was thereafter decided not to include the mixed-layer mineral.

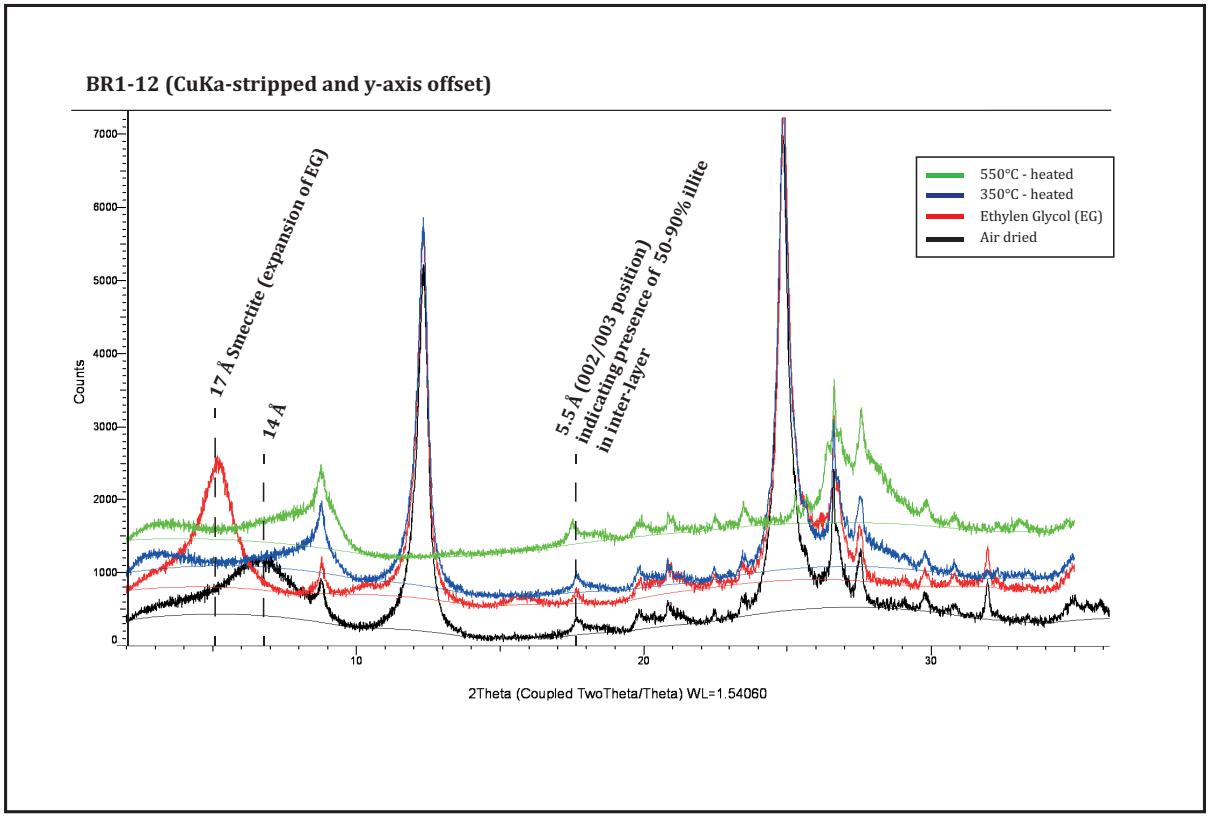

Figure 3.48: Diffractogram of sample BR1-12 illustrating the approach for mixed-layer phase determination, as explained above.

4 | Discussion

The discussion of mineral formations underlaying the generation of primary crystal dissolution and precipitation of observed secondary clay mineral phases will constitute the first part of this discussion. Ensuing, depositional parameters, such as paleoclimatic indications, groundwater effects and paleo-tectonic implications for the sedimentary coverage of the weathering formation will be suggested. Last, the acquired results of the Bornholm locality will be compared to the selected paleo-weathering locality at Ivö Klack in southern Sweden and the recent weathering locality at Oporto, in NW Portugal. In addition, comparable aspects will be attempted in connection with the offshore weathering succession found in drill cores from the Utsira high.

4.1 The formation of secondary mineral associations

Tardy et al. (1973) characterized granitic saprolite profiles as a ”dynamic system, which constitutes multiple populations of closed or partly opened micro-environments with no clearly determined dependency on each other”. This corresponds with formerly encountered results from the Nygård locality, where vertical and lateral trends of mineral distribution in the profile could hardly be observed in a constant strain. As a first approach to weathering classification macroscopical and physical observations of the saprolite section at the Nygård kaolin pit established the general weathering facies. The mineralogical and petrographical analysis depict the backbone for the following discussion of the established weathering facies.

4.1.1 Weathering facies I

For further discussion of higher weathering degrees it is inevitable to elucidate the parent rock paragenesis comprehensively, as the characteristic mineralogical composition of the weathering bedrock determines the formation secondary minerals tremendously (Nesbitt and Young, 1984; Pedro, 1983; Gerrard, 1994).

4.1.1.1 Primary mineral associations of the Rønne Granite

U-Pb determinations of 25 zircon grains from Stubbegård granite quarry (Waight et al., 2012), revealed an estimated concordia age of 1456±5Ma. This result complements earlier U-Pb-dating approaches of Zariņš and Johansson (2009), which elaborated an age of 1450±5Ma of the Rønne Granite, Mesoproterozoic time.

The petrogenesis of unweathered parent rock constitutes a granite in 'sensu stricto'. Plagioclase exceeds the abundance of K-feldspar marginally and comprises together with quartz the main felsic component in the pristine plutonite. The predominance of the Ca-/Na-rich felspar compared to the potassium feldspar has led former geologists to the conclusion that the melanocratic appearing rock should rather be classified as a granodiorite (Callisen, 1934; Bondam, 1968, 1984). XRD semi-quantifications and point counting analysis of the fresh samples Q1-12 and Q2-12 were plotted in a Streckeisen diagram (Figure 3.2) (according IUGS Subcommision of Igneous Rocks). The results solidated the classification of crystalline bedrock as a granite with the tendency to a quartz-monzonite.

Plagioclase crystals commonly show internal, cryptocrystalline sericitization. Sericitization is pronounced in two different orientations which represents a ubiquitous feature in such minerals. Weaver and Pollard (1973) concluded, that sericite in most cases can be viewed as a metamorphic or deuteric-igenous product which cannot be produced as primary phase in the weathering profile. Henceforth, it is notional that the sericitization of plagioclase in the fresh granite is a preceding process, which stands in no connection to the later subaerial alteration.

Sericite resembles a fine-grained muscovite often viewed as a hydrothermally derived alteration product of potassium-/aluminium-rich mica (Meunier and Velde, 1982). First, sericite is adjusted along principal, polysynthetic twinning directions along the 001 direction of plagioclase crystals (see Figure 3.5). Second, sericite inclusions appear along meso-fractures (Figure 3.6). While studying the sericite inclusions with high magnification under the microscope (20x10 and 40x10) it seems striking, that the two directions of orientation may depict two different hydrothermal events, due to the degrees of alteration. This was apart from their cryptocrystalline appearance easy to distinguish according to the high birefringence color (Figure 3.5). Que and Allen (1996) postulated that the prior appearance of sericite along polysynthetic albite twins is a result of externally derived, secondary, hydrothermal fluids which intruded in the mineral interior via pores during retrograde metamorphism. This happened at fluid temperatures of about 600 °C to 400 °C where crystallizing feldspar paragenesis is still immature. The K-feldspar association surrounding the sericitized plagioclase core, as commonly observed (see Figure 3.6), is mainly constituted of the low temperature variety microcline typically crystallizing in a temperature window between 450 °C to 200 °C. This supports the assumption, that potassic-feldspar microcline crystallized around and intrinsically at a later stage than plagioclase. Perthitic exsolution of albite lamellas could be found in the

surrounding microcline K-feldspar (see Figure 3.6). The exsolution of lenticuliar perthites may be attributed to the fact that exsolution and crystallization of the two feldspars are taking place simultaneously, providing the optimum conditions for the formation of microcline (Spencer, 1938). This indicates that there has been a late stage plagioclase formation which may have coincided with the crystallization of K-feldspar, since the exsolutional growth of albite into the K-feldspar could be determined seamless (sample Q2-12, Figure 3.6). In contrary, partly sericitized meso-fractures were restricted to the plagioclase interior, whereas in micro fractures cutting through the surrounding microcline rim sericite was absent. The formation of the micro-fractures and fissures is imputed to contractional stresses during magma cooling. This might coincide with the latter intrusion of retrograde formation of sericite via hydrothermal fluid apparently corroding the Ca-rich anorthite [1] (Que and Allen, 1996).

SEM investigations revealed that the anorthite abundance of about $An_{<40}$ observed in thin sections was increasing towards the sericitized parts of the mineral grain, implying the connection between anorthite and the sericitization. The absence of sericite within the albitic perthites may consolidate this finding. Based on the degree of alteration studied in the described sericitation appearances, two hydrothermal events may be distinguished, which may also be related with the latter formation of pegmatite veins in the plutonite. The sericitization within polysynthetic twinned (albite/anorthite) lamellas can be associated with an early fractionation and retrograde metamorphosis. This constituted in the samples of the fresh Rønne Granite a slightly argillaceous association of sericite, due to alteration along the twin planes. In comparison, sericite crystallization in micro-fractures often displays high birefringence and less alteration. This could be attributed to a later intrusion of hydrothermal fluids into plagioclase micro-fissures, induced by contractional cooling dislocation or tectonic exfoliation at decreasing temperatures (Que and Allen, 1996). The mid-temperature variant orthoclase could only be examined in minor phenocrysts, not in direct vicinity to plagioclase. The assumption of post magmatic, hydrothermal alteration is further supported by the minor presence of chlorite along biotite mineral fringes observed in samples Q1-12 and Q2-12 (see Figure 3.8). Eggleton and Banfield (1985) formulated the alteration of plagioclase to sericite in terms of unit cells, involving the translation of biotite to chlorite as following:

$$1\,\mathrm{Bio} + 0\cdot 21\,\mathrm{An} + 1\cdot 64\,\mathrm{H_2O} + 1\cdot 46\,\mathrm{H^+} + 0\cdot 08\,\mathrm{O_2} \longrightarrow 0\cdot 46\,\mathrm{Chl} + 0\cdot 11\,\mathrm{Sph} + 0\cdot 10\,\mathrm{Ep} + 0\cdot 56\,\mathrm{Musc} + 0\cdot 63\,\mathrm{Qtz} + 0\cdot 02\,\mathrm{Mag} + 1\cdot 46\,\mathrm{K^+}$$

According to Que and Allen (1996) alteration reactions of plagioclase to sericite and biotite to chlorite are in a thermodynamic equilibrium with similar weathering fluid conditions. The authors further attests, that plagioclase transformation into sericite is common in biotite granites.

[1] Hydrothermal fluids may constitute temperatures in the order of 400 °C to 600 °C (Que and Allen, 1996), associated with burial depths of about 10 km, and are therefore distinguished as preceding weathering mechanisms, to the later subaerial weathering.

Biotite was observed as a subordinate mafic mineral phase with an estimated average abundance of 6% from point counting analysis, to the Ca-rich amphibole polymorph hornblende, present with 14% in both studied thin sections Q1-12 and Q2-12. XRD semi-quantification of fresh granite samples revealed in contrary a biotite abundance of ordinary 16 XRD%. Hornblende was estimated in accordance to the point counting results of 13 XRD% and examined the subordinate presence to a more equal abundance. Semi-quantitative estimations comprises, as pointed out before, a rather imprecise method and are therefore a more reluctant estimate compared to the optical point counting analysis. Callisen (1957) found that some parts of the hornblende crystals resemble regions of embayed, fine grained quartz, opaques and apatite, which may represent "relic cores of clinopyroxene". The presence of polycrystalline, embayed quartz in minor areas of hornblende, mostly distributed along the mineral margins, could be affirmed by optical analysis of fresh thin section samples. It is suggestested, that the size diminished and embayed quartz grains may comprise an earlier crystallization, compared to the much larger intrinsic grains found adjacent (Tom Andersen (UIO), personal communication). The mode of quartz crystallization, usually associated with the latest stage of fractionation crystallization of igneous magma, may therefore contribute to the formerly suggested diverse and inconstant cooling history of the crystalline parent rock, which might be associated with strong tectonic influences during the Bornholm horst block formation (Petersen et al., 2003).

4.2 Corestones

The corestone associations in the profile are well preserved, less weathered boulder formations. Lateral changes from the western margin (left hand side of the profile) to east have been recorded. The western margin comprises a more massive corestone complex and the profile becomes increasingly heterogeneous in eastern direction (compare Figure 3.11). This lateral trend of weathering stands in contrast to the general hydraulic gradient at present state (Figure D.2). The corestones appear oriented along certain fracture elongation and are very divers in their appearance. Due to the general appearance of high weathering facies below the corestone complex, it might be concluded, that the observed outcrop represents only a spars part of the saprolitic layer. Gamma ray measurements acquired from profile B and D are in acquiescence to the increasing heterogeneity (see Figure 3.21). The measurements in profile B reflect lower values in the medium part of the profile, constituted by the less weathered corestone complex. Increased γ- radiation could be recorded for higher weathering facies.

4.2.1 Weathering facies II to IV

In this section the precipitation and genesis of secondary mineral associations of pre- to syn-burial weathering conditions are elucidated. In agreement with Nesbitt and Young (1989), who stated that "unlike the mineralogical compositions of weathering profiles, the bulk compositional trends are not noticeably modified by climate" it seems appropriate to use bulk compositional trend observations of recent weathering successions as an example to which ancient weathering profiles can be compared. Pedro (1983) stated, that the paragenesis of secondary minerals depend more on the primary mineral paragenesis, than on general bio climatic conditions. Gerrard (1994) postulated in acquiescence that the nature of secondary minerals is rather dependent on particular leaching conditions, than on specific climatic conditions. Based on these assumptions the mineralization sequence and the formation of secondary phases at the Nygård saprolite profile will be discussed in a mineralogical manner, disregarding paleoclimatic parameters, which will be encountered in subsection Post burial and re-exposure of the weathering profile.

4.2.1.1 Feldspar

As presumed from thin section analysis and assent with XRD-bulk analysis, the abundance of plagioclase is vastly diminished to an ordinary concentration of approximately 5 XRD% and a slightly higher estimated value of about 8% from point counting observations in weathering profile B and D. According to Nesbitt and Young (1984) plagioclase constitutes the most abundant mineral of the exposed, unweathered, continental crust and is among the most prone and brisk weathering silicates. Experimental studies of Busenberg and Clemency (1976) revealed, that during the denudation large amounts of kaolinitic clay minerals are formed by the direct expense of plagioclase. This appraisal is in accordance with the petrographical observations formerly presented, which confirmed that progressing weathering led to the dissolution of plagioclase and the direct precipitation of kandites (kaolinite group minerals) (Figure 4.1) in closest vicinity to the altered mineral grain (Figure 3.31). Further more, ratio calculations presented in Figure 3.39 and Figure 3.42 of kaolinite plotted versus total feldspar, such as kaolinite against plagioclase, revealed an inverse proportional trend indicating the relation between plagioclase weathering and ultimate kaolinite precipitation. The chemical alteration of plagioclase during the exposure to meteorically derived drainage fluids to kaolinite may be expressed after Blum (1994) under consideration of a) the dissolution of plagioclase in solution and b) the subsequent precipitation kaolinite which leads to:

$$2\,NaAlSi_3O_8 + 9\,H_2O \longrightarrow Al_2Si_2O_5(OH)_4 + 4\,H_4SiO_4 + 2\,Na^+ \qquad (4.2.1)$$

Incipient weathering of plagioclase associated with weathering facies II, may be illustrated as in Figure 3.24, where plagioclase mineral-margins and -interiors are comparably corroded. With prograding weathering, water associated with incipient and intermediate weathering solutions become increasingly aggressive (Meunier and Velde, 1976) due to the enrichment of silicic acid ($4\,H_4SiO_4$) as displayed in (4.2.1). Dissolved, mobile ions, like Mg,Na, Ca presume in solution and the evacuation of mobile phases lead to a relative accumulation of immobile phases, like K, Si, Fe, Al or Ti in the weathered residuals (Schmitz, 2008). Hereby the progressing denudation of plagioclase may be explained, as displayed in Figure 3.30 e) for weathering facies III, g) for class IV and i) for V. As a result, disordered kaolinite flakes can be observed in weathered pore space adjacent to more prone mineral phases like K-feldspar. Potassium-rich feldspar in return appears to be more weathering resistant and weathers more slowly than plagioclase (Busenberg and Clemency, 1976; Nesbitt and Young, 1984) (Figure 3.31).

4.2.1.2 Mafic mineral associations

Hornblende The second most abundant mafic mineral in the pristine parent rock is the Ca-/Na-rich amphibole hornblende. XRD estimations of the parent rock association revealed 13 XRD%, whereas semi-quantitations of the weathered samples were almost entirely devoid of the amphibole (average 1 XRD%), indicating a high and fast weathering rate of hornblende. Typical cleavage directions of 60°and 120°may benefit the fast denudation of the mineral phase by giving pathways for intruding weathering solutions and forming ferruginous and aluminous products like kaolinite, gibbsite and goethite[2] (Velbel, 1989). No ferruginous weathering products were determined in the performed analysis within the Nygård saprolite profile, leading to the conclusion, that the alteration of hornblende rather contributed to the formation of the aluminous kaolinite. Detailed thin section analysis of sparsely distributed hornblende fragments revealed partial transformation into chlorite phases. This is in agreement with Tiba et al. (1970), who observed the formation of chlorite and subsequent chlorite-inter layer phases in Japanese soils. Anand and Gilkes (1984) recorded in doleritic samples from a western Australian saprolite that hornblende and feldspars weathered congruently, producing etch pits along cleavage planes. This is in accordance with the studies presented by Velbel (1989), but could not be observed in any sample from Nygård. The general absence of etch pitted surfaces is thought to be connected with the almost entirely devoid association of hornblende and may also be attributed to the limited outcrop found at Nygård where only partial mineral fragments are remained. Hornblende may constitute an important ion source for Na, Ca, Mg and Mn to the weathering solution, which could explain the formation of Mn-rich clinochlor in the later stage of weathering (Anand and Gilkes, 1984) (discussed in later section).

[2]named in consecutive formation order

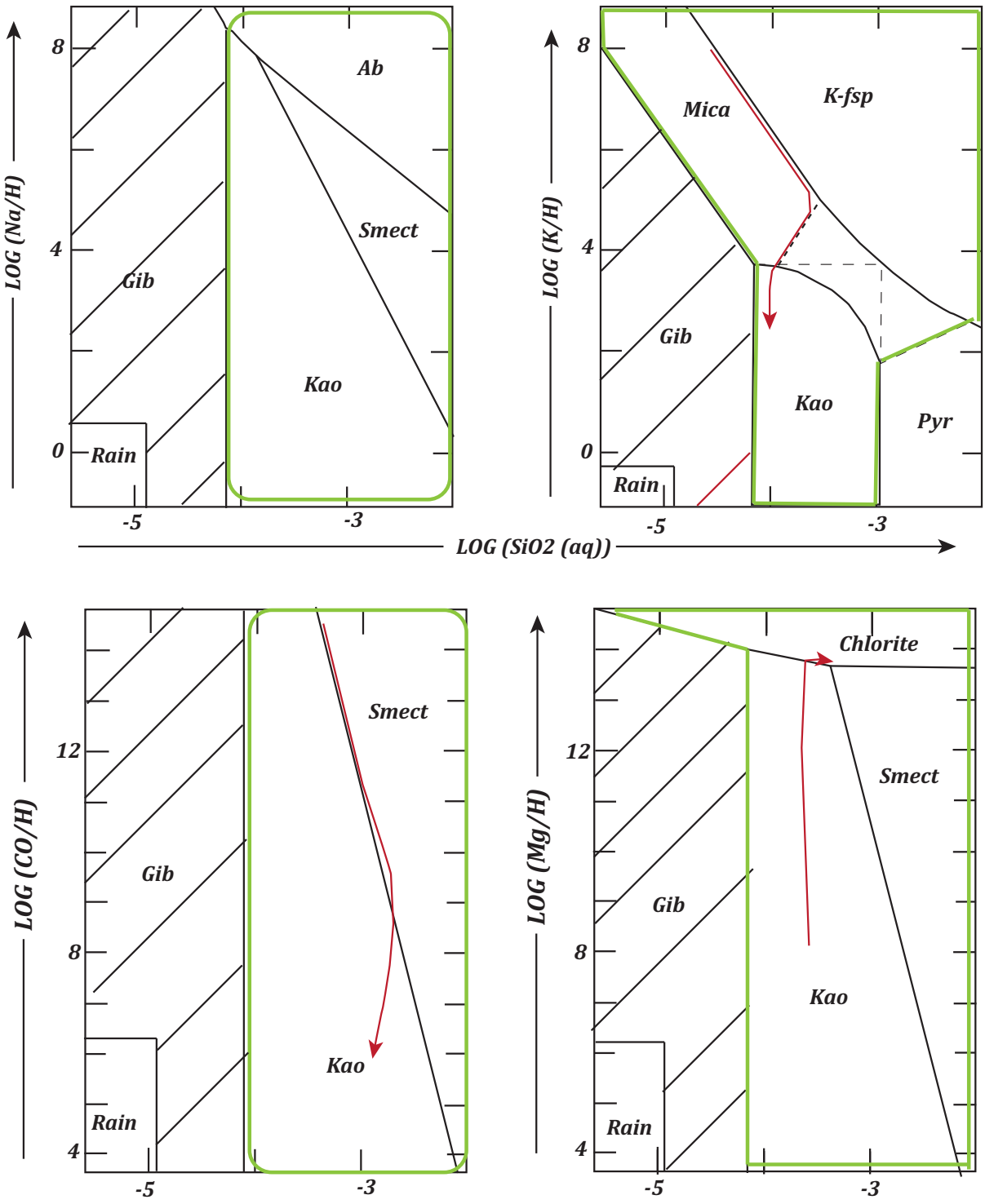

Figure 4.1: Simplified, thermodynamic stability relations between mineral associations, weathering solutions and shallow ground waters (modified after Nesbitt and Young (1984)). Principal stability paths from primary minerals to secondary clay minerals are schematically illustrated by the red line. Studied mineral associations are lightened by green color. Dashed lines represent metastable mineral phases.

Biotite Biotite micas may resemble a commonly more weathering resistant mineral phase, as studied at in the Nygård sectioncompared to feldspar or amphiboles (Goldich, 1938). Weathering of the trioctahedral phylosilicate is associated with the subordinate formation of intermediate 2:1 layer silicate phases, like vermiculite and/or smectite, illite and inter-layered clay minerals during incipient weathering, such as the transformation into the end member kaolinite (Murphy et al., 1998). Petrographical observations and point counting estimations of the weathered material disclosed an intense decrease in biotite when compared to the unweathered parent rock. Original concentrations ranged at approximately 6%, based on point counting and latter XRD-bulk quantifications revealed an average biotite abundance of about 16 XRD% in the analyzed fresh Rønne Granite. The concentration loss calculated after Nesbitt (1979) (see Table C.3), by using quartz instead of zircon (as suggested in the paper) as pristine, immobile phase, was based on fairly steady values estimated in XRD. The changes, based on this assumption exhibited concentration changes of mica in the weathered section of about -80% to -93% in profile B and with an much higher range of -4 %- -82% in profileD. The strong variance of mineral loss in the latter profile may be related to the lithological heterogeneity in this profile (Figure 3.17).

The weathering sequence of the Al-rich mica comprises the most complex of all mineral associations within the observed samples. Analysis of the particle fraction $< 2\,\mu m$ revealed the presence of 5 secondary clay mineral associations. Kaolinite, chlorite (incpient), smectite, illite and illite/smectite mixed-layers [3], may be affiliated directly or subordinary as weathering products of biotite. Microscopical results (Figure 3.30) illustrate weathering sequence of plagioclase and biotite. Random samples from profiles (B and D) were used for this figure, since no weathering constrain could have been established based on a consequent order. Assuming that the illustarted trend (Figure 3.30) is representative in a general sense, we can observe, that single wafers of biotite become increasingly widened (see Figure 3.32). According to Fordham et al. (1990) this may be related to increasing oxidation of Fe^{2+} to Fe^{3+} during the incipient weathering phase, causing ”internal stresses”. These interal stresses ease into ”physical deformation” of the crystal lattice through reduced layer charges, preferrable along 001 crystal plane (Murphy et al., 1998). Fordham et al. (1990) further stated, that these remnant layers of the biotite-like mineral may stay relatively unweathered and frame in XRD analysis typical illite characteristics (clay sized biotite). This is in accordance with conducted XRD and SEM analysis of such ”splayed” biotite crystals in samples from the Nygård locality. Detailed back scattering images (BEI) and elemental analysis of thin section BR19-12 (Figure 3.32) showed, that the wafer remnants of biotite still preserved the original texture, whereas the layer interspace was characterized by pure kaolinite with no detectable intermediate zone (again Figure 3.32). The transition between single ”splayed” layers and the kaolinite was extremely sharp (compare Braga et al. (2002)).

[3] Named in consecutive decreasing concentration as found in samples at Nyggård.

Two principal mechanisms are suggested for the formation of kaolinite out of biotite. 1.incipient crystallization of chlorite (Figure 3.8) associated with weathering class I becomes increasingly transformed into intermediate mineral phases of smectite, leading through K^+ liberation due to the inter-layer expansion into the 2:1 silica phase, to the subordinate formation of illite/smectite mixed layer phase (Murphy et al., 1998). Different studies (Grant, 1964; Fordham et al., 1990; Kretzschmar et al., 1997; Murphy et al., 1998) suggested vermiculite as common intermediate phase of biotite to kaolinite transformation. This could not be affirmed for the Nygård saprolite, where distinct XRD analysis confirmed the presence of smectite and the general absence of vermiculite. Furthermore it is suggested, that Na-, Ca- and Mg-enriched weathering solutions, derived from the dissolution of plagioclase and the often studied adjacency of biotite to hornblende minerals may be beneficial for the formation of smectite over vermiculite. The clay fraction analysis suggests that smectite is represented by the Ca-/Mg-rich polymorph montmorillonite [4]. Prograding leaching and break down of single biotite wafers could be observed in weathered samples with advanced alteration from Nygård. Figure 3.30 displays in image f) a dissolved biotite, with remnant layer structure, associated with intermediate clay mineral phases. The possible chemical reaction involving the transformation of biotite to kaolinite, via an intermediate phase can be displayed after Rebertus et al. (1986):

$$K_2(Fe_3Mg_3)(Al_2Si_6)O_{20}(OH)_4 + 4\,Al(OH)_2^+ + 10\,H^+ \longrightarrow 1.5Al_3Si_4O_{10}(OH)_2 + 2\,K^+ + 3\,Fe^{2+} + 3\,Mg^{2+} + 5\,H_2O \tag{4.2.2}$$

The 2. mechanism disregards the formation of a 2:1 intermediate phase and includes the direct reaction from trioctahedral biotite to 1:1 kaolinite. Ahn and Peacor (1987) suggested the reaction:

$$K_2(Fe_3Mg_3)(Al_2Si_6)O_{20}(OH)_4 + 6\,Al^{3+} + 2\,H_4SiO_4 + 4\,H_2O \longrightarrow 2\,Al_4Si_4O_{10}(OH)_8 + 2\,K^+ + Fe^{2+} + 3\,Mg^{2+} + 4\,H^+ \tag{4.2.3}$$

Ahn and Peacor (1987) further stated that the direct formation of kaolinite from biotite might involve ”drastic changes”, which must be caused by the dissolution of and along biotite layers, where H_2O, Al and Si entering the intra-mineral and dissolve H, K, Fe and Mg out of the mineral lattice. These observations were exhibited in a hydrothermally altered biotite (Ahn and Peacor, 1987). The mature state of the weathering profile at the Nygård resembles a rather low temperature regime that will be further elucidated. Generally both formation paths could be studied in the samples by using the previously mentioned analytical methods. It is arguable, if the denudation of biotite to kaolinite is rather restricted to earlier diagenetic events, which might have comprised late hydrothermal influence, or if both weathering sequences could have

[4]Typical XRD-clay curve (see Figure 3.48) shows a smooth 14 Å-peak for the air dried curve, which strongly expands to 17 Å after ethylene glycol solvation and collapse to 10 Å after heating treatment.

appeared simultaneously, only depended on the micro chemical environment in a dynamic system, as postulated by Tardy et al. (1973).

The appearance of smectites and 2:1 clay mineral associations in kaolinitic weathering or saprolite profiles indicate hydrological circumstances during the formation of swelling clays. Borchardt (1989) recorded smectites found in only poorly drained conditions, wheras Murphy et al. (1998) detected smectitic clays where strong "mottling indicates periodic water logging and reduction" [5]. In contrary, Kapoor (1972) studied the appearance of smectite within well, freely drained weathering profiles in Norwegian podzols and recorded beside the presence of "smectite, vermiculite and hydrobiotite" the absence of kaolinite. This is indicating the importance of hydrological influences, such as climatic controls for the weathering formation and rather poor draining conditions during earlier phases of weathering at Nygård. Prograding weathering of primary phases may have induced changes in the drainage capacity over time, by increasing secondary porosities within the profile. This might have contributed the enhanced precipitation of kaolinite under more mature drainage.

4.2.1.3 Quartz

Microscopical observations of random quartz grains from thin sections of weathering class I to IV showed progressional decrease in size. Statistical estimation of quartz grain degradation have not been performed in this research and are strongly recommended in further perspective. The progressing reactivity of quartz, could only be detected by optical investigations in SEM and microscope. X-ray analysis resembled rather constant concentrations of average 12 XRD% in both studied profiles (B and D) compared to the samples of fresh granite, where 10 XRD% were estimated by semi-quantification. The petrographical observations, where backscattering electron microscopy was used on stub samples from profile D, revealed frequent, strong surface dissolution features on quartz grains (Figure 3.35), in form of fairly symmetric, triangular etch pits. Knauss and Wolery (1988) studied by *flow-through apparatus* experiments, conducted at 70 °C the dissolution rate of quartz as a function of pH. The results presented in the paper display progressive formation of triangular shaped etch pits with increasing alkalinity, similar etch pits were observed in sample DR9-12 (Figure 3.35). Initial development of etch pits was observed by Knauss and Wolery (1988) from the pH of 9 and the coalescence further increased to a pH of 12. Based on this observations it might be concluded, that the formation of etch pits, presented in sample DR9-12 may have undergone strong dissolution at increasing alkaline conditions. The high symmetry and coalescence of the quartz surfaces studied in SEM (BEI) responds to strong surface dissolution effects. The chemical reaction may be written as:

$$2\,SiO_2 + H_2O \longrightarrow H_4SiO_4 \tag{4.2.4}$$

[5] Murphy et al. (1998) on recent tropical, humid weathering at the Luquillo Mountains, Puerto Rico.

Sverdrup and Warfvinge (1988) stated that the dissolution of quartz and thereby connected liberation of H_4SiO_4 to the weathering solution may lead to an increase in acidity, which exhibits an increase in the weathering rate of minerals in general. Whereas, the dissolution of Al containing minerals and the connected liberation of Al-cation may decrease or inhibit certain weathering rates in other minerals in the paragenesis (Sverdrup and Warfvinge, 1988).

4.2.2 Weathering facies V

The previously discussed weathering processes of the Rønne Granite, are thought to be the driving agents for the formation of the residual kaolin at the Nygård locality. Bondam (1968), one of the first to analyze the kaolin deposits mineralogically and geochemically, found two distinct clay horizons within the profile (see Figure 1.6) and named them I-paragenesis and K-paragenesis. The first (I-type) constituted a calcite containing clay assemblage, further determined by an appreciable amount of illite. The K-paragenesis was in contrary calcite free and foremost distinguished by kaolinite and devoid of illite. Saprolites studied along the inactive kaolin quarry were found to display rather I-type characteristics. In this perspective the weathering facies V was difficult to confine and sample RaF 3B-1985 was chosen as standard for the highest degree of weathering. Highly weathered samples taken in 2012 were classified into lower weathering facies. They display important examples for late diagenetic reactions, leading to mineral associations (e.g. siderite, chlorite and hematite) formed during syn- and post-burial of the weathering succession.

XRD-clay analysis of sample RaF 3B-1985 display 98 XRD% of kaolinite. The bulk analysis revealed 33 XRD% kaolinite 12 XRD% quartz, which could be confirmed by microscopical analysis (Figure 3.29). Thin section observations resembled size diminished quartz phenocrysts, beside kaolinite. This may a high weathering maturation in the samples. It is suggested that the high purity kaolinite horizon must have undergone drastic rearrangements since no such order and booklet formation was observed for kaolinite directly adjacent to weathering products. According to Nesbitt and Young (1989) weathering reactions only happen between solid rock material and precipitating waters penetrating the rock mass. By the time most kaolinite was formed the succession was covered by a residual soil layer of unknown thickness (compare Figure 1.11). The soil cover was further associated with strong vegetation, due to the suggested tropical, humid climate conditions during the Mid-Mesozoic times (Lidmar-Bergström, 1983). This may have resulted in enhanced profile differentiation induced by processes of lessivation and podzolization (Blume et al., 2010).

Lessivation describes the readjustment of solid substance <2 µm in soil profiles, where solid particles of top soils are transported along the hydraulic gradient in the profiles and may accumulate downstream (Blume and Schwertmann, 1969). This may lead to profile differentiation, where e.g. calcium carbonate dissolves and precipitates along the hydraulic

gradient (Schmitz, 2008). The removal of ions in the top soil layers can trigger undersaturation within the upper most, leached parts of the profile, which may lead to the dispersion of clay mineral phases (Schmitz, 2008). The dispersion, most effective for smectitic clays, may induce the dislocation of these clay phases into lower parts of the profile and thereby to the accumulation of clay layers (Blume et al., 2010). This process may lead to relative accumulation of kaolinite in the upper weathering horizons, because the 1:1 layer mineral is less dispersive (Gjems, 1967). Weathering solutions during such advanced stages of weathering are more acidified through the passage of the organic rich top soil (Nesbitt and Young, 1989). This may lead to increased weathering rates of the remaining primary residuals, the enhanced production of kaolinite (Meunier and Velde, 1976) and advanced profile differentiation (Bondam, 1968). The lessivation increases the erodibility of soil (Blume and Schwertmann, 1969). This is why possible remains of the top soil paleo-acrisoles and -alisoles may have been removed entirely through the covering of the Rabekke Formation.

Podzolization, here used in sense of profile differentiation, is a vertically downward directed process (Figure 4.2) under enhanced acidic circumstances, where organic material, together with Al and Fe^{2+}, is dumped and deposited in lower areas of the soil profile (Schmitz, 2008).

The above elucidated processes of primary mineral dissolution and precipitation are mostly associated with early diagenetic (weathering) processes, which may occur in pre-burial to early burial state of the weathering succession under low temperatures ($< 250\,^{\circ}C$). Nesbitt and Young (1989) stated, that early diagenetic reactions often result in ”abnormally high accumulation” of carbonates, which may be used as indicators for the plaeo-water table.

4.2.2.1 Late diagenetic reations

In comparison to early-, late-diagenetic reactions are rather associated with the syn- or post burial state of the weathering profile (Nesbitt and Young, 1989). As previously discussed, soil profile differentiation processes like lessivation and other profile differentiation processes could be responsible for a relative accumulation of carbonates in the lower weathering profile horizons (see Figure 4.2). The abnormally high siderite in profile B (saprolite horizon) and more pore space restricted calcite concentrations in the saprolitic profile at Nygård may be reason to believe that the mineral associations are rather related to syn-burial of the weathering section, under increased temperatures. Original 27 XRD% of siderite and 7 XRD% calcite were estimated in profile B. Thin section analysis revealed a strongly pervasive character of the iron carbonate, often overgrowing kaolinite in inter-mineral spaces (see Figure 3.24 a)). SEM images of stub samples, illustrated in Figure 3.36, display spheritic siderite rhomboheders overlaying visibly weathered and etch pitted K-feldspar. The pervasive overgrowth of siderite over kaolinite, as well as the overgrowth over formerly weathered K-feldspar indicates an younger age for the carbonates. Siderite is further more thought to have formed under increased

temperature conditions, more likely associated with burial (Helge Hellvang (UIO) personal communication). The appearance of the iron carbonate within larger pore spaces in thin sections was found to form ”blossom-like” structures, whereas meso- and micro-fractures were often associated with more massive filling. This observation suggests precipitation conditions strongly related to the hydrological influence of percolating groundwaters. Remarkable in comparison of the two profiles (B and D) was that in profile D more heterogeneous corestone association was found. The siderite concentration dropped to 7 XRD% while an increase in calcite of 9 XRD% could be recorded. This indicates an relation of carbonate precipitation to the hydraulic conductivity. Profile B, constituted of a rather massive and less weathered corestone complex, which obviously enhanced the formation of siderite. This may be related to the decreased porosity and a higher field capacity of the capillaries, exhibiting the liberation

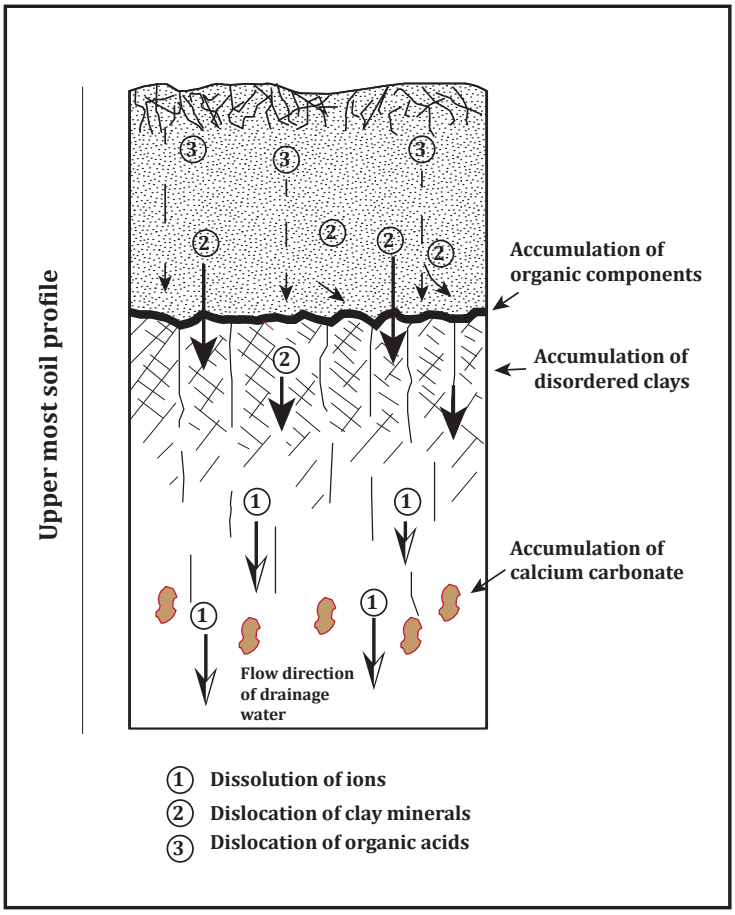

Figure 4.2: Simplified mechanism of podzolization (modified after Righi and Meunier (1995))

of Fe^{2+} at higher temperatures.

Gravesen et al. (1982) recorded common sideritic nodules within the lower-most Rabekke Formation, interfering with coarse to medium sized, unsorted sandstone. The sedimentology of the Rabekke Formation, together with the local tectonically setting, may lead to the suggestion that the paleogeological setting during burial of the formation was associated with a fresh water lacustrine environment. This observation may be supported by the presence of recrystallized K-feldspar, found in the samples of the weathering succession (see Figure 3.36) which, in comparison to older, etch pitted K-feldspar (Figure 3.34), yields no sign of alteration. Nesbitt and Young (1989) summarized the transformation of illite or partially altered K-feldspar to neogenetic K-feldspar under buried conditions as K-metasomatosis, which is dependent on temperature and the concentration of Na^+/K^+ in the weathering solution (see Figure 4.4). Nesbitt and Young (1989) postulated that K-matasomatosis is only common for continental settings. Ar/Ar-age dating for the neogenetic K-feldspar seem a reasonable approach and is strongly recommended for further work, to receive more information about timing of the late diagenetic processes in the succession. In addition, geochemical studies seem necessary to find out more about the disposition of intermediate clay phases and neogenetically formed mineral phases.

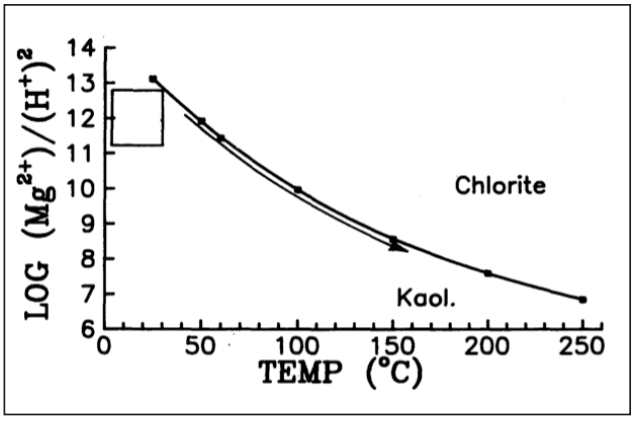

Figure 4.3: Temperature related changes in ratio of Mg^{2+}/H^+, displaying the chlorite/kaolinite solution equilibrium relations. The diagram displays the increasing stability of chlorite with temperature at the expense of kaolinite at decreasing Mg^{2+}/H^+ concentration in the weathering solution (Nesbitt and Young (1989)).

With increasing temperature during burial, chlorite may form at the expense of kaolinite Nesbitt and Young (1989). This reaction is controlled by the amount of solved Mg^{2+}/H^+ (Figure 4.3) in the weathering solution and the prevailing thermodynamically conditions associated with low temperature (< 250 °C) (Nesbitt and Young, 1989). The formation of partly Mn-enriched clinochlor could be observed in SEM stub samples of profile B, displayed in Figure 3.36. Cauliflower structures were most common, growing on recrystallized K-feldspar (Figure 3.36 c)) and rhombohedral siderite (Figure 3.36 a1) and a2)), implying late diagenetic reactions during the weathering profile may have been entirely in contact with oozing ground

waters. The formation of neogenetic K-feldspar and chlorite are strongly associated with fresh water conditions, where less acidic conditions are anticipated than in sea water influenced conditions. Nesbitt and Young (1989) suggested the following reaction for the late diagenetic formation of chlorite at the expense of kaolinite:

$$Al_2Si_2O_5(OH)_4 + SiO_2 + 5\,Mg^{2+} + 7\,H_2O \longrightarrow Mg_5Al_2Si_3 + 10\,(OH)_8 + 10\,H^+ \qquad (4.2.5)$$

4.2.2.2 Post burial and re-exposure of the weathering profile

During the latest stage of diagenesis and re-exposure of the weathering profile, heavy oxidation was probably introduced to the profile, several origins are possible. Climatic changes from a formerly humid, tropical climate to more dry and arid conditions (see Figure 1.8 and Lidmar-Bergström (1983)) could have led to prolonged seasonal ground water oscillations. Other reasons may be found in the tectonical development of the area along the western margin of Bornholm. During the Late Cretaceous to the Early Cenozoic transpressional tectonic movements within the Sorgenfrei-Tornquist Zone are recorded as a product of the Alpine orogenesis, including fault reactivation and inversion tectonics, reactivation resulted in the Neogene-Pleistocene regional uplift of the area, which comprised the vast erosion of the Bornholm Mesozoic sediments(Gry, 1969; Gravesen et al., 1982; Liboriussen et al., 1987; Michelsen and Nielsen, 1991, 1993).

Fracture measurements conducted in field, at the Klippeløkken granite quarry and the approximately 800 m distant weathering profile at Nygård (see Table 3.3 and Figure 3.20) revealed, that dominant strike directions in the fresh granite coincides well with the suggested macro-geological trends of the mosaic like horst-block zone along the south-western margin of Bornholm (see Graversen (2010) for more details). General fault directions, both in the Palaeozoic and in the Mesozoic rock groups are dominated by WNW- ESE and NNW-SSE strikes (Graversen, 2010). These trends could be affirmed by fracture measurements in the Rønne Granite, where dominant strike directions of NNW to SSE (350°) and WNW to ESE (70°) agree well with the overall regional trend. The fracture measurements at the Nygård kaolin pit display very agreeable strike directions, 80 % of the fractures were pronounced in NNW-SSE direction. This indicates, that there has been no or very little tectonic activity between the two localities. Textural analysis of thin sections show similar observations, since the preserved friable rock structure was almost entirely preserved in the saprolite. Henceforth it can be suggested that the area around the weathering profile at Nygård was uniformly exposed to tectonic movement during the formation of the thick kaolinitic weathering crust and the saprolite profile was only influenced by tectonics on a larger scale. Thereby the last essential parameter, tectonic stability, is fulfilled beside climatic and mineralogical conditions as preliminaries for the formation of thick kaolinitic crusts, as postulated by Petrov (1967);

Störr and Bellmann (1975) (see section: *formation of weathering crusts*).

Eggleton and Taylor (1998) described, that prolonged seasonal oscillations of the water table can lead to the "gradational removal" of Fe^{2+} of the preexisting rock matter, within the fringe zone of intermitted saturation. The liberated ferrous iron is then likely to precipitate on oxidation ($Fe^{3+} -> Fe^{2+} + OH^-$) at the wet water table (Eggleton and Taylor, 1998). It is likely that the observed iron oxidized horizon in the Nygård profile constitutes the paleo-water table.

4.3 Comparison with other localities

4.3.1 Recent weathering

4.3.1.1 Oporto and Braga, NW-Portugal

Weathering of Quaternary, granitic saprolites in Northwestern Portugal, studied by Braga et al. (2002) represent an important example for recent alteration under temperate, arid climatic conditions. Various profiles from two field localities displayed secondary clay mineral phases of gibbsite and kaolinite, under currently prevailing climatic conditions characterized by average annual precipitation rates between 1200 mm to 1600 mm and mean temperatures of 14 °C to 17 °C (Braga et al., 2002).

The general weathering sequence, of plagioclase before mafic phases like biotite seem comparable to Nygård. Especially the mode of biotite denudation is strikingly similar, extremely sharp mineral margins with interlaying kaolinite and/or mixed layer clay associations could be observed in SEM (Braga et al., 2002). Detailed studies of the secondary mineral assemblage revealed strong differences from those at Nygård where kaolinitic argillization was dominating, in contrast to the Portugal profiles, which were characterized by arenization. Main secondary phases distinguished in the Portogese samples, were 0% to 45% of 2:1 clay minerals (illite, chlorite and mixed layers) and 10% to 85% of 1:1 clay minerals (kaolinite, metahalloysite) as well as iron and aluminium oxy-hydroxides (primarily gibbsite and goethite) (Braga et al., 2002). The authors determined gibbsite and kaolinite as the most abundant secondary phases in the granitic saprolite, indicating the high maturity of the studied sections. This stands in strong contrast to the weathering profile at Nygård, where no gibbsite or goethite was found and the profile is rather dominated by the iron-oxide hematite.

Braga et al. (2002) defined three principal characteristics for the studied profiles, which all were "more than 10m deep, had an remarkably high material loss of 40% (calculated by isovolumetric approach) and all represented an relatively low clay content an high degree of mineralogical evolution". It is especially the high material loss and the arenization ('sandification') which contrasts to the weathering profile in Nygård. Arenization in temperate weathering profiles may be partly explained by the formerly introduced mechanism

of podzolization (see Figure 4.2), which coincides with increasing acidification and vertically downward dislocation of clay minerals in the profile. The leached top soil remains more easily erodible and relatively enriched with pristine quartz, which could explain the high material loss. (Braga et al., 2002) argued, that arenization may yield an important weathering process in temperate climate zones. This is in agreement with Eggleton and Banfield (1985) who suggested that the process of arenization and mechanisms of podzolization may explain some of the white sand formations studied in western Australia. Pédro et al. (1997) and Braga et al. (2002) suggested a climatic zonality for the appearance of secondary minerals in weathering profiles, distinguished according a southward gradation recorded from Scandinavia in the north to Portugal in the south. Pédro et al. (1997) suggested the following zonal dependency:

- Cold and wet: tendency towards vermiculite
- Temperate: kaolinite group (kandites)
- Warm: kaolinite

It can be concluded that the formation of the Nygård kaolin took place under different, more humid and tropical conditions. The arenitic paragenesis studied in Oporto and Braga, with relatively low kaolinite concentration and high abundance of gibbsite reflect arid to temperate conditions, which contrasts the weathering sequences elucidated in this thesis.

4.3.2 Paleo-weathering

4.3.2.1 Ivö Klack

In Scania, a 200 m wide and 22 m thick saprolite section is exposed in the Ivö Klack kaolin quarry (Naqvi, 2013) (Figure 1.1). The site is located on the island Ivö, a part of the Kristianstad basin. The present section represents a Campanian rocky coast (Surlyk and Sørensen, 2010) covered by Cretaceous, fossiliferous carbonates, showing the upper border of the weathering profile. The clay mineral assemblages at Ivö Klack display a shift from smectite- rich red beds, to kaolinite-rich, coal-bearing successions. According to Ahlberg et al. (2003) this corresponds to the change from Early-/ Mid- Triassic, semi- arid conditions to more permanently warm and year-round humid climate during the Rhaetian, Lower Jurassic. Lidmar-Bergström (1995) pointed out, that the kaolinitic weathering may have been initiated during the Late Triassic to Early Jurassic and continued, under prevailing humid and tropical weathering conditions throughout the Jurassic. Time range of weathering and the general mineralogy, seem to coincide with the Bornholm locality. The thickness of the kaolinite deposit at Ivö Klack was recorded by Lidmar-Bergström (1983) of approximately 50 m. Kaolinite deposits at Nygård were determined by Bondam (1967) of maximum 30 m. The thickness variation between the two localities, may indicate longer weathering for the Ivö locality from Late Triassic (Rhaetian)

Lidmar-Bergström (1995), whereas the weathering time for Nygård is assumed at latest from Early Jurassic.

The bedrock geology, recently discussed by Naqvi (2013) revealed a syenite- to monzosyenite granite paragenesis of the Vånga parent rock. Naqvi (2013) suggested according point counting analysis 38% quartz, 23% plagioclase and 39% K-feldspar as main constituents of the Vånga Granite source rock. The much higher quartz concentration, as well as the predominance of K-feldspar over plagioclase give the Vånga Granite a rather leucocrate appearance, in comparison to the more mafic Rønne Granite. Sericitization in plagioclase minerals is well developed along twinning planes, but absent along micro-fractures in the Vånga Granite (Naqvi, 2013). This stands in contrast to the plagioclase association of the Rønne Granite where sericitization in both orientations could be found and might indicate differences in igneous melt cooling and retrograde metamorphic appearances for the two localities. The dominance of K-feldspar over plagioclase supports a more continuous cooling history for the Vånga Granite. Perthitic albite exsolution was frequent within K-feldspar crystals and SEM analysis revealed in accordance to the Nygård result the substitution of albite towards kaolinitic clays at early weathering stage.

At Ivö it was possible to sample the entire weathering sequence from solid bedrock to the kaolinite residual, while at Nygård only the saprolite horizon could be studied and fresh samples had to be analyzed from the 800 m distant Klipeløkken granite quarry.

This close profile sampling revealed a contrasting weathering sequence at the Ivö Klack locality, where Naqvi (2013) recorded a general trend of kaolinite$>>$ illite $>$ smectite, in contrary to the Nygård locality which was represented by kaolinite $>>>$ chlorite $>>$ smectite $>$ illite for the secondary clay association. Further more, a vermiculite intermediate phase was noted in SEM observations as interstage product of biotite weathering at Ivö Klack, which in this case may be addressed to the absence of hornblende. The general trend observed in sections at Ivö Klack reflects an distinct tendency of prograding kaolinite accumulation in the upper parts and in contrast an relative abundance of smectite in the lower parts of the profiles at the bedrock saprolite boundary. This trend is hardly consistent for the profiles studied at Nygård where the clay mineral distribution seem more heterogeneous.

Naqvi (2013) distinguished two main types of carbonates, namely calcite and dolomite, in the sections studied by XRD analysis. He further stated, that the carbonate association could be attributed as fine grained veins or concretions derived from the overlaying, leaching sub-Cretaceous limestone cover studied in thin section. The general absence of siderite concretions associated with late diagenetic processes during burial in Nygård may include significant information about the profile evolution at Ivö Klack. Nesbitt and Young (1989) stated, that the introduction of calcium carbonate to a mature weathering profile is likely to be inhibited, due to the ”acidic nature” of such well developed profiles. This absence could be addressed to a higher concentration of felsic compartments, which may lead to higher acidity of the

weathering solutions baring more diluted silicic acid.

Other reasonable solutions may lay in the observation of Naqvi (2013), who distinguished recrystallized plagioclase in some sections. Nesbitt and Young (1989) postulated a feasibility for the diagenetic formation of plagioclase in sea water dominated weathering profiles with rather high Na^+/K^+ values (as dissolved ions) or of a sea water derivate influenced, buried profiles (Figure 4.4). The recrystallization of plagioclase in a buried profile may then be exhibited at relatively low diagenetic temperatures (below 200 °C). In contrast to that, the Nygård profile exposed the presence of recrystallized K-feldspar (see Figure 3.36 c)) which according to Nesbitt and Young (1989) may be related to rather low values of dissolved Na^+/K^+ in solution, associated with dilute continental waters. Nesbitt and Young (1989) further pointed out, that continental waters would plot within the K-feldspar field for all temperatures below 250 °C (Figure 4.4). This observation may bare the evidence, that the mature, buried weathering profile at Ivö Klack was rather seawater dominated, whereas the weathering profile at Nygård belonged to a continental realm. The presence of high values of Na^+/K^+ in the weathering solution may yield higher weathering rates of minerals, since sea water is thought to be more reactive than fresh water. This could have led to the formerly described suppression of carbonate formation during the burial of the weathering profile at Ivö Klack and suggests that the low concentrations of calcite and dolomite are rather related to the carbonate dissolution and re-precipitation from the overlaying, Campanian fossiliferous limestone. In the contrast to the Nygård profile, where siderite formation could be distinguished having diagenetic characteristics and thus may have formed under less acidic conditions, which is further supported by the relatively high presence of post burially formed chlorite, associated with comparable temperature conditions (Nesbitt and Young, 1989).

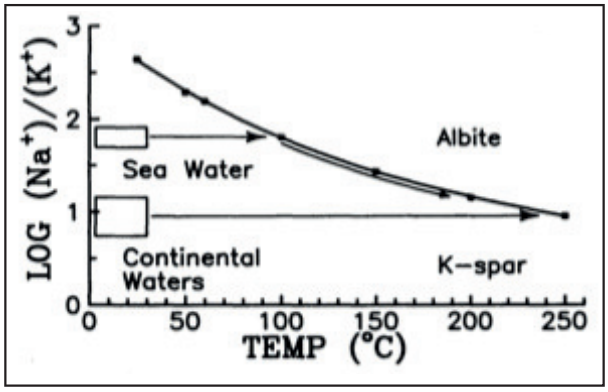

Figure 4.4: Temperature related changes in ratio of Na^+/K^+, displaying the albite/K-feldspar solution equilibrium relations. The lower K-spar stability field is restricted to continental fluids, whereas the the neogenesis of albite takes place under sea water, with higher concentrations of dissolved Na^+/K^+ Nesbitt and Young (1989).

4.4 Implications for the Utsira-project

Two drill cores from the Edvard Grieg field and the Johan Svedrup (Well 16/3-4) field on the Utsira High, an intra-basinal structural high, displaying well developed weathering sequences. Preliminary dating, conducted at the NGU (Norges geologiske undersøkelse) suggest Mid to Late Triassic age of the weathering formation. Prevailing warmer and drier climatic conditions

may explain the low presence of kaolinitic particles within the upper most part of the profile. The two acquired drill cores give only a limited insight on highly heterogeneous, 3 dimensional weathering profiles and the lateral component is missing. The lateral behavior might change on centimeter scale and is thereby hard to detect from a strictly vertical core. The study presented in this work and the equivalent work performed by Naqvi (2013), may therefore contribute valuable information for the interpretation of such profiles found in cores. The low kaolinite concentrations in the upper part of the profile and the climatic conditions prevailing during the preliminary estimated time of weathering, may indicate similar processes studied in Portugal of arenization. In contrary both onshore localities in Ivö and Bornholm were rather dominated by processes of argillization and characterized by thick kaolinite deposits, which suits more tropical conditions. The geological setting of the weathering profile found on the Utsira High and that at Nygård both located within horst block structure, may carry similarities.

Internal mineral associations as presented in this work contain key informations about the profile development and paleo-climatic conditions. Neo genetic formations, e.g. plagioclase or K-feldspar can be used to differentiate, wether the profile formed under continental or marine circumstances and dating approaches for authigenic K-feldspar or plagioclase are recommended. Further geochemical analysis might comprise important information about the succession generation. In general it can be stated, that detailed mineralogical analysis of the drill core material may contain the potential to reconstruct a formation model, based on the comparison to onshore localities. If the Jurassic weathering profiles in Bornholm and Ivö Klack comprise appropriate onshore analogues for the Utsira profiles, will be elucidated by the work of Lars Riber (UIO).

5 | Conclusion

The study of clay sedimentary particles at the saprolitic, deep weathering profile at Nygård, revealed the presence of different mineralization generations (see summary Figure 5.1) in the section. The subdivision into four distinct generations was established.

1. Post magmatic, retrograde metamorphism; hydrothermally alteration of plagioclase, foremost anorthite, to sericite. Two orientations of sericitization could be studied, implying discontinuous retrograde cooling and multiple, hydrothermal intrusions. The paragenesis of the Rønne granite constitutes a monzo-granite with marginally predominance of plagioclase over K-feldspar.

2. Sub-aerial weathering of primary mineral associations and the precipitation of secondary clay mineral phases associated with the reaction of percolating groundwaters may have formed the incipient zone of the weathering profile. It is assumed to have started within the Early Jurassic.

3. Late weathering reactions associated with the formation of carbonate and authigenic K-feldspar are assumed to have resulted during and following burial. The interplay between continental ground waters and mechanisms of podzolization may have induced further profile differentiation.

4. Post burial, recurrent exposure of the profile through fault reactivation and inversion tectonics in the Early Cretaceous-Laten Cenozoic, such as climatic changes towards a more arid situation during the Late Mesozoic, may resulted the erosion of the vulnerable acrisoles covering the formation and to the re-exposure of the residual clay horizon.

Early diagenetic dissolution reactions were established according the primary mineral associations of plagioclase, hornblende and biotite, as most prone to weathering phases observed. Plagioclase ultimately formed kaolinite, hornblende precipitated incipiently from chlorite to a undetermined intermediate phase (likey smectite) and finally to kaolinite. Biotite likewise formed incipient chlorite intermediate illite, illite/smectite mixed-layer clay minerals and terminated in the precipition of kaolinite.

Late diagenetic reactions in the weathering section are foremost constituted by the formation of sideritic carbonate, which indicates a relatively high pH and temperature situation within the profile during burial. This might also explain the etch pitted surface of quartz grains which is associated with alkalic pH values. The neo-formation of K-feldspar may be addressed to the high content of dissolved K^+/H^+ in the weathering solution, during burial. The formation of potassium-rich feldspar on the expense of illite and/or kaolinite, such as the observed formation of Mn-rich clinochlor encourages the assumption that the weathering profile at Nygård was mainly influenced by continental waters under lacustrine circumstances, than by sea water entrapment. Sea water entrapment may lead to the recrystallization of plagioclase, as observed by Naqvi (2013) at Ivö Klack. Ar/Ar- or K/Ar-dating is highly recommended for the age determination of the K-feldspar at Nygård and for the plagioclase in Ivö Klack, to gain more information about the formation of the two onshore localities.

The strong oxidation staining observed macroscopically and in latter petrographical analysis is a suggested product of prolonged seasonal ground water oscillations. The hydrological variance may be a result of two unlinked agents. Late Cretaceous- Early Cenozoic inversion tectonics may have introduced regional uplift and increased erosion of the covering layers and climatic changes towards more arid conditions were recorded during the Mid Cretaceous. This could have led to enhanced seasonal differentiation and terminated in the precipitation of iron oxide upon the pale water table. Fracture/joint measurements at the kaolin pit and at the 800 m distant granite quarry revealed no differing fracture orientation, which exhibits that no internal movements occurred within the studied area and the weathering profile matured under tectonically stable conditions.

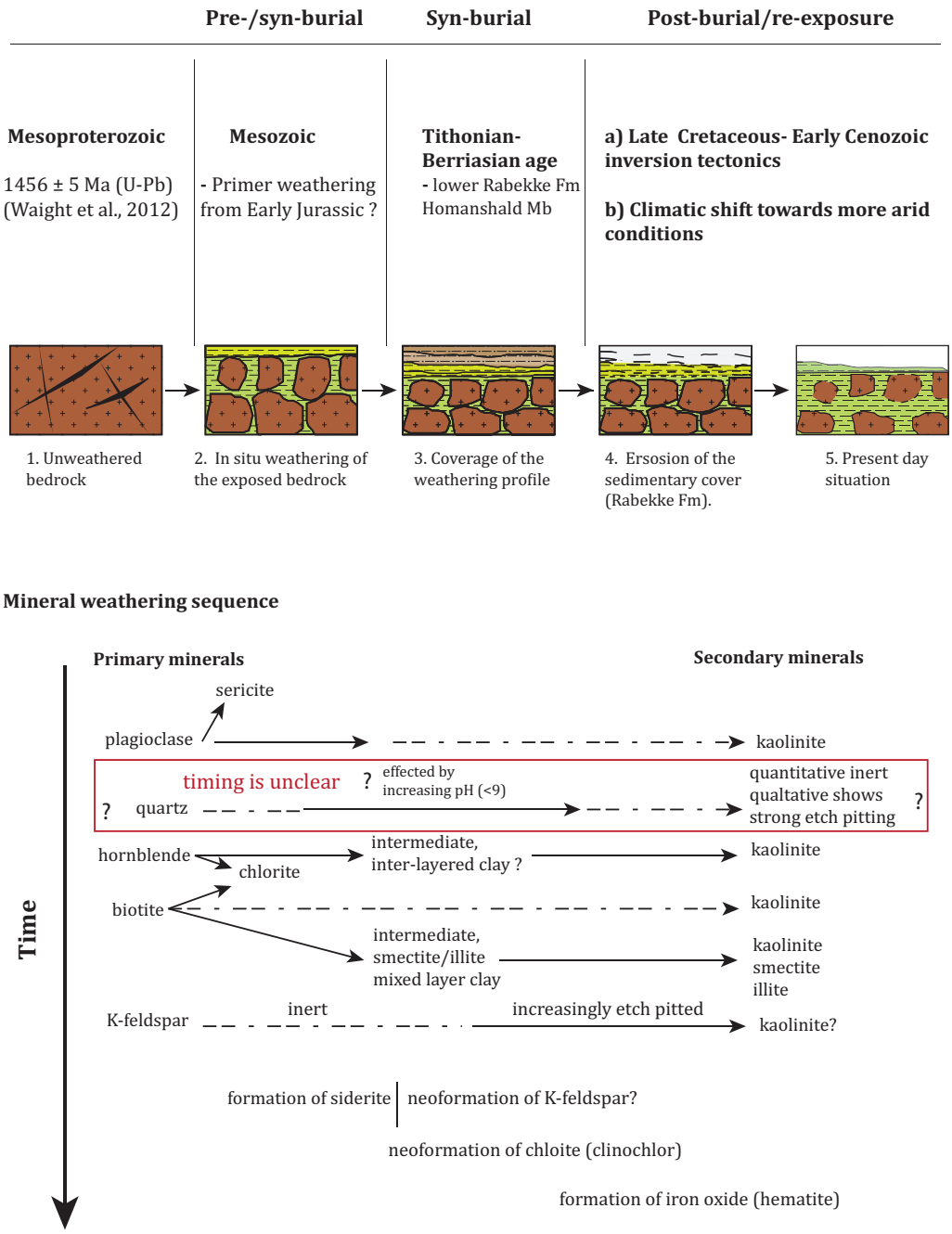

Figure 5.1: Summary figure for the formation constrain of the weathering profile and the associated weathering sequence from primary to secondary minerals.

References

Ahlberg, A., Olsson, I., and Šimkevičius, P. (2003). Triassic-Jurassic weathering and clay mineral dispersal in basement areas and sedimentary basins of southern Sweden. *Sedimentary Geology*, 161(1):15–29.

Ahn, J.-H. and Peacor, D. R. (1987). Kaolinization of biotite–TEM data and implications for an alteration mechanism. *American Mineralogist*, 72(3):353–6.

Anand, R. and Gilkes, R. (1984). Weathering of hornblende, plagioclase and chlorite in meta-dolerite, Australia. *Geoderma*, 34(3):261–280.

Baartman, J. and Christensen, O. (1975). *Contributions to the interpretation of the Fennoscandian Border Zone*. I kommission hos CA Reitzel.

Bates, R. and Jackson, J. (1987). Glossary of Geology: American Geological Institute. *Alexandria, Virginia*, 788.

Berthelsen, A. (1998). The Tornquist Zone northwest of the Carpathians: an intraplate pseudosuture. *GFF*, 120(2):223–230.

Blum, A. E. (1994). Feldspars in weathering. In *Feldspars and their reactions*, pages 595–630. Springer.

Blume, H. and Schwertmann, U. (1969). Genetic evaluation of profile distribution of aluminum, iron, and manganese oxides. *Soil Science Society of America Journal*, 33(3):438–444.

Blume, H.-P., Brümmer, G. W., Horn, R., Kandeler, E., Kögel-Knabner, I., Kretzschmar, R., Stahr, K., and Wilke, B.-M. (2010). *Scheffer/Schachtschabel: Lehrbuch der Bodenkunde*. Spektrum Akademischer Verlag.

Boggs, S. (2006). Principles of sedimentology and stratigraphy: Pearson Education. *Inc., Upper Saddle River, New Jersey*.

Bölau, D. (1973). Die Kimmerischen Bewegungen im tektonischen Bilde Schonens. *GFF*, 95(2):165–180.

Bondam, J. (1967). Undersøgelser vedrørende de geokemiske forhold i kaolinforekomsten ved Rønne på Bornholm. *Bulletin of the Geological Society of Denmark*, 17:297–356.

Bondam, J. (1968). Investigations in the geochemical distribution of the major elements in some kaolin deposits. *XXIII Intern. Geol. Congr. 14, 32*, 37.

Bondam, J. (1984). Kaolinized granodiorite and its sedimentary cover on Bornholm. *Non-metallic mineral ores*, 15:319.

Bondam, J. and Störr, M. (1988). Transition in chemical and mineralogical composition around unweathered relicts of granodiorite in the kaolin deposit on Bornholm, Denmark. *Bull. gcol-Soc. Denmark*, 37:1–2.

Borchardt, G. (1989). Smectites. *Minerals in soil environments*, (mineralsinsoile):675–727.

Braga, S., Paquet, H., and Begonha, A. (2002). Weathering of granites in a temperate climate (NW Portugal): granitic saprolites and arenization. *Catena*, 49(1):41–56.

Brinkmann, R. and Sanders, J. (1969). *Geologic evolution of Europe*. Enke (Publisher).

Buchwald, J. (1971). Zur Genese der Oberlausitzer Kaoline und Tone. *Geologie, Berlin*, 20:38–61.

Burst, J. F. (1969). Diagenesis of Gulf Coast clayey sediments and its possible relation to petroleum migration. *AAPG bulletin*, 53(1):73–93.

Busenberg, E. and Clemency, C. V. (1976). The dissolution kinetics of feldspars at 25° C and 1 atm CO< sub> 2</sub> partial pressure. *Geochimica et Cosmochimica Acta*, 40(1):41–49.

Callisen, K. (1934). *Das grundgebirge von Bornholm*. I kommission hos CA Reitsels forlag.

Callisen, K. (1957). Hornblende with pyroxene core in the Rønne Granite, Bornholm. *Meddelser Dansk Geologisk Forening*, 13:236–237.

Dörhöfer, G. and Norris, G. (1977). Discrimination and correlation of highest Jurassic and lowest cretaceous terrestrial palynofloras in north-west Europe.

Eggleton, R. and Taylor, G. (1998). Selected thoughts on laterite. In *New Approaches to an Old Continent: Proceedings of the 3rd Australian Regolith Conference*, pages 209–226.

Eggleton, R. A. and Banfield, J. F. (1985). The alteration of granitic biotite to chlorite. *American Mineralogist*, 70(9-10):902–910.

EUGENO-S (1988). Crustal structure and tectonic evolution of the transition between the Baltic Shield and the North German Caledonides (the EUGENO-S Project). *Tectonophysics*, 150(253):3.

Fordham, A. et al. (1990). Weathering of biotite into dioctahedral clay minerals. *Clay Minerals*, 25(1):51–63.

Fritz, S. J. and Ragland, P. C. (1980). Weathering rinds developed on plutonic igneous rocks in the North Carolina Piedmont. *American Journal of Science*, 280(6):546–559.

Gerrard, J. (1994). Weathering of granitic rocks: environment and clay mineral formation. *Rock weathering and landform evolution*, 10:1.

Gjems, O. (1967). Studies on clay minerals and clay-mineral formation in soil profiles in Scandinavia. *Norwegian Forest Research Institute, Vollebekk, Norway*.

Goldich, S. S. (1938). A study in rock-weathering. *The Journal of Geology*, pages 17–58.

Goldstein, J., Newbury, D. E., Joy, D. C., Lyman, C. E., Echlin, P., Lifshin, E., Sawyer, L., and Michael, J. R. (2003). *Scanning electron microscopy and X-ray microanalysis*. Springer.

Graff-Petersen, P. and Bondam, J. (1963). *Hasle Klinkerfabrik Clay Pit and Rabekke Clay Pit: A Short Geological and Clay-mineralogical Description*. A/S Hasle Klinker & Chamottestensfabrik.

Grant, W. H. (1964). Chemical weathering of biotite-plagioclase gneiss. *Clays Clay Miner*, 12(3):455–463.

Graversen, O. (2004). Upper Triassic–Cretaceous stratigraphy and structural inversion offshore SW Bornholm, Tornquist Zone, Denmark. *Bulletin of the Geological Society of Denmark*, 51:111–136.

Graversen, O. (2010). Structural analysis of superposed fault systems of the Bornholm horst block, Tornquist Zone, Denmark. *Bulletin of the Geological Society of Denmark*, 57:25–49.

Gravesen, P., Andersen, S., and Naturstyrelsen, S.-o. (1996). *Geologisk set: Bornholm: en beskrivelse af områder af national geologisk interesse*. Geografforlaget.

Gravesen, P., Rolle, F., and Surlyk, F. (1982). Lithostratigraphy and sedimentary evolution of the Triassic, Jurassic and Lower Cretaceous of Bornholm, Denmark. *Geol. Surv. Denmark*.

Gry, H. (1956). Wealdenaflejringerne på Bornholm. *Meddelelser fra Dansk Geologisk Forening, København*, pages 13–134.

Gry, H. (1960). *Geology of Bornholm: guide to excursions nos. A 45 and C 40*.

Gry, H. (1969). Megaspores from the Jurassic of the island of Bornholm, Denmark. *Meddelelser fra Dansk Geologisk Forening*, 19:69–89.

Hays, J. and Pitman, W. (1973). Lithospheric plate motion, sea level changes and climatic and ecological consequences. *Nature*, 246(5427):18–22.

Heim, D. (1990). *Tone und Tonminerale: Grundlagen der Sedimentologie und Mineralogie*. Enke.

Jackson, M. and Sherman, G. (1953). Chemical weathering of minerals in soils. *Adv. Agron*, 5:219–318.

Jørgart, T. (2000). The basement geology of Bornholm. In *An excursion guide. Paper for the field conference "TransBaltic Precambrian Correlations", the Visby Programme/Swedish Institute and EUROBRIDGE/ESF. Bornholm-Blekinge*, pages 17–30.

Kapoor, B. (1972). Weathering of micaceous clays in some Norwegian podzols. *Clay Miner*, 9(4):383–394.

Knauss, K. G. and Wolery, T. J. (1988). The dissolution kinetics of quartz as a function of pH and time at 70 C. *Geochimica et Cosmochimica Acta*, 52(1):43–53.

Kominz, M., Browning, J., Miller, K., Sugarman, P., Mizintseva, S., and Scotese, C. (2008). Late Cretaceous to Miocene sea-level estimates from the New Jersey and Delaware coastal plain coreholes: An error analysis. *Basin Research*, 20(2):211–226.

Kretzschmar, R., Robarge, W., Amoozegar, A., and Vepraskas, M. (1997). Biotite alteration to halloysite and kaolinite in soil-saprolite profiles developed from mica schist and granite gneiss. *Geoderma*, 75(3):155–170.

Krumb, J. H. (1998). *Bedingungen, Prozesse und Stoffbilanz der Kaolinisierung-das Beispiel der Lagerstätten Sachsens*. Ed. Bodoni.

Laursen, I., Fugelli, E., and Lervik, K. (1995). Sequence stratigraphic framework of the Paleocene and Eocene successions, block 16/1, Norwegian North Sea. *Norwegian Petroleum Society Special Publications*, 5:471–481.

Liboriussen, J., Ashton, P., and Tygesen, T. (1987). The tectonic evolution of the Fennoscandian Border Zone in Denmark. *Tectonophysics*, 137(1):21–29.

Lidmar-Bergström, K. (1983). Pre-Quaternary geomorphological evolution in southern Fennoscandia. *Dissertation abstracts international. C. European abstracts*, 44(3).

Lidmar-Bergström, K. (1995). Relief and saprolites through time on the Baltic Shield. *Geomorphology*, 12(1):45–61.

Lindgren, J., Currie, P. J., Rees, J., Siverson, M., Lindström, S., and Alwmark, C. (2008). Theropod dinosaur teeth from the lowermost Cretaceous Rabekke Formation on Bornholm, Denmark. *Geobios*, 41(2):253–262.

Meunier, A. (2005). *Clays*. Springer.

Meunier, A. and Velde, B. (1976). Mineral reactions at grain contacts in early stages of granite weathering. *Clay Minerals*, 11(3):235–240.

Meunier, A. and Velde, B. (1982). Phengitization, sericitization and potassium-beidellite in a hydrothermally altered granite. *Clay Minerals*, 17(3):285–299.

Michelsen, O. and Nielsen, L. (1991). Well records on the Phanerozoic stratigraphy in the Fennoscandian Border Zone, Denmark. *DGU, Danmarks Geologiske Undersøgelse. Serie A*, (29):4–37.

Michelsen, O. and Nielsen, L. (1993). Structural development of the Fennoscandian border zone, offshore Denmark. *Marine and petroleum geology*, 10(2):124–134.

Millot, G., Farrand, W. R., and Paquet, H. (1970). *Geology of clays: weathering, sedimentology, geochemistry*. Springer-Verlag New York and Berlin.

Moore, D. M., Reynolds Jr, R. C., et al. (1989). *X-ray diffraction and the identification and analysis of clay minerals.* Oxford University Press (OUP).

Murphy, S., Brantley, S., Blum, A., White, A., and Dong, H. (1998). Chemical weathering in a tropical watershed, Luquillo Mountains, Puerto Rico: II. Rate and mechanism of biotite weathering. *Geochimica et Cosmochimica Acta*, 62(2):227–243.

Nahon, D. B. (1991). Self-organization in chemical lateritic weathering. *Geoderma*, 51(1):5–13.

Naqvi, S. A. A.-E.-M. (2013). Weathering of Precambrian basement and formation of sedimentary particles in Scania. Master's thesis, University of Oslo.

Nesbitt, H. and Young, G. (1984). Prediction of some weathering trends of plutonic and volcanic rocks based on thermodynamic and kinetic considerations. *Geochimica et Cosmochimica Acta*, 48(7):1523–1534.

Nesbitt, H. and Young, G. M. (1989). Formation and diagenesis of weathering profiles. *The Journal of Geology*, pages 129–147.

Nesbitt, H. W. (1979). Mobility and fractionation of rare earth elements during weathering of a granodiorite.

Norling, E. and Bergström, J. (1987). Mesozoic and Cenozoic tectonic evolution of Scania, southern Sweden. *Tectonophysics*, 137(1):7–19.

Ollier, C. (1971). Causes of spheroidal weathering. *Earth-Science Reviews*, 7(3):127–141.

Ollier, C. et al. (1984). *Weathering.* Longman Group, second edition edition.

Ollier, C., Pain, C., et al. (1996). *Regolith, soils and landforms.* John Wiley & Sons.

Pedro, G. (1983). Structuring of some basic pedological processes. *Geoderma*, 31(4):289–299.

Pédro, G., Paquet, H., Clauer, N., et al. (1997). Clay minerals in weathered rock materials and in soils. *Soils and sediments: mineralogy and geochemistry.*, pages 1–20.

Petersen, H. I., Bojesen-Koefoed, J. A., and Nytoft, H. P. (1996). Depositional environment and burial history of a lower cretaceous carbonaceous claystone, bornholm, denmark. *Bulletin of the Geological Society of Denmark*, 43(2):133–142.

Petersen, H. I., Nielsen, L. H., Bidstrup, T., and Thomsen, E. (2003). Burial depth and post-early cretaceous uplift of lower–middle jurassic strata in the fennoscandian border zone based on organic maturity. *The Jurassic of Denmark and Greenland. Geological Survey of Denmark and Greenland Bulletin*, 1:611–630.

Petrov, V. (1967). Fundamentals In Study Of Ancient Weathering Crusts.

Pitman, W. and Talwani, M. (1972). Sea-floor spreading in the North Atlantic. *Geological Society of America Bulletin*, 83(3):619–646.

Prasad, G. and Sarracino, R. (1989). Initial stages in spheroidal weathering. *Sciences géologiques*.

Que, M. and Allen, A. R. (1996). Sericitization of plagioclase in the Rosses granite complex, Co. Donegal, Ireland. *Mineralogical Magazine*, 60(403):927–936.

Rebertus, R., Weed, S., and Buol, S. (1986). Transformations of biotite to kaolinite during saprolite-soil weathering. *Soil Science Society of America Journal*, 50(3):810–819.

Righi, D. and Meunier, A. (1995). Origin of clays by rock weathering and soil formation. In *Origin and mineralogy of clays*, pages 43–161. Springer.

Schmitz, M. (2008). *vorgelegt von Diplom-Geologe Martin Schmitz.* PhD thesis, TU Berlin.

Scotese, C. (2002). PALEOMAP website.

Sorgenfrei, T. and Buch, A. (1964). *Deep tests in Denmark 1935-1959*.

Spencer, E. (1938). The potash-soda feldspars II. Some applications to petrogenesis. *Mineralogical Magazine*, 25(162):87–118.

Störr, M. (1983). *Die Kaolinlagerstätten der Deutschen Demokratischen Republik*. Akad.-Verlag.

Störr, M. and Bellmann, H. (1975). *Kaolin Deposits of the GDR in the Northern Region of the Bohemian Massif*. Ernst-Moritz-Arndt-Universität Greifswald Sektion Geologische Wissenschaften.

Streckeisen, A. (1976). To each plutonic rock its proper name. *Earth-Science Reviews*, 12(1):1–33.

Surlyk, F. (1980). Geology of the European countries. In *Denmark, Finland, Iceland, Norway, Sweden. Denmark. Published in corporation with the Comit6 Fran˜ ais de G˜ ologiem (CNFG) on the occasion of the 26th international geological congress. Paris: Graham and Trotman Ltd*.

Surlyk, F. and Sørensen, A. (2010). An early Campanian rocky shore at Ivö Klack, southern Sweden. *Cretaceous Research*, 31(6):567–576.

Sverdrup, H. and Warfvinge, P. (1988). Weathering of primary silicate minerals in the natural soil environment in relation to a chemical weathering model. *Water, Air, & Soil Pollution*, 38(3):387–408.

Tardy, Y., Bocquier, G., Paquet, H., and Millot, G. (1973). Formation of clay from granite and its distribution in relation to climate and topography. *Geoderma*, 10(4):271–284.

Tiba, T., Hashinoto, M., and Kato, A. (1970). An anthophyllite-hornblende pair from Japan. *Lithos*, 3(4):335–340.

Turcotte, D. (1986). Fractals and fragmentation. *Journal of Geophysical Research*, 91(B2):1921–1926.

Vejbæk, O. and Andersen, C. (2002). Post mid-Cretaceous inversion tectonics in the Danish Central Graben—regionally synchronous tectonic events. *Bulletin of the Geological Society of Denmark*, 49:129–144.

Velbel, M. A. (1989). Weathering of hornblende to ferruginous products by a dissolution-reprecipitation mechanism: Petrography and stoichiometry. *Clays and Clay Minerals*, 37(6):515–524.

Velde, B., Dubois, J., Moore, D., and Touchard, G. (1991). Fractal patterns of fractures in granites. *Earth and Planetary Science Letters*, 104(1):25–35.

Waight, T., Frei, D., and Storey, M. (2012). Geochronological constraints on granitic magmatism, deformation, cooling and uplift on Bornholm, Denmark. *Geological Society of Denmark. Bulletin*, 60:23–46.

Weaver, C. E. and Pollard, L. D. (1973). *The chemistry of clay minerals*, volume 83. Elsevier Amsterdam.

Zariņš, K. and Johansson, Å. (2009). U–Pb geochronology of gneisses and granitoids from the Danish island of Bornholm: new evidence for 1.47–1.45 Ga magmatism at the southwestern margin of the East European Craton. *International journal of earth sciences*, 98(7):1561–1580.

A | Gamma ray measurements

Table A.1: Summary table of gamma ray measurements

Gamma Ray Measurements Nygård					
Hight above def. datum (cm)	**Profile A**	**Profile B**	**Profile C**	**Profile D**	**Profile E**
440		80	104		
430					
420		68			
410					
400					
390		61			
380		57		110	
370		58		120	
360					
350		53			
340		58	102		83
330		60	100	88	85
320		69	91	93	78
310		60	90	92	87
300	50	70	92	85	115
290		100	92	90	105
280		105	93	80	112
270			93	84	105
260	50		100	85	103
250	54		86	84	99
240			90	82	85
230			89	92	80
220		63	100	81	98
210	47	61	86	82	95
200	50	55	83	85	73
190	48	63	89	65	65
180			85	70	75
170	51	63	84	65	67
160	48	59	77	68	72
150	45	56	75	68	70
140	49	57	82	69	65
130	50	59	78	67	70
120	48	58	87	67	78
110	55	59	81	70	80
100	57	59	90	75	76
90	60	65	80	63	80
80	65	62	90	64	80
70	57	71	91	65	85
60	57	70	96	65	85
50	60	73	90	69	100
40	60	95	89	70	85
30	73	95	93	70	95
20	80	100	94	77	85
10	80	104	93	80	
0					

B | Thin section analysis

Sample	Texture	Mineral Size and developement	Mineral content 1.	2.	Pheno-crysts	Zoning and Twinning	Staining	Degree of weathering	Comments
AR 3-12 (friable, strongly weathered)	Holocrystalline, porespace filled by clay (dominantly Kaolinite)	Phaneritic (fine grained <1mm) Anhedral very spars to non min.-min. bound	Qtz, K-fsp. (Microcl.), Plag (<) Zr	Kaolinite Siderite Apatite Hematite Pyrite	Quartz, K-fsp, Plagioclase	No zoning observed, twinning of K-fesp. extremly blury	Siderite `blossom structures and iron oxide along highly fractured Fsp.	Ⅳ	Biotite compl. weathered, Plag. nearly out, poresp. filled with Kaolinite,Siderite pervasive, after Kaolinitization.
AR 18-12 (within corestone outer shale)	Holocrystalline porspace filled by Siderite and Dolomite,Kaolinite	Phaneritic-Aphanitic (fine grained <1mm) Anhedral	Qtz, K-fsp Zr	Kaolinite< Siderite>> Apatite Hematite Pyrite	Qtz, K-fsp	No zoning observed, twinning of K-fesp. extremly blury	Siderite blossom structures and iron oxide along highly fractured Fsp.	Ⅳ	Qtz and K-fsp only micrsocopically distinguishable, remains of primary minerals.
AR 28-12 (corestone)	Holocrystalline	Phaneritic fine-/medium grained (<1-5mm); Sub-Anhedral	Qtz, K-fsp, Plag (<) Bio Zr	Kaolinite< Siderite>> Apatite Hematite>	Quartz, K-fsp., >Plag., >>Biotite	Discontinous zonation and"Tartan" -twinning observed in K-fsp	Staining in microfrct. and scattered k-fesp., filling iron oxide	Ⅲ	Biotite and Plg. poorly present,porespace filled with Kaolinite, little Siderite.
CR 3-12 (weathered zone)	Holocrystalline, Mixed accumulated mineral associations in thin section	Phaneritic (fine grained <1mm); Anhedral very spars to non min.-min. bound	Qtz, K-fsp. >>Bio >>Plag	Kaolinite> Illite Hematite<	Quartz, K-fsp., Plag.<, Biotite<<	Discontinous zonation and"Tartan" -twinning observed in K-fsp	Staining along the k-fsp mineral sufaces	Ⅲ - Ⅳ	On the splaying ends of Biotite,small K-fsp recristallyzation could be observed
CR 14-12 (modertate hard)	Holocrystalline porspace filled by Siderite and calcite, Kaolinite	Phaneritic fine-/medium grained (<1-5mm); Sub-Anhedral	Qtz, K-fsp Bio Zr	Kaolinite< Siderite>> Calcite Hematite>	Quartz, K-fsp., very alterated Biotite	"Tartan" twinning and exosolution lamellas appear altered	Siderite and ironoxide is increased compared to CR3-12	Ⅳ	Plg. altered comletely, Biotite is present in remnants of splayed pieces. Sample high in calcite
CR 25-12 (very weathered, friable)	Holocrystalline porspace filled by Siderite and Dolom., Kaolinite	Phaneritic fine-/medium grained (<1-5mm); Sub-Anhedral	ZrQtz, K-fsp Bio Zr	Kaolinite< Siderite>> Dolomite Hematite>	Quartz, K-fsp. extremely alterated Biotite	"Tartan" twinning, exosolution lamellas appear altered	Siderite "blossom" structures along K-fsp grain surfaces	Ⅳ	Plg. altered comletely, Biotite is present in remnants of splayed pieces.
ER 1-12 (friable)	Holocrystalline,	Phaneritic fine-/medium grained (<1-5mm); Sub-Anhedral	Qtz, K-fsp, Bio Zr	Kaolinite> Hematite< Pyrite	Quartz, K-fsp., >>Biotite	No zoning observed, twinning of K-fsp. extremly blury	Oxidized minerals (ironoxide) present along K-fsp borders	Ⅲ - Ⅳ	Quartz is sericitized. Biotite mostly gone Plagioclase gone
ER 14-12 (very fractured, brittle)	Holocrystalline, porespace filled by clay	Phaneritic fine-/medium grained (<1-5mm); Sub-Anhedral	Qtz, K-fsp Hbl-remnants Bio Zr	Kaolinite> Illite Hematite<	Quartz, K-fsp.	No zoning observed, twinning of K-fsp. extremly blury	Oxidized minerals presenet along K-fsp borders	Ⅲ - Ⅳ	Quartz is sericitized. Biotite mostly gone Plagioclase gone
ER 30-12 (base of core stone, loose)	Holocrystalline porspace filled by Siderite and Dolom. Kaolinite	Phaneritic (fine grained <1mm) An-subhedral	Qtz, K-fsp Bio	Kaolinite> Calcite Siderite Hematite<	Quartz, K-fsp., Biotite	No zoning observed, twinning of K-fsp. extremly blury	Oxidized minerals presenet along K-fsp borders	Ⅲ	Biotite very splayed kaolinititization along c-axis common. Plg completely altered to Kaolinite.
RaF 3B-1985 (pure kaolinite Qtz clasts)	Holocrystalline Matrix supported sediment. Matrix: Kaolinite	Aphanitic Anhedral	Quartz	Kaolinite	Quartz	—	—	Ⅳ	Pure Kaolinite with some quartz phenocrysts in groundmass
Quarry 1-12 (Fresh Granite)	Holocrystalline	Phaneritic fine-medium <1mm-5mm close to equigranular eu- to subhedral	Qtz, Bio, Hbl, K-fsp, Plag., Rt., Zr	Sericite in Plag. Pyrite	Quartz, K-fsp/ Plag, Hornblende, Bio	Zoned Fledpar, Plagioclase, surounded by K-fsp	Staining along {001} in Biotite and along micro-fractures in Hornblende	Ⅰ	Slightly weathered around Biotite. Plg sericitized in center
Quarry 2-12 (Fresh Granite)	Holocrystalline	Phaneritic Fine-medium <1mm-5mm close to equigranular eu- to subhedral	Qtz, Bio, Hbl, K-fsp, Plag., Rt., Zr	Sericite in Plag. Pyrite	Quartz, K-fsp/ Plag, Hbl, Biotite	Plag Q2-12 shows internal zoning, "Tartan twinning" in K-fsp less blury as in Q1-12	Staining along {001} in Biotite and along micro-fractures in Hornblende	Ⅰ	As Q1-12 first signs of pervasive alteration, along c-axis in Biotite. Hbl shows primer Qtz

Figure B.1: Thin section description

Sample	Texture	Mineral Size and developement	Mineral content 1.	Mineral content 2.	Pheno-crysts	Zoning and Twinning	Staining	Degree of weathering	Comments
BR 1-12	Holocrystalline void space filled with kaolinite, remants of biotite and iron oxide +siderite	Phaneritic subhedral to anhedral mineral surfaces	Qtz, K-fsp, Plag Biot (altered) Hbl (very alt.) Zr	Kaolinite Siderite Iron oxide Calcite Chlorite<<	Qtz, K-fsp, Biot (altered) Hbl (very alt.) Zr	No zoning `Tartan` twinning in K-fsp, poly-synthetic, some Karlsbad in Plag.	Strong staining along veins and micro-fractures. Siderite does not show `blooming` structure	III — IV	Stained veines contain also calcite (high bire-fringance), Hbl and Bio most affected by dis-coloration of iron oxide
BR 2-12	Holocrystalline void space filled with kaolinite, remants of biotite and iron oxide +siderite	Phaneritic subhedral to anhedral mineral surfaces	Qtz, K-fsp, Plag Biot (altered) Hbl (very alt.) Zr	Kaolinite Siderite Iron oxide Calcite Chlorite<<	Qtz, K-fsp, Biot (altered) Hbl (very alt.) Zr	No zoning `Tartan` twinning in K-fsp, poly-synthetic, some Karlsbad in Plag.	Staining increased compared to BR1-12 some `blooming ` appears	IV	well distinct veins, filled with siderite and iron oxide radioting from Bio minerals.
BR 4-12	Holocrystalline Hbl relief stronger determined as before	Phaneritic subhedral to anhedral mineral surfaces	Qtz, K-fsp, Plag, Biot (alt.) Hbl (very alt.) Zr, Pyrite	Kaolinite Siderite Iron oxide Calcite Chlorite<<	Qtz, K-fsp, Plag Biot (alt.) Hbl (very alt.) Zr, Pyrite	No zoning `Tartan` twinning in K-fsp, poly-synthetic, some Karlsbad in Plag.	Less staining, increased pore-space	IV	Pyrite content increased very high birefringance of some Qtz (Flashfigure). Plag gone
BR 5-12	Holocrystalline Hbl gone	Phaneritic subhedral to anhedral mineral surfaces	Qtz, K-fsp, Plag Biot (alt.) Hbl (very alt.) Zr, Pyrite	Kaolinite Siderite Iron oxide Calcite Chlorite<<	Qtz, K-fsp, Plag Biot (alt.) Hbl (very alt.) Zr, Pyrite	No zoning `Tartan` twinning in K-fsp, poly-synthetic, some Karlsbad in Plag.	Strong staining, well determined Siderite `blooms` + Calcite in veins	IV	Sample high in Kaolinite, oxidation state highest in profile so far.
BR 7-12	Holocrystalline Biotite, present only in remnats	Phaneritic subhedral to anhedral mineral surfaces	Qtz, K-fsp, Plag, Biot <<(alt.) Hbl (very alt.) Pyrite	Kaolinite Siderite Iron oxide Calcite<< Chlorite<<	Qtz, K-fsp, Plag Biot (alt.) Hbl (very alt.) Pyrite	No zoning `Tartan` twinning in K-fsp, poly-synthetic, some Karlsbad in Plag.	Very strong staining siderite nearly not visible--> highly oxidized (isotrpic)	IV	As BR-12
BR 13-12	Holocrystalline Biotite, present only in remnats	Phaneritic subhedral to anhedral mineral surfaces	Qtz, K-fsp, Plag, Biot <<(alt.) Hbl (very alt.) Pyrite	Kaolinite Siderite Iron oxide Calcite<< Chlorite<<	Qtz, K-fsp, Plag Biot (alt.) Hbl (very alt.) Pyrite	No zoning `Tartan` twinning in K-fsp, poly-synthetic, some Karlsbad in Plag.	Very strong staining siderite nearly not visible--> highly oxidized (isotrpic)	IV	Remaining K-fsp minerals empty in center, Plag weathered out, highly fractured
BR 16-12	Holocrystalline Biotite, present only in remnats	Phaneritic subhedral to anhedral mineral surfaces	Qtz, K-fsp, Plag, Biot <<(alt.) Hbl (very alt.) Pyrite	Kaolinite Siderite Iron oxide Calcite<< Chlorite<<	Qtz, K-fsp, Biotite (very altered shows no birefringance)	No zoning `Tartan` twinning in K-fsp, poly-synthetic, some Karlsbad in Plag.	Very strong staining siderite nearly not visible--> highly oxidized (isotrpic)	IV	Calcite content increased in pore space Scattered Biotite
BR 19-12	Holocrystalline Biotite, present only in remnats	Phaneritic subhedral to anhedral mineral surfaces	Qtz, K-fsp, Plag, Biot <<(alt.) Hbl (very alt.) Pyrite	Kaolinite Siderite Iron oxide Calcite<< Chlorite<<	Qtz, K-fsp, Biotite (very altered shows no birefringance)	No zoning `Tartan` twinning in K-fsp, poly-synthetic, some Karlsbad in Plag.	Very strong staining siderite nearly not visible--> highly oxidized (isotrpic)	IV	Calcite content increased in pore space Scattered Biotite
BR 21-12	Holocrystalline Biotite, present only in remnats	Phaneritic subhedral to anhedral mineral surfaces	Qtz, K-fsp, Plag, Biot <<(alt.) Hbl (very alt.) Pyrite	Kaolinite Siderite Iron oxide Calcite<< Chlorite<<	Qtz, K-fsp, Biotite (very altered shows no birefringance)	No zoning `Tartan` twinning in K-fsp, poly-synthetic, some Karlsbad in Plag.	Very strong staining siderite nearly not visible--> highly oxidized (isotrpic)	IV	Particles more scattered as in previous samples
BR 23-12	See sample BR21-12	See sample BR21-12	See sample BR21-12	See sample BR21-12	See sample BR21-12	See sample BR21-12	See sample BR21-12	IV – V	See sample BR21-12
BR 28-12	See sample BR21-12	See sample BR21-12	See sample BR21-12	See sample BR21-12	See sample BR21-12	See sample BR21-12	See sample BR21-12	IV – V	See sample BR21-12

Figure B.2: Thin section description

Sample	Texture	Mineral Size and developement	Mineral content 1.	2.	Pheno-crysts	Zoning and Twinning	Staining	Degree of weathering	Comments
DR 3-12 (Friable, weathered material)	Holocrystalline, void space filled with siderite, kaolinite and calcite	Phaneritic to aphanitic (medium-very fine grained) subhedral	Qtz, K-fsp, Plag Bio Hbl<	Kaolinite Siderite Calcite Pyrite	K-fsp Bio Qtz	Polylamellar twinning, exsolution in K-fesp	Staining along mineral margins and microfractures, mostly calcite and ironoxide	III — IV	Siderite vein dominant, high on calcite in pore space Plag. partlypreserved
DR 7-12 (Less friable, outer core stone)	Holocrystalline, siderite, kaolinite and calcite in poresp.	Phaneritic to aphanitic subhedral	Qtz, K-fsp, Plag Bio<< Hbl<<<	Kaolinite Siderite Calcite Pyrite	K-fsp Bio Qtz Hbl	Polylamellar twinning, exsolution in K-fesp	Staining along mineral margins and microfractures, mostly calcite and ironoxide	III — IV	TS shows the last stage in Hbl weathering
DR 9-12 (Weathered core stone)	Holocrystalline calcite, kaolinite and siderite in ps.	Phaneritic-aphanitic sub- to anhedral	Qtz, K-fsp Plag Bio<< Hbl<<<	Kaolinite Siderite Calcite Pyrite	K-fsp Bio Qtz Hbl	Polylamellar twinning, exsolution in K-fesp	Along microfrctures developement of siderite "flowers"	III — IV	TS shows the last stage in Hbl weathering
DR 10-12 (Less weathered corestone)	Holocrystalline calcite, kaolinite and siderite (ps.)	Phaneritic (Medium-fine grained) subhedral	Qtz, K-fsp Plag Bio<< Hbl<	Kaolinite Siderite Calcite Pyrite	K-fsp Bio Qtz Hbl	Polylamellar twinning, exsolution in K-fesp	Less stained, oxidation along fractures	III	Hbl better preserved than in DR3,7,9-12 Plag waethering -->plg+kao in k-fesp
DR 13-12 (Less weathered corestone)	Holocrystalline calcite, kaolinite and siderite (ps.)	Phaneritic (Medium-fine grained) subhedral	Qtz, K-fsp Plag Bio< Hbl>	Kaolinite Siderite Calcite Pyrite	K-fsp Bio Qtz Hbl	Polylamellar twinning, exsolution in K-fesp	Less stained, oxidation along fractures	III	Hbl preserved and siderite intergrown within Hbl
DR 19-12 (Core stone)	Holocrystalline calcite>>, kaolinite> (ps.)	Phaneritic (Medium-fine grained) subhedral	Qtz, K-fsp Plag Bio< Hbl>	Kaolinite Calcite Pyrite	K-fsp Bio Qtz Hbl	Polylamellar twinning, exsolution in K-fesp	Very little dis-coloration due to oxidation. High calcite content	II — III	High calcite content in void space, microcrystalline
DR 20-12 (Corestone)	Holocrystalline calcite, kaolinite> (ps.)	Phaneritic (Medium-fine grained) subhedral	Qtz, K-fsp Plag Bio<	Kaolinite Calcite Pyrite	K-fsp Bio Qtz	Polylamellar twinning, exsolution in K-fesp	Very little dis-coloration due to oxidation. High calcite content	II — III	Siderite microsc. not present. Transition Plag-Kao
DR 24-12 (Less weathered corestone)	Holocrystalline calcite, kaolinite>> (ps.)	Phaneritic (Medium-fine grained) subhedral	Qtz, K-fsp Plag Bio<<	Kaolinite Calcite	K-fsp Bio Qtz	Polylamellar twinning, exsolution in K-fesp	Very little dis-coloration due to oxidation. High calcite content	III	Amount of calcite decreased
DR 28-12 (Less weathered corestone)	Holocrystalline calcite>>, kaolinite> (ps.)	Phaneritic (Medium-fine grained) subhedral	Qtz, K-fsp Plag Bio<	Kaolinite Calcite	K-fsp Bio Qtz	Polylamellar twinning, exsolution in K-fesp	Very little dis-coloration due to oxidation. High calcite content	III	Amount of calcite increased
DR 31-12 (Corestone)	Holocrystalline calcite>>, kaolinite> (ps.)	Phaneritic (Medium-fine grained) subhedral	Qtz, K-fsp Plag Bio<	Kaolinite Calcite	K-fsp Bio Qtz	Polylamellar twinning, exsolution in K-fesp	Fractures and porespace filled with calcite and Kao>>	III	Prediminantly Kaolinite in pore spaces
DR 37-12 (outermost shale of core stone)	Holocrystalline, kaolinite> (ps.)	Phaneritic (Medium-fine grained) subhedral	Qtz, K-fsp Plag Bio<	Kaolinite	K-fsp Bio Qtz	Polylamellar twinning, exsolution in K-fesp	Very little dis-coloration due to oxidation. High calcite content	II — III	Prediminantly Kaolinite in pore spaces

Figure B.3: Thin section description

Table B.1: Point counting summary table

Point Counting										
Sample	Quartz	Plagioclase	K-Feldspar	Biotite/Illite	Hornblende	Chlorite	Siderite	Hematite	Kaolinite	Pyrite
BR1-12	19.2%	3.2%	25.5%	10.2%	1.2%	0.5%	8.0%	1.7%	28.0%	2.5%
BR2-12	8.0%	8.2%	18.5%	13.7%	2.0%	5.5%	11.2%	3.2%	27.2%	2.5%
BR4-12	12.2%	9.2%	30.2%	9.5%	4.2%	0.0%	0.7%	2.9%	30.7%	0.4%
BR5-12	8.5%	4.0%	19.5%	6.2%	4.0%	0.7%	17.0%	18.0%	21.2%	0.9%
BR7-12	6.2%	11.0%	23.7%	3.9%	4.7%	0.0%	9.5%	18.2%	22.0%	0.8%
BR13-12	4.7%	10.0%	20.0%	7.2%	6.5%	0.0%	20.0%	8.7%	21.0%	1.9%
BR16-12	14.7%	7.2%	26.7%	5.2%	0.5%	0.0%	21.0%	2.2%	22.5%	0.0%
BR19-12	15.2%	7.2%	19.5%	7.2%	0.5%	1.5%	28.7%	2.7%	16.5%	1.0%
BR21-12	13.0%	2.5%	15.0%	10.5%	1.2%	0.2%	25.5%	13.7%	18.2%	0.2%
BR23-12	12.7%	3.7%	13.7%	16.7%	0.5%	1.8%	13.7%	19.7%	17.5%	0.0%
BR28-12	13.0%	3.7%	13.5%	10.2%	2.2%	1.5%	9.7%	25.2%	20.2%	0.8%
DR3-12	19.7%	5.5%	30.0%	6.0%	0.1%	1.0%	13.7%	1.0%	23.0%	0.0%
DR7-12	17.5%	5.5%	32.5%	5.2%	0.0%	1.0%	16.2%	3.0%	19.0%	0.1%
DR9-12	16.5%	3.6%	31.9%	8.1%	0.0%	1.0%	20.6%	2.0%	15.9%	0.4%
DR10-12	15.0%	2.7%	23.7%	3.5%	0.0%	2.2%	17.2%	9.7%	25.7%	0.3%
DR13-12	16.7%	4.2%	25.0%	7.7%	0.0%	1.5%	7.2%	10.2%	27.2%	0.3%
DR19-12	17.0%	9.7%	27.2%	11.2%	0.0%	0.2%	15.2%	1.0%	18.2%	0.3%
DR20-12	15.5%	11.2%	23.2%	10.5%	2.5%	2.7%	13.2%	2.5%	18.5%	0.2%
DR24-12	12.8%	7.4%	28.9%	15.2%	0.8%	2.6%	4.7%	0.0%	27.1%	0.5%
DR28-12	5.5%	11.2%	12.7%	22.7%	5.0%	3.2%	20.0%	2.0%	17.0%	0.7%
DR31-12	13.5%	6.2%	24.7%	10.7%	1.2%	5.7%	11.7%	3.0%	22.7%	0.6%
DR37-12	10.9%	8.7%	27.8%	12.8%	0.3%	6.2%	0.0%	2.1%	30.7%	0.5%
Q1-12	15.5%	37.5%	26.0%	6.8%	14.2%	0.0%	0.0%	0.0%	0.0%	0.0%
Q2-12	19.0%	34.0%	23.0%	10.2%	13.7%	0.0%	0.0%	0.0%	0.0%	0.1%

C | XRD-analysis

Table C.1: Estimated XRD-% of the bulk sample analysis

Sample	Quartz	Plagioclase	K-Feldspar	Micas	Ilmenite	Hornblende	Siderite	Dolomite	Calcite	Hematite	Kaolinite	Chlorite/Smectite	Pyrite	Zircon
d-value	4,25 Å	3,19 Å	3,24 Å	10 Å	2,75 Å	8,4 Å	2,79 Å	2,89 Å	3,04 Å	2,69 Å	3,58 Å	14 Å	2,71 Å	3,3 Å
AR 3-12	8	2	13	1	3	1	39	4	4	2	13	1	2	6
AR 18-12	6	3	8	2	5	2	41	5	3	4	12	1	5	5
AR 28-12	13	7	25	9	3	1	8	5	5	2	10	1	3	7
BR 1-12	18	4	19	4	5	1	14	7	6	2	8	1	2	9
BR 2-12	20	4	22	5	5	1	9	7	7	2	6	1	2	9
BR 4-12	21	5	24	4	4	1	3	7	6	2	9	3	3	9
BR 5-12	9	2	9	2	3	1	20	3	33	1	7	1	2	5
BR 7-12	12	3	9	2	5	1	35	5	5	3	11	1	3	6
BR 13-12	10	3	16	2	3	1	34	5	3	4	11	1	3	5
BR 16-12	8	2	16	1	4	1	38	4	3	3	10	1	3	4
BR 19-12	11	3	17	2	5	1	35	1	4	2	10	1	3	6
BR 21-12	8	3	16	1	4	1	37	4	3	3	11	1	3	4
BR 23-12	13	4	24	2	4	1	19	5	3	3	8	1	4	8
BR 28-12	7	3	16	2	4	1	36	4	2	3	10	1	4	5
CR 3-12	20	5	23	6	6	1	3	8	5	3	6	1	3	10
CR 14-12	11	5	17	4	4	1	24	5	9	2	9	2	2	6
CR 25-12	13	6	20	3	4	1	2	6	22	2	9	2	2	9
DR 3-12	14	4	17	5	5	1	22	5	5	2	8	2	3	6
DR 7-12	14	8	23	4	5	1	14	6	3	3	5	4	3	8
DR 9-12	13	6	22	7	4	2	14	6	7	2	7	2	2	7
DR 10-12	13	5	17	11	4	1	12	5	10	2	8	2	3	7
DR 13-12	13	5	20	13	4	1	12	5	9	2	6	2	2	6
DR 19-12	11	5	20	11	3	1	2	5	22	2	7	1	2	6
DR 20-12	15	6	21	6	4	1	3	6	16	2	7	1	3	9
DR 24-12	14	7	29	3	4	1	3	6	1	2	13	4	2	9
DR 28-12	11	7	22	13	3	1	2	5	19	1	6	1	2	7
DR 31-12	15	6	19	8	3	1	3	6	15	2	8	1	3	9
DR 37-12	15	5	29	4	4	1	2	6	2	2	16	1	2	10
ER 1-12	21	5	22	6	6	1	3	7	3	2	9	1	3	11
ER 14-12	15	10	21	2	4	1	14	6	2	3	9	3	3	9
ER 30-12	14	7	13	9	4	2	2	6	22	2	8	1	2	8
Q 1-12	8	18	16	18	3	17	2	3	1	2	2	0	4	6
Q 2-12	12	22	16	15	3	10	2	3	2	2	2	1	2	8
RaF 3B-1985	20	1	3	2	2	1	3	2	1	2	57	1	2	5

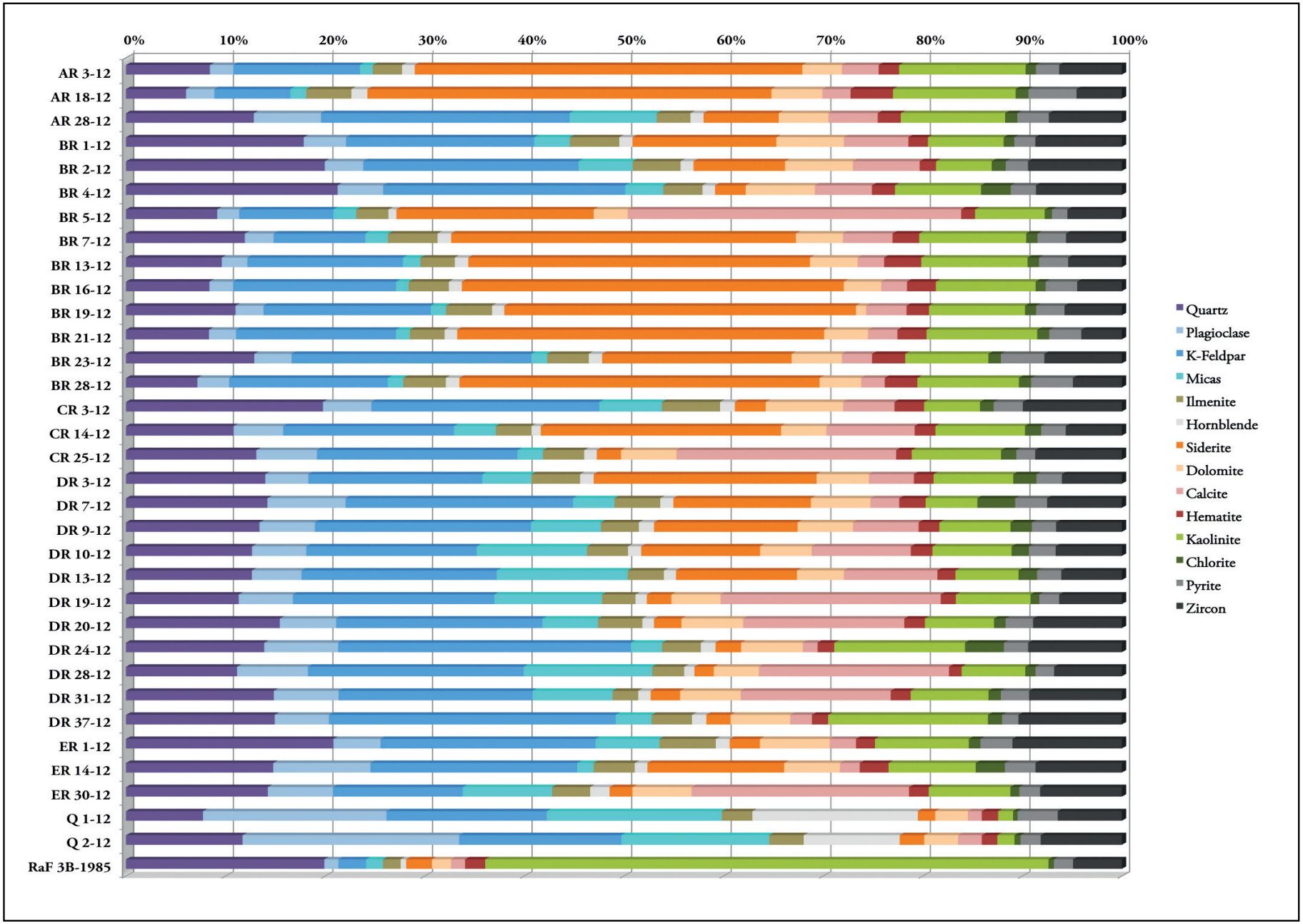

Figure C.1: Graphical representation of the xrd-bulk analysis, histogram displays the mineral content of the analyses samples inXRD-%. For data reference see Table C.1.

Table C.2: Mineral ratio calculations, based on semi-quantification of XRD -bulk analysis.

	Qz/(Fsp+Qz)	Pl/K-fspl+Pl)	Pl/(K-fsp+Pl)	Kao/(fsp+kao)	Pl/(Kao+Pl)	Kao/(Bio+Kao)	Hbl/(Chl+Hbl)	Hbl/(Sid+Hbl)	Sid/(Ca+Sid)
BR 1-12	0.44	0.18	0.18	0.24	0.36	0.70	0.50	0.07	0.70
BR 2-12	0.43	0.16	0.16	0.17	0.44	0.50	0.50	0.10	0.60
BR 4-12	0.42	0.16	0.16	0.22	0.36	0.70	0.25	0.25	0.38
BR 5-12	0.45	0.18	0.18	0.39	0.22	0.78	0.50	0.05	0.37
BR 7-12	0.48	0.25	0.25	0.45	0.23	0.83	0.50	0.03	0.87
BR 13-12	0.35	0.12	0.12	0.37	0.17	0.83	0.50	0.03	0.92
BR 16-12	0.31	0.11	0.11	0.36	0.17	0.91	0.50	0.03	0.93
BR 19-12	0.37	0.16	0.16	0.32	0.25	0.90	0.50	0.03	0.89
BR 21-12	0.31	0.17	0.17	0.38	0.21	0.92	0.50	0.03	0.92
BR 23-12	0.31	0.15	0.15	0.23	0.33	0.89	0.50	0.05	0.86
BR 28-12	0.28	0.17	0.17	0.36	0.23	0.91	0.50	0.03	0.95
Average	0.38	0.16	0.16	0.32	0.27	0.81	0.48	0.06	0.76
DR 3-12	0.39	0.21	0.21	0.27	0.36	0.64	0.33	0.05	0.83
DR 7-12	0.32	0.27	0.27	0.13	0.64	0.57	0.25	0.08	0.85
DR 9-12	0.32	0.20	0.20	0.19	0.45	0.50	0.33	0.07	0.68
DR 10-12	0.36	0.24	0.24	0.25	0.42	0.41	0.33	0.08	0.55
DR 13-12	0.33	0.18	0.18	0.21	0.40	0.33	0.33	0.08	0.58
DR 19-12	0.31	0.21	0.21	0.23	0.42	0.41	0.50	0.33	0.09
DR 20-12	0.38	0.20	0.20	0.22	0.42	0.58	0.50	0.25	0.17
DR 24-12	0.28	0.19	0.19	0.26	0.35	0.79	0.25	0.33	0.67
DR 28-12	0.27	0.26	0.26	0.18	0.54	0.33	0.50	0.33	0.10
DR 31-12	0.37	0.25	0.25	0.23	0.46	0.50	0.50	0.25	0.18
DR 37-12	0.30	0.17	0.17	0.32	0.26	0.82	0.50	0.33	0.50
Average	0.33	0.22	0.22	0.23	0.43	0.54	0.39	0.20	0.47
Q1-12	0.19	0.53	0.52	0.03	0.15	0.06	0.11	0.60	0.25
Q2-12	0.24	0.57	0.48	0.05	0.17	0.12	0.17	0.60	0.40
Average	0.22	0.55	0.50	0.04	0.16	0.09	0.14	0.60	0.33

Table C.3: Mineral change in %, calculated after (2.2.1)

	Qz/Pl-change%	Qz/K-fsp - change%	Qz/Mica - change%	Qz/Hbl - change%	Kao/Qz - change %
BR 1-12	-87	-20	-86	-93	157
BR 2-12	-88	-17	-79	-94	64
BR 4-12	-87	-12	-87	-93	143
BR 5-12	-87	-25	-82	-87	386
BR 7-12	-84	-38	-85	-89	468
BR 13-12	-87	25	-82	-87	594
BR 16-12	-86	50	-90	-85	681
BR 19-12	-84	9	-93	-89	411
BR 21-12	-79	41	-90	-85	759
BR 23-12	-81	44	-93	-90	317
BR 28-12	-76	61	-89	-83	793
DR 3-12	-81	-6	-73	-90	365
DR 7-12	-67	19	-80	-90	208
DR 9-12	-76	25	-60	-90	313
DR 10-12	-76	0	-33	-90	365
DR 13-12	-79	23	-13	-89	341
DR 19-12	-74	30	-27	-89	398
DR 20-12	-81	0	-73	-92	292
DR 24-12	-71	57	-80	-90	573
DR 28-12	-60	50	-4	-88	375
DR 31-12	-76	-3	-60	-91	313
DR 37-12	-78	45	-82	-91	673

Table C.4: XRD-clay fraction summary table, showing semi-quantification given as XRD-% of clay minerals as present in weathering section. Note that sample Q1-12 was neglected in this estimation. The values presented display a strictly clay fraction related internal distribution, since the amount of the clay share, compared to the bulk volume was not distinguished.

Mineral		**Smectite (Montm.)**	**Chlorite**	**Illite**	**Kaolinite**
d-value		17Å	3.54Å	10Å	3,57Å
Sample	Substrate nr.				
AR 3-12	1	11	30	5	53
AR 18-12	2	7	28	7	58
AR 28-12	3	4	12	2	82
BR 1-12	4	18	22	8	52
BR 2-12	5	21	20	6	53
BR 4-12	6	4	33	3	60
BR 5-12	7	11	21	6	62
BR 7-12	8	10	22	4	65
BR 13-12	9	8	27	3	62
BR 16-12	10	7	20	3	70
BR 19-12	11	9	23	3	65
BR 21-12	12	5	31	3	62
BR 23-12	13	12	24	4	60
BR 28-12	14	18	23	4	55
RaF 3B-1985	15	0	0	2	98
CR 3-12	16	5	13	2	80
CR 14-12	17	4	18	3	75
CR 25-12	18	4	15	2	79
DR 3-12	19	2	9	3	85
DR 7-12	20	1	26	4	69
DR 9-12	21	1	33	3	63
DR 10-12	22	3	19	3	75
DR 13-12	23	2	13	2	83
DR 19-12	24	4	10	2	84
DR 20-12	25	6	14	1	79
DR 24-12	26	2	23	2	72
DR 28-12	27	2	7	2	89
DR 31-12	28	8	1	4	86
DR 37-12	29	4	11	2	84
ER 1-12	30	5	13	1	81
ER 14-12	31	2	19	3	76
ER 30-12	32	4	13	1	82

Table C.5: Summary table of samples used for XRD- clay analysis.

Sample	Substrate nr.	Air dried	EG	350 °C	550 °C
AR 3-12	1	1578	1622	1970	2124
AR 18-12	2	1545	1588	1964	2116
AR 28-12	3	1528	1543	1605	1631
BR 1-12	4	1563	1583	1605	1627
BR 2-12	5	1534	1572	1597	1621
BR 4-12	6	1564	1586	1609	1630
BR 5-12	7	1566	1584	1610	1629
BR 7-12	8	1538	1570	1601	1616
BR 13-12	9	1536	1574	1595	1615
BR 16-12	10	1562	1582	1606	1635
BR 19-12	11	1548	1591	1968	2118
BR 21-12	12	1565	1585	1611	1628
BR 23-12	13	2140	2148	2154	2175
BR 28-12	14	1547	1590	1967	2117
RaF 3B-1985	15	2139	2149	2155	2176
CR 3-12	16	2127	2146	2157	2178
CR 14-12	17	2141	2150	2156	2177
CR 25-12	18	1580	1625	1969	2125
DR 3-12	19	1535	1573	1596	1619
DR 7-12	20	2126	2147	2158	2179
DR 9-12	21	1546	1589	1966	2120
DR 10-12	22	1537	1575	1594	1620
DR 13-12	23	1530	1567	1603	1636
DR 19-12	24	1531	1568	1592	1613
DR 20-12	25	1526	1541	1604	1634
DR 24-12	26	1533	1576	1593	1614
DR 28-12	27	1524	1539	1607	1633
DR 31-12	28	1525	1540	1600	1612
DR 37-12	29	1529	1571	1599	1617
ER 1-12	30	1532	1569	1598	1618
ER 14-12	31	1577	1623	1971	2122
ER 30-12	32	1579	1626	1972	2121
Q 1-12	33	1581	1624	1973	2119

D | Illustrations

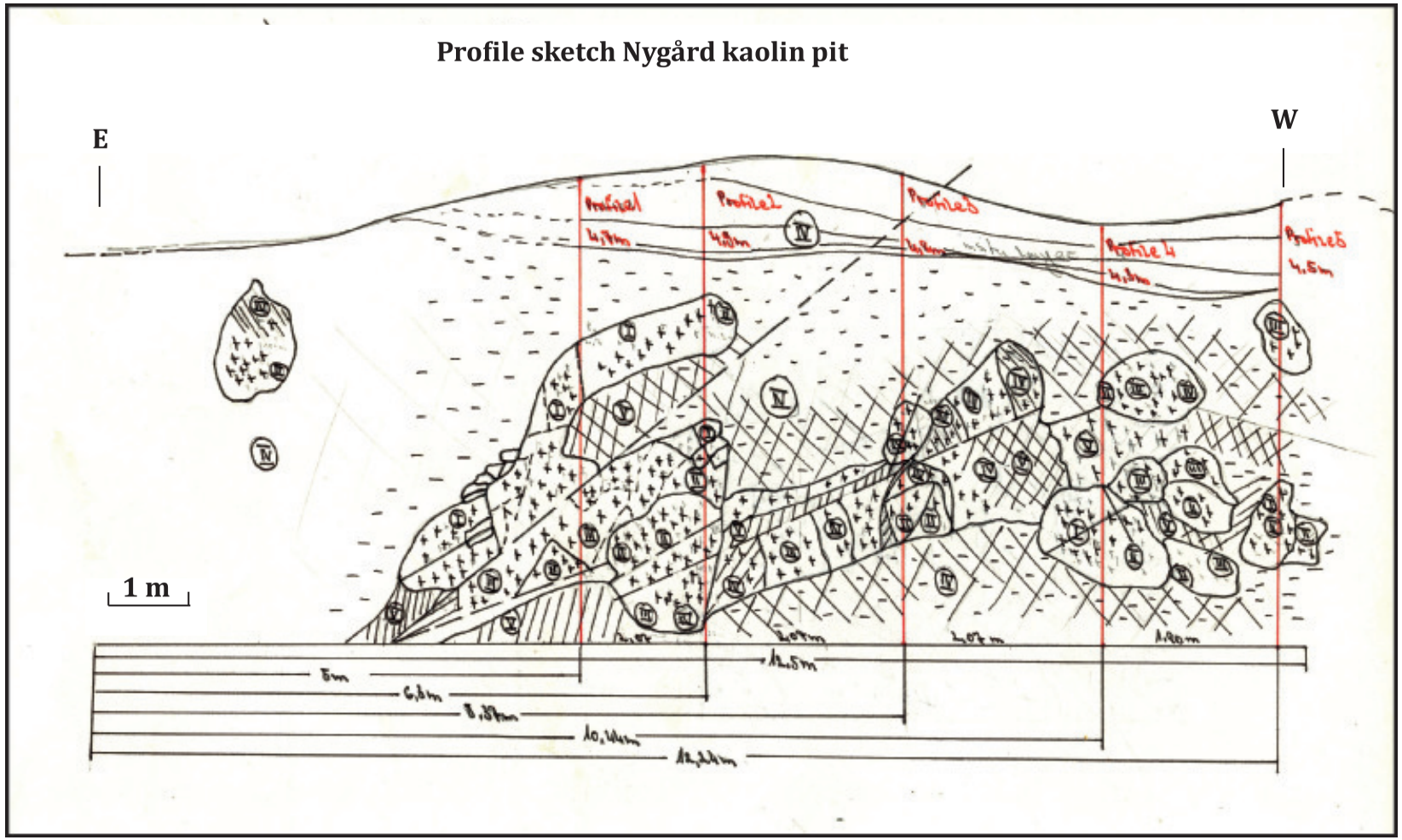

Figure D.1: Field sketch of the weathering profile at the Nygård kaolin pit, drawn in 1:10.

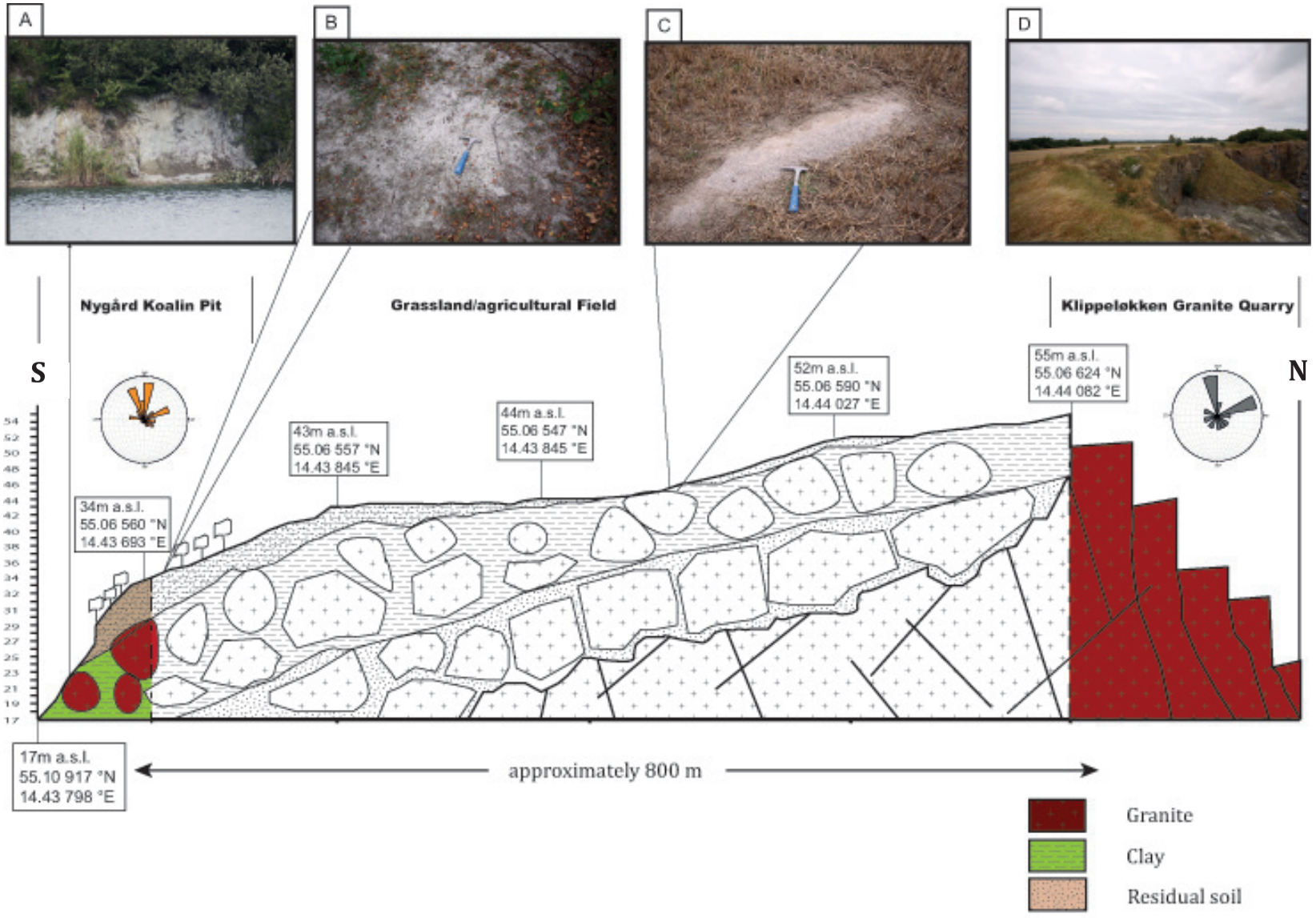

Figure D.2: The figure represents a interpolated, schematic and sketch of the elevation profile between the study site at Nygård (western margin) and the Klippeløkken granite quarry (east). The interpolation is based on GPS elevation measurements, combined with field photographies (a)-d)) indicating subaerially exposed changes of lithology of the substratum. The strictly hypothetical and interpolated area of the profile is left transparent, colored areas represent accessible outcrops.

Acknowledgements

I would like to express my deepest thanks to my supervisor Henning Dypvik, who by always sharing his valuable time and knowledge, helped me mature my scientific abilities, thank you Henning. In this manner I also would like to thank my co-supervisor Lars Riber, who through his busy days as a PhD candidate never hesitated to give support with fund professional expertise and delighting comments, both were highly appreciated, thank you.

My sympathy and regards go to Kamran Javed and Syed Asmar Aal-E-Muhammad Naqvi, who constituted an inevitable part of the working group, I would like to thank you for your teamwork and good working manner, which always was a delight to me.

I would like to thank the Lundin Petroleum AS for funding the field work and the analytical investigations of this master thesis.

The many hours of analytical work would not have been as enjoyable and pleasant without the people that helped to enable them. Therefore, I wish to send my gratitude to Maarten Aerts, for guiding me sedulously through the laboratory techniques and sample preparation for my XRD analysis and further more for being my LaTeX 2ε-keeper, thank you, this thesis would not look like this without you. Times at the electron microscope would not have been as constructive and illuminating without Berit Løken Berg, your guidance was inevitable and inspiring, thank you for saving me of getting lost in the micro cosmos. Staying in the micro cosmos, but rather on larger scale, it would not be without Lars Magne Kirksæter from the Petrological Service and Salahlldin Akhavan from the UIO, who did an outstanding job on preparing the thin sections, even of the highest weathering degree, thank you for your effort. My gratitude has to be addressed to Tom Andersen and Helge Hellvang for valuable discussions.

My dearest appreciation goes to my family and to my friends, who always blessed me with their infinite faith and love. In particular to Bertha Louise, words can not express my gratitude for your patience and your support, thank you for being there. My son Konrad, who by his radiance and presence reminded me that there is not that much difference between the eyes of a geologist and those of a child, it is the inspiration and the inner faith that drives them.